Title

Exogenous and endogenous mitochondrial regulators

Author

Khasin, Liliya

Publication Date

2020

Peer reviewed|Thesis/dissertation

Exogenous and Endogenous Mitochondrial Regulators

By

Liliya Khasin

A dissertation submitted in partial satisfaction

of the requirements for the degree of

Doctor of Philosophy

in

Molecular & Cell Biology

in the

Graduate Division

of the

University of California, Berkeley

Committee in charge:

Professor Polina V. Lishko, chair

Professor Rebecca Heald

Professor Daniel Feldman

Professor Andreas Stahl

Spring 2020

Abstract

Exogenous and Endogenous Mitochondria Regulators

By

Liliya Khasin

Doctor of Philosophy in Molecular and Cellular Biology

University of California, Berkeley

Professor Polina V Lishko, Chair

Mitochondria play a pivotal role in the cellular physiology. Besides orchestrating cellular energy generation, they are also crucial to numerous other processes, including the maintenance of intracellular Ca2+ homeostasis and the production of reactive oxygen species [1–4]. This thesis focuses on the two aforementioned functions and their regulation by endogenous and exogenous factors.

Mitochondria sustain calcium homeostasis by actively buffering cytosolic calcium. Calcium uptake into the mitochondrial matrix, in turn, regulates metabolism and energy production[1]. It is now well established that the primary mechanism of Ca2+ uptake in mitochondria is carried via the mitochondrial calcium uniporter (MCU) [5–8]. Interestingly, to date, only a few endogenous regulators of the MCU channel have been identified [9–12]. By using a targeted lipid mass spectrometry analysis and direct patch-clamp recordings from the inner mitochondrial membrane, we show that phosphatidylinositol-4,5-bisphosphate (PIP2) is a novel endogenous regulator of the MCU complex.

The byproduct of mitochondrial calcium uptake and subsequent increased metabolism is the generation reactive oxygen species (ROS)[13]. While low levels of ROS are essential for various physiological processes, ROS over-production can destroy mitochondria and lead to cell death[14–17].

A significant portion of this thesis deals with the effects of increased formation of ROS, triggered by environmental toxins, on sperm fertility. Specifically, we tested four ubiquitous chemicals found in plastics: bisphenol A (BPA), di-2-ethylhexyl phthalate (DEHP), diethyl phthalate (DEP), and dimethyl phthalate (DMP) on sperm fertilizing ability. Of all the tested toxins, DEHP demonstrated the most damaging impact on sperm fertility by increasing ROS production, altering the sperm maturation process, and impairing the acrosome reaction. We have concluded that even acute exposure to phthalates, such as DEHP, presents a significant risk to male fertility.

References

1. Contreras, L., Drago, I., Zampese, E. & Pozzan, T. Mitochondria: The calcium connection. *Biochimica et Biophysica Acta - Bioenergetics* vol. 1797 607–618 (2010).
2. Giorgi, C. *et al.* Mitochondrial calcium homeostasis as potential target for mitochondrial medicine. *Mitochondrion* vol. 12 77–85 (2012).
3. Chaudhari, N., Talwar, P., Parimisetty, A., d'Hellencourt, C. L. & Ravanan, P. A molecular web: Endoplasmic reticulum stress, inflammation, and oxidative stress. *Frontiers in Cellular Neuroscience* vol. 8 (2014).
4. Starkov, A. A. The role of mitochondria in reactive oxygen species metabolism and signaling. in *Annals of the New York Academy of Sciences* vol. 1147 37–52 (Blackwell Publishing Inc., 2008).
5. Finkel, T. *et al.* The ins and outs of mitochondrial calcium. *Circulation Research* vol. 116 1810–1819 (2015).
6. Santo-Domingo, J. & Demaurex, N. Calcium uptake mechanisms of mitochondria. *Biochimica et Biophysica Acta - Bioenergetics* vol. 1797 907–912 (2010).
7. Kirichok, Y., Krapivinsky, G. & Clapham, D. E. The mitochondrial calcium uniporter is a highly selective ion channel. *Nature* **427**, 360–364 (2004).
8. Pan, X. *et al.* The Physiological Role of Mitochondrial Calcium Revealed by Mice Lacking the Mitochondrial Calcium Uniporter. *Nat. Cell Biol.* **15**, 1464–1472 (2013).
9. Shanmughapriya, S. *et al.* Ca2+ signals regulate mitochondrial metabolism by stimulating CREB-mediated expression of the mitochondrial Ca2+ uniporter gene MCU. *Sci. Signal.* **8**, ra23 (2015).
10. Dong, Z. *et al.* Mitochondrial Ca2+ Uniporter Is a Mitochondrial Luminal Redox Sensor that Augments MCU Channel Activity. *Mol. Cell* **65**, 1014-1028.e7 (2017).
11. Rizzuto, R., Bernardi, P. & Pozzan, T. Mitochondria as all-round players of the calcium game. *Journal of Physiology* vol. 529 37–47 (2000).
12. Joiner, M. L. A. *et al.* CaMKII determines mitochondrial stress responses in heart. *Nature* **491**, 269–273 (2012).
13. Zorov, D. B., Juhaszova, M. & Sollott, S. J. Mitochondrial reactive oxygen species (ROS) and ROS-induced ROS release. *Physiological Reviews* vol. 94 909–950 (2014).
14. Bolisetty, S. & Jaimes, E. A. Mitochondria and reactive oxygen species: Physiology and pathophysiology. *International Journal of Molecular Sciences* vol. 14 6306–6344 (2013).
15. Aitken, R. J. & Drevet, J. R. The importance of oxidative stress in determining the functionality of mammalian spermatozoa: A two-edged sword. *Antioxidants* vol. 9 (2020).

16. Saleh, R. A. & Agarwal, A. Oxidative stress and male infertility: From research bench to clinical practice. *J. Androl.* **23**, 737–752 (2002).

17. Zhang, J. *et al.* ROS and ROS-Mediated Cellular Signaling. *Oxid. Med. Cell. Longev.* **2016**, (2016).

Table of Contents

Chapter III

The Impact of di-2-ethylhexyl Phthalate on Sperm Fertility

Chapter IV

Conclusion

ACKNOWLEDGMENTS

First and foremost, I want to thank Professor Polina Lishko, my mentor, teacher, and friend. Thank you for all your support, encouragement, and help! You affected my career as a researcher and life as a mother in so many ways. You are always pushing me to be better and aim higher.

I would also like to thank Andrew Modzelewski, Ida Björkgren, Lenka Vyklicka, Monika Haoui and John Della Rosa for all your help, support and friendship over the years. Thank you all!

I want to thank my mom, Neta, and my sister Angelina. I love you so much!
you are both ready to fly 10,000 miles anywhere anytime just to help me. I also thank my dad, Mark, who I love and miss every day.

I want to thank my in-laws, Amira and Michael. You both supported me so much over the years. Michael – you never missed one poster, paper, application, or fellowship I wrote. You always find time for me.

Most importantly, I thank my husband and daughter, George and Roni. You are my whole world. Without George's support, I would have never applied to a graduate school. Thank you all!

Chapter I

Introduction

1. Outline

As the powerhouse of the cell, mitochondria control nearly all cellular processes by providing a continuous supply of energy in the form of ATP. However, energy production is just one of many roles of mitochondria. Mitochondria are critical to cellular metabolism, fatty acid synthesis, generation of reactive oxygen species, calcium homeostasis, autophagy, and programmed cell death. Regulation of the cellular and mitochondrial calcium homeostasis and generation of reactive oxygen species are the main focus of this work.
The subsequent subsections summarize the current state of knowledge about these two important functions and pinpoints the areas where the current work has made its most significant contributions.

2. The basics of the cellular and mitochondrial calcium homeostasis regulation

2.1 Cellular calcium homeostasis regulation

Calcium homeostasis is essential for numerous cellular processes and is actively regulated by mitochondria[1]. Numerous cellular processes are governed by changes in calcium concentrations, making calcium one of the most important cellular second messengers [2]. At rest, calcium concentrations within the cell are kept low - around 100 nM. This low resting cytosolic concentration of calcium is maintained exclusively by plasma membrane Ca2+ transporters, ATPases, and the Na+ /Ca2+exchanger [3]. Following a stimulus, intracellular Ca2+ levels rise up to 1 μM, subsequently activating a targeted cellular reaction [4]. The rise in Ca2+ is achieved by either calcium entry from the extracellular space or the release from intracellular stores. The influx of calcium from the extracellular space is regulated by four types of plasma membrane channels: the voltage-operated calcium channels (VOCCs), the receptor-operated calcium channels (ROCCs), the store-operated calcium channels (SOCCs), and the second messenger-operated calcium channels (SMOCs) [5]. Within cells, the major calcium store is the endoplasmic reticulum (ER) or its equivalent in muscle cells - the sarcoplasmic reticulum (SR) [6]. Calcium release from the ER/SR is carried by the inositol 1,4,5-trisphosphate receptor (IP3R) or the ryanodine receptor (RyR). Both receptors are structurally related and are members of the same gene family [7].

The rise in Ca2+ needed to evoke a cellular response is mainly through release from intracellular stores, i.e. the ER. When a cellular stimulus is initiated, an extracellular soluble agonist binds a G-coupled protein receptor, thereby activating the enzyme phospholipase C (PLC). PLC then cleaves phosphatidylinositol 4,5 bisphosphate (PIP2) molecules resulting in the formation of diacylglycerol (DAG) and inositol-1,4,5-trisphosphate (IP3). Both DAG and IP3 are important second messengers. While DAG remains in the membrane to activate the protein kinase C signaling cascade, IP3 induces the opening and subsequent release of Ca2+ from the ER,

resulting in a rise in cytosolic Ca2+ and activation of various Ca2+-dependent intracellular events. The cellular outcome depends on the time and location of the generated Ca2+ signal [8]. After the signaling function is fulfilled, calcium must be quickly removed from the cytosol. This removal is achieved by calcium reuptake via the sarco-endoplasmic reticulum Ca2+-ATPase (SERCA), refilling the ER/SR Ca2+ stores. Calcium can also be extruded to the extracellular space by either the plasma membrane Ca2+ ATPases (PMCA pumps) or via the Na+/Ca2+ (NCX) and Na+/Ca2+-K+ exchangers (NCKX) [5].

Mitochondria play an equally important role in buffering cytosolic calcium. Mitochondria have a large calcium buffering capacity; they can manage up to 500 nM of cytosolic calcium concentrations, and by doing so, can handle transient changes in calcium levels and buffer cellular calcium overload [9–11]. Interestingly, mitochondrial calcium uptake does not just serve as a buffer for the cytosolic calcium, it also regulates numerous processes within the cell including muscle contraction, vesicular secretion, cell motility and migration, neuronal and cardiac electrical excitability, aerobic metabolism and cell survival [12–14].

2.2 Mitochondrial calcium homeostasis regulation

2.2.1 The physiological and pathophysiological role of mitochondrial calcium uptake

Mitochondrial calcium is tightly coupled to the energetic needs of the cell: a rise in mitochondrial calcium concentration indicates an increased cellular demand for energy, in the form of ATP [15]. In the mitochondrial matrix, calcium activates three key TCA cycle enzymes: pyruvate dehydrogenase, isocitrate dehydrogenase, and α-ketoglutarate dehydrogenase [16] as well as the F_1F_0-ATP synthase [17]. The net effect of such activation is enhanced electron transport, an increase in H+ pumping, and, subsequently, an increase in ATP synthesis [18].

When mitochondria accumulate excessive amounts of Ca2+, the mitochondrial function can become impaired, leading to an altered ATP production and an increased synthesis of reactive oxygen species (ROS). Moreover, when mitochondria are overloaded with calcium, a large channel in the mitochondrial inner membrane, also known as the mitochondrial permeability transition pore (mPTP) opens up [19]. mPTP opening increases the mitochondrial permeability to molecules smaller than 1500 Da. This results in mitochondrial osmotic shock, changes in the mitochondrial potential, and release of apoptotic factors into the cytoplasm [20].

2.2.2 Mechanisms of mitochondrial Ca2+ uptake

A. Transport across the mitochondrial membranes

To reach the mitochondrial matrix, calcium must cross two phospholipid membranes- the outer mitochondrial membrane (OMM) and the inner mitochondrial membrane (IMM). The OMM separates the cytosol from the intermembrane space and is relatively permeable to ions and small proteins (MW < 10 kDa) through the voltage-dependent anion channels (VDAC) also known as mitochondrial porin [21–23]. There are three different VDAC isoforms (VDAC1, VDAC2, and VDAC3). VDAC1 is considered to control Ca2+ permeability and act as the mitochondrial gatekeeper [24–27]. The inner mitochondrial membrane (IMM) separates the intermembrane space (IMS) from the mitochondrial matrix and is ion impermeable. Thus, calcium ions can only get across the IMM via a highly selective transport protein. The transporter, which is responsible for the majority of mitochondrial calcium uptake, is known as the mitochondrial calcium uniporter (MCU) [28,29].

B. Calcium uptake by the MCU

The mitochondrial respiratory chain establishes a proton (H+) gradient across the inner membrane. The H+ gradient generates a concentration gradient and an electrical gradient (ΔΨ) across the inner mitochondrial membrane of -180 mV (negative inside). These gradients provide a strong driving force for calcium uptake via the MCU and accumulation in the mitochondrial matrix [29]. Interestingly, the chemiosmotic gradient in the energized mitochondria is not sufficient for calcium uptake. This is mainly because one of the main characteristics of the MCU is its low affinity for Ca2+ (Kd of 20–30 μm under physiological conditions). This high Kd suggests that the cytosolic Ca2+ concentration must be at least 5 μm to reach a sizable mitochondrial Ca2+ influx. However, the intracellular levels of calcium in a healthy cell never reach such values. This discrepancy can be explained by the formation of high Ca2+ microdomains at the ER/SR-mitochondrial junctions [30–33]. These junctions are known as the mitochondria-associated ER membranes (MAMs). There, the calcium concentration can be >10μM, guaranteeing a quick uptake of Ca2+ by the MCU inside the mitochondrial matrix [31,34]. Many close contacts exist between the ER and the mitochondria. Also, similar microdomains exist between the mitochondria and the plasma membrane. The latter allows mitochondria to regulate better cytosolic calcium and various cellular functions [9].

2.2.3 The MCU components and regulation

The MCU is a highly selective calcium channel located in the inner mitochondrial membrane. The uniporter forms a 480 kDa multimeric complex consisting of MCU, MICU1/2, EMRE, MCUb, and MCUR. MCU, the essential pore-forming subunit [35–38] has two auxiliary subunits, MICU1, and MICU2, that work together to regulate the MCU by sensing calcium concentration through their EF-hand domains [39–44]. EMRE is an essential MCU regulator that connects MICU1/2 to MCU [45]. MCUb is a negative regulator of the MCU [46], and lastly, MCUR is an essential positive regulator of the MCU [47,48] (Figure 1).

In addition to these regulatory subunits of the MCU, further layers of regulation also exist to control the uniporter's activity. These include transcriptional and post-transcriptional regulation of MCU such as the cAMP response element-binding protein (CREB), which is a Ca2+-regulated transcription factor, and microRNAs, such as miR-25, which down-regulate MCU levels [49,50]. Post-translational modifications include Ca2+/calmodulin-dependent protein kinase II (CamKII) and the proline-rich tyrosine kinase 2 (Pyk2). CamKII is a positive regulator of MCU activity [51]. Pyk2 phosphorylates MCU residues and, by doing so, spurring MCU oligomerization and activity [52]. MCU is also regulated by the transport of nucleotides and anions to the mitochondrial matrix [53–56]. Such transport increases ΔΨm, and thus generates a more potent driving force for calcium uptake by MCU. Lastly, there is oxidative regulation of MCU. MCU has three conserved cysteines that can be oxidized. Of the three, Cys-97 had been previously identified as the primary target of oxidation by mitochondrial ROS. Cys-97 oxidation increases calcium uptake by the MCU [57]. When an aberrant increase in mitochondrial ROS occurs, such as during inflammation or ischemic heart injury reperfusion, mitochondrial ROS modifies MCU activity, which leads to mitochondrial Ca2+ overload and cell death [58].

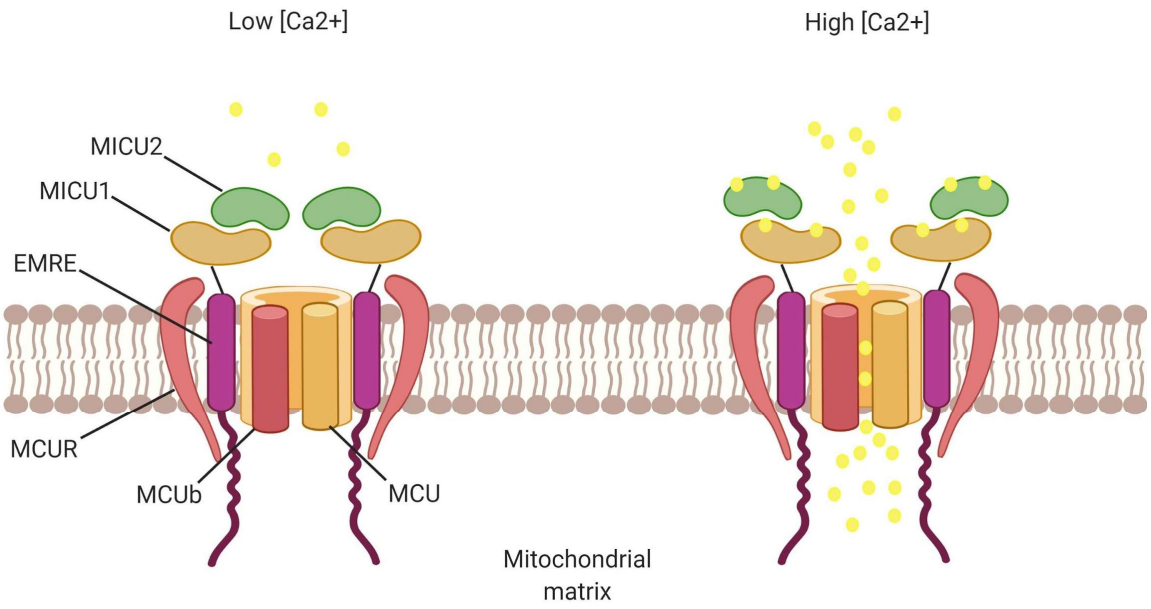

Figure 1. The mitochondrial calcium uniporter (MCU) complex. MCU is the Ca2+-selective ion channel that resides in the inner mitochondrial membrane (IMM) and is part of a macromolecular complex that includes the channel-forming subunit MCU and its regulators MICU1, MICU2, MCUb, EMRE, and MCUR1. Image created with BioRender.

2.2.4 Bioactive lipids

In the past few years, bioactive lipids emerged as a notable regulator of a diverse array of ion channels and transporters. Lipids are amphipathic molecules that are indispensable for the cellular and organellar membrane structure and function [59]. The most abundant membrane lipids are the phospholipids. Phospholipids can be modified by different enzymes, such as phospholipases or kinases, to produce bioactive lipid mediators [60]. The phospholipid, phosphatidylinositol 4,5-bisphosphate (PIP2), is the best-studied bioactive lipid. PIP2 is an anionic lipid found in the cytoplasmic leaflet of the plasma membrane, where it comprises less than 1% of all phospholipids [61,62]. Although PIP2 is principally found in the plasma membrane, its presence was also confirmed in organellar membranes, including the mitochondria [63,64].

It is well established that bioactive lipids regulate numerous mitochondria functions, including the electron transport chain (ETC) and ATP synthesis, mitochondrial protein import, as well as the integrity of the organellar membrane [65–69]. However, whether mitochondrial calcium uptake by the MCU can also be regulated by bioactive lipids has not been known. Since PIP2 is present in mitochondrial membranes and is known to govern the activity of various ion channels and transporters [70–73], we hypothesized that it can also regulate the activity of MCU. One of the main objectives of the present work was to explore this hypothesis.

3. The physiological and pathophysiological roles of ROS in sperm

3.1 Basics of ROS

As previously stated, mitochondrial Ca2+ uptake controls numerous mitochondrial and cellular processes [74–76]. One critical process regulated by the mitochondrial calcium is generation of reactive oxygen species (ROS), such as superoxide anion (O_2•−), hydrogen peroxide (H_2O_2), and hydroxyl radicals (HO•). Mitochondria are considered the primary location for ROS production, with at least eleven different sites associated with ROS generation [77]. Calcium and ROS are intimately linked: calcium is imperative for ROS generation, and ROS, in turn, regulates cellular calcium signaling [78]. Although this relationship is essential for normal cellular physiology, it also seems to play a critical role in many pathophysiological conditions [79,80]. The reason is that, in some sense, ROS acts as a double-edged sword. On the one hand, low levels of ROS function as a signaling molecule to regulate physiological processes [81,82] while on the other hand, overproduction of ROS can lead to increased levels of free radicals that cause oxidative stress. Unwarranted levels of free radicals can cause lipid peroxidation, damage the structure and the activity of proteins and DNA, and eventually lead to cellular death [83].

3.2 ROS and sperm fertility

A significant portion of this work focuses on the effects of ROS on sperm fertility and the exogenous regulation of mitochondrial ROS production by environmental toxins. ROS generation is a common feature of all living cells, including sperm cells. Spermatozoa are transcriptionally and translationally silent cells. Ejaculated spermatozoa must undergo a series of maturation steps in the female reproductive tract to be able to penetrate the protective vestments of the egg and fertilize. These maturation steps are accomplished by modifications of existing proteins rather than changes in gene expression [84]. ROS is one of the players required for such protein adjustments and the maturation process of sperm.

Small amounts of ROS are essential for sperm fertility. ROS raises the levels of cAMP, which then activates protein kinase A (PKA) [85]. An increase in the activity of PKA leads to an increase in the level of tyrosine phosphorylation, which is the primary driving force for sperm maturation, known as capacitation [86]. Increased protein phosphorylation also leads to sperm hyperactivation, a dramatic change in the motility pattern, which is required for sperm to be able to swim through the female reproductive tract and drill through the zona pellucida to fertilize the egg [87]. In addition, protein phosphorylation in the head region of the sperm enables spermatozoa to undergo the acrosome reaction, which allows sperm to fuse with the egg. [88–92]. High levels of ROS, on the other hand, are harmful to sperm fertility. Elevated ROS levels cause oxidative damage, which leads to chromatin instability and DNA fragmentation, lipid peroxidation that results in the loss of sperm membrane fluidity, and subsequently cell death [93–95]. In fact, elevated levels of ROS are considered as one of the causes of male infertility as aberrant levels of ROS have been reported in 40% of infertile men [96–98]

3.3 Sources of sperm ROS

Sperm cells heavily rely on mitochondria for ATP production due to the continuous requirement for energy to power their motility [99]. Spermatozoa harbor large numbers of mitochondria in the midpiece region of the sperm flagellum. The primary source of ROS in spermatozoa is the electron leakage from mitochondria, induced by various factors that disrupt the

electron transport chain[100]. Another endogenous source of ROS in sperm is the membrane-derived NADPH oxidase (NOX) [101]. In addition, sperm encounters additional sources of ROS in semen and inside the reproductive tract of females. Semen is responsible for the transport of sperm inside the reproductive tract of the female. Mammalian semen contains not only mature sperm cells but also leukocytes, a few Sertoli cells, and various developmental stages of sperm [102]. Leukocytes and immature spermatozoa with an abnormal morphology produce large amounts of ROS [103104105]. Mitochondria are the primary source of ROS within these cells. When seminal ROS exceeds normal production, spermatozoa experiences increased oxidative stress and subsequent cellular damage. The female reproductive tract also contains significant amounts of mitochondrial ROS. Although ROS is important for normal fertilization, the overproduction of ROS plays a role in the pathogenesis of infertility [106,107].

Due to the vital importance of maintaining ROS levels at bay for normal sperm functioning, it can be expected that environmental pollutants affecting mitochondrial physiology and ROS levels would cause severe adverse effects to sperm fertility. Over the past 40 years, male infertility rates have risen dramatically, with 1 in 20 men facing difficulties to father a child [108]. Male infertility is a complex, multifactorial condition in which genetic predisposition and environmental factors account for its development. Over the last decade, a class of chemical pollutants named endocrine-disrupting chemicals (EDCs) has been associated with increased rates of infertility [109,110]. These chemicals can alter signal transduction of sex steroid and thyroid hormones, trigger epigenetic changes [111,112], alter cellular metabolism by targeting mitochondrial function as well as target numerous other mechanisms that affect the endocrine and reproductive systems. [113–115]. Endocrine disruptors are a highly diversified group of chemicals that includes several industrial solvents/lubricants and their byproducts, including but not limited to plasticizers such as bisphenol A (BPA), phthalates and pesticides [113].

The second objective of the present work was to assess the impact of four ubiquitous environmental EDCs: bisphenol A (BPA), di-2-ethylhexyl phthalate (DEHP), diethyl phthalate (DEP), and dimethyl phthalate (DMP) on ROS generation in sperm and the effects on sperm fertilizing ability.

4. References

1. Giorgi, C. *et al.* Mitochondrial calcium homeostasis as potential target for mitochondrial medicine. *Mitochondrion* vol. 12 77–85 (2012).
2. Carafoli, E. & Krebs, J. Why calcium? How calcium became the best communicator. *J. Biol. Chem.* **291**, 20849–20857 (2016).
3. Brini, M. & Carafoli, E. The Plasma Membrane Ca2+ ATPase and the plasma membrane Sodium Calcium exchanger cooperate in the regulation of cell Calcium. *Cold Spring Harb. Perspect. Biol.* **3**, 1–15 (2011).
4. Leybaert, L. & Sanderson, M. J. Intercellular Ca2+ waves: Mechanisms and function. *Physiological Reviews* vol. 92 1359–1392 (2012).
5. De Stefani, D., Rizzuto, R. & Pozzan, T. Enjoy the Trip: Calcium in Mitochondria Back and Forth. *Annu. Rev. Biochem.* **85**, 161–192 (2016).
6. Koch, G. L. E. The endoplasmic reticulum and calcium storage. *BioEssays* vol. 12 527–531 (1990).
7. Santulli, G., Nakashima, R., Yuan, Q. & Marks, A. R. Intracellular calcium release channels: an update. *Journal of Physiology* vol. 595 3041–3051 (2017).
8. Bagur, R. & Hajnóczky, G. Intracellular Ca2+ Sensing: Its Role in Calcium Homeostasis and Signaling. *Molecular Cell* vol. 66 780–788 (2017).
9. Hartmann, J. & Verkhratsky, A. Relations between intracellular Ca $^{2+}$ stores and store-operated Ca $^{2+}$ entry in primary cultured human glioblastoma cells. *J. Physiol.* **513**, 411–424 (1998).
10. Budd, S. L. & Nicholls, D. G. A Reevaluation of the Role of Mitochondria in Neuronal Ca2+ Homeostasis. *J. Neurochem.* **66**, 403–411 (2002).
11. Imbert, N., Cognard, C., Duport, G., Guillou, C. & Raymond, G. Abnormal calcium homeostasis in Duchenne muscular dystrophy myotubes contracting in vitro. *Cell Calcium* **18**, 177–186 (1995).
12. Romero-Garcia, S. & Prado-Garcia, H. Mitochondrial calcium: Transport and modulation of cellular processes in homeostasis and cancer (Review). *International Journal of Oncology* vol. 54 1155–1167 (2019).
13. Tsai, F. C. *et al.* A polarized Ca2+, diacylglycerol and STIM1 signalling system regulates directed cell migration. *Nat. Cell Biol.* **16**, 133–144 (2014).
14. Yang, S. & Huang, X. Y. Ca2+ influx through L-type Ca2+ channels controls the trailing tail contraction in growth factor-induced fibroblast cell migration. *J. Biol. Chem.* **280**, 27130–27137 (2005).

15. Glancy, B., Willis, W. T., Chess, D. J. & Balaban, R. S. Effect of calcium on the oxidative phosphorylation cascade in skeletal muscle mitochondria. *Biochemistry* **52**, 2793–2809 (2013).

16. Denton, R. M. & McCormack, J. G. On the role of the calcium transport cycle in heart and other mammalian mitochondria. *FEBS Letters* vol. 119 1–8 (1980).

17. Territo, P. R., Mootha, V. K., French, S. A. & Balaban, R. S. Ca2+ activation of heart mitochondrial oxidative phosphorylation: Role of the F0/F1-ATPase. *Am. J. Physiol. - Cell Physiol.* **278**, (2000).

18. Rizzuto, R., De Stefani, D., Raffaello, A. & Mammucari, C. Mitochondria as sensors and regulators of calcium signalling. *Nature Reviews Molecular Cell Biology* vol. 13 566–578 (2012).

19. Hunter, D. R., Haworth, R. A. & Southard, J. H. Relationship between configuration, function, and permeability in calcium treated mitochondria. *J. Biol. Chem.* **251**, 5069–5077 (1976).

20. Stansfield, W. E. *et al.* The Pathophysiology of Cardiac Hypertrophy and Heart Failure. in *Cellular and Molecular Pathobiology of Cardiovascular Disease* 51–78 (Elsevier Inc., 2014). doi:10.1016/B978-0-12-405206-2.00004-1.

21. Simamura, E., Shimada, H., Hatta, T. & Hirai, K. I. Mitochondrial voltage-dependent anion channels (VDACs) as novel pharmacological targets for anti-cancer agents. *J. Bioenerg. Biomembr.* **40**, 213–217 (2008).

22. Bayrhuber, M. *et al.* Structure of the human voltage-dependent anion channel. *Proc. Natl. Acad. Sci. U. S. A.* **105**, 15370–15375 (2008).

23. Mihara, K. & Sato, R. Molecular cloning and sequencing of cDNA for yeast porin, an outer mitochondrial membrane protein: a search for targeting signal in the primary structure. *EMBO J.* **4**, 769–774 (1985).

24. Gincel, D., Zaid, H. & Shoshan-Barmatz, V. Calcium binding and translocation by the voltage-dependent anion channel: A possible regulatory mechanism in mitochondrial function. *Biochem. J.* **358**, 147–155 (2001).

25. Báthori, G., Csordás, G., Garcia-Perez, C., Davies, E. & Hajnóczky, G. Ca2+-dependent control of the permeability properties of the mitochondrial outer membrane and voltage-dependent anion-selective channel (VDAC). *J. Biol. Chem.* **281**, 17347–17358 (2006).

26. Tan, W. & Colombini, M. VDAC closure increases calcium ion flux. *Biochim. Biophys. Acta - Biomembr.* **1768**, 2510–2515 (2007).

27. Rapizzi, E. *et al.* Recombinant expression of the voltage-dependent anion channel enhances the transfer of Ca2+ microdomains to mitochondria. *J. Cell Biol.* **159**, 613–624 (2002).

28. Kirichok, Y., Krapivinsky, G. & Clapham, D. E. The mitochondrial calcium uniporter is a highly selective ion channel. *Nature* **427**, 360–364 (2004).

29. Rizzuto, R., Bernardi, P. & Pozzan, T. Mitochondria as all-round players of the calcium game. *Journal of Physiology* vol. 529 37–47 (2000).

30. Copeland, D. E. & Dalton, A. J. An association between mitochondria and the endoplasmic reticulum in cells of the pseudobranch gland of a teleost. *J. Biophys. Biochem. Cytol.* **5**, 393–396 (1959).

31. Rizzuto, R. *et al.* Close contacts with the endoplasmic reticulum as determinants of mitochondrial Ca2+ responses. *Science (80-.).* **280**, 1763–1766 (1998).

32. Vance, J. E. MAM (mitochondria-associated membranes) in mammalian cells: Lipids and beyond. *Biochimica et Biophysica Acta - Molecular and Cell Biology of Lipids* vol. 1841 595–609 (2014).

33. Burgoyne, T., Patel, S. & Eden, E. R. Calcium signaling at ER membrane contact sites. *Biochimica et Biophysica Acta - Molecular Cell Research* vol. 1853 2012–2017 (2014).

34. Jouaville, L. S., Pinton, P., Bastianutto, C., Rutter, G. A. & Rizzuto, R. Regulation of mitochondrial ATP synthesis by calcium: Evidence for a long-term metabolic priming. *Proc. Natl. Acad. Sci. U. S. A.* **96**, 13807–13812 (1999).

35. Baughman, J. M. *et al.* Integrative genomics identifies MCU as an essential component of the mitochondrial calcium uniporter. *Nature* **476**, 341–345 (2011).

36. De Stefani, D., Raffaello, A., Teardo, E., Szabó, I. & Rizzuto, R. A forty-kilodalton protein of the inner membrane is the mitochondrial calcium uniporter. *Nature* **476**, 336–340 (2011).

37. Chaudhuri, D., Sancak, Y., Mootha, V. K. & Clapham, D. E. MCU encodes the pore conducting mitochondrial calcium currents. *Elife* **2013**, (2013).

38. Kovaćs-Bogdán, E. *et al.* Reconstitution of the mitochondrial calcium uniporter in yeast. *Proc. Natl. Acad. Sci. U. S. A.* **111**, 8985–8990 (2014).

39. Patron, M. *et al.* MICU1 and MICU2 finely tune the mitochondrial Ca2+ uniporter by exerting opposite effects on MCU activity. *Mol. Cell* **53**, 726–737 (2014).

40. Liu, J. C. *et al.* MICU1 Serves as a Molecular Gatekeeper to Prevent In Vivo Mitochondrial Calcium Overload. *Cell Rep.* **16**, 1561–1573 (2016).

41. Perocchi, F. *et al.* MICU1 encodes a mitochondrial EF hand protein required for Ca2+ uptake. *Nature* **467**, 291–296 (2010).

42. Kamer, K. J., Grabarek, Z. & Mootha, V. K. High-affinity cooperative Ca 2+ binding by MICU 1– MICU 2 serves as an on–off switch for the uniporter . *EMBO Rep.* **18**, 1397–1411 (2017).

43. Mallilankaraman, K. *et al.* MCUR1 is an essential component of mitochondrial Ca2+ uptake that regulates cellular metabolism. *Nat. Cell Biol.* **14**, 1336–1343 (2012).

44. Csordás, G. *et al.* MICU1 controls both the threshold and cooperative activation of the mitochondrial Ca2+ uniporter. *Cell Metab.* **17**, 976–987 (2013).

45. Sancak, Y. *et al.* EMRE is an essential component of the mitochondrial calcium uniporter complex. *Science (80-.).* **342**, 1379–1382 (2013).

46. Raffaello, A. *et al.* The mitochondrial calcium uniporter is a multimer that can include a dominant-negative pore-forming subunit. *EMBO J.* **32**, 2362–2376 (2013).

47. Chaudhuri, D., Artiga, D. J., Abiria, S. A. & Clapham, D. E. Mitochondrial calcium uniporter regulator 1 (MCUR1) regulates the calcium threshold for the mitochondrial permeability transition. *Proc. Natl. Acad. Sci. U. S. A.* **113**, E1872–E1880 (2016).

48. Tomar, D. *et al.* MCUR1 Is a Scaffold Factor for the MCU Complex Function and Promotes Mitochondrial Bioenergetics. *Cell Rep.* **15**, 1673–1685 (2016).

49. Shanmughapriya, S. *et al.* Ca2+ signals regulate mitochondrial metabolism by stimulating CREB-mediated expression of the mitochondrial Ca2+ uniporter gene MCU. *Sci. Signal.* **8**, ra23 (2015).

50. Marchi, S. *et al.* Downregulation of the mitochondrial calcium uniporter by cancer-related miR-25. *Curr. Biol.* **23**, 58–63 (2013).

51. Joiner, M. L. A. *et al.* CaMKII determines mitochondrial stress responses in heart. *Nature* **491**, 269–273 (2012).

52. O-Uchi, J. *et al.* Adrenergic signaling regulates mitochondrial Ca2+ uptake through Pyk2-dependent tyrosine phosphorylation of the mitochondrial Ca2+ uniporter. *Antioxidants Redox Signal.* **21**, 863–879 (2014).

53. Litsky, M. L. & Pfeiffer, D. R. Regulation of the mitochondrial Ca2+ uniporter by external adenine nucleotides: The uniporter behaves like a gated channel which is regulated by nucleotides and divalent cations. *Biochemistry* **36**, 7071–7080 (1997).

54. Amigo, I. *et al.* Glucagon regulation of oxidative phosphorylation requires an increase in matrix adenine nucleotide content through Ca2+ activation of the mitochondrial ATP-Mg/Pi carrier SCaMC-3. *J. Biol. Chem.* **288**, 7791–7802 (2013).

55. Kwong, J. Q. *et al.* Genetic deletion of the mitochondrial phosphate carrier desensitizes the mitochondrial permeability transition pore and causes cardiomyopathy. *Cell Death Differ.* **21**, 1209–1217 (2014).

56. Wei, A. C., Liu, T. & O'Rourke, B. Dual effect of phosphate transport on mitochondrial Ca2+ dynamics. *J. Biol. Chem.* **290**, 16088–16098 (2015).

57. Dong, Z. *et al.* Mitochondrial Ca2+ Uniporter Is a Mitochondrial Luminal Redox Sensor that Augments MCU Channel Activity. *Mol. Cell* **65**, 1014-1028.e7 (2017).

58. Lee, S. K. *et al.* Structural Insights into Mitochondrial Calcium Uniporter Regulation by Divalent Cations. *Cell Chem. Biol.* **23**, 1157–1169 (2016).

59. Fahy, E. *et al.* Update of the LIPID MAPS comprehensive classification system for lipids. *Journal of Lipid Research* vol. 50 (2009).

60. Dennis, E. A. Liberating chiral lipid mediators, inflammatory enzymes, and lipid maps from biological grease. *J. Biol. Chem.* **291**, 24431–24448 (2016).

61. Rusten, T. E. & Stenmark, H. Analyzing phosphoinositides and their interacting proteins. *Nature Methods* vol. 3 251–258 (2006).

62. McLaughlin, S., Wang, J., Gambhir, A. & Murray, D. PIP2 and proteins: Interactions, organization, and information flow. *Annual Review of Biophysics and Biomolecular Structure* vol. 31 151–175 (2002).

63. Watt, S. A., Kular, G., Fleming, I. N., Downes, C. P. & Lucocq, J. M. Subcellular localization of phosphatidylinositol 4,5-bisphosphate using the pleckstrin homology domain of phospholipase C δ1. *Biochem. J.* **363**, 657–666 (2002).

64. Vicinanza, M. *et al.* OCRL controls trafficking through early endosomes via PtdIns4,5P 2-dependent regulation of endosomal actin. *EMBO J.* **30**, 4970–4985 (2011).

65. Daum, G. Lipids of mitochondria. *BBA - Reviews on Biomembranes* vol. 822 1–42 (1985).

66. Hoch, F. L. Cardiolipins and biomembrane function. *BBA - Reviews on Biomembranes* vol. 1113 71–133 (1992).

67. Petrushka, E., Quastel, J. H. & Scholefield, P. G. Role of phospholipids in oxidative phosphorylation and mitochondrial. *Can. J. Biochem. Physiol.* **37**, 989–998 (1959).

68. Shinzawa-Itoh, K. *et al.* Structures and physiological roles of 13 integral lipids of bovine heart cytochrome c oxidase. *EMBO J.* **26**, 1713–1725 (2007).

69. Jiang, F. *et al.* Absence of cardiolipin in the crd1 null mutant results in decreased mitochondrial membrane potential and reduced mitochondrial function. *J. Biol. Chem.* **275**, 22387–22394 (2000).

70. Hilgemann, D. W. & Ball, R. Regulation of Cardiac Na + , Ca2l Exchange and Potassium Channels by PIP2 KATp. *Science (80-.).* **273**, 956–959 (1996).

71. Hilgemann, D. W., Feng, S. & Nasuhoglu, C. The complex and intriguing lives of PIP2 with ion channels and transporters. *Science's STKE : signal transduction knowledge environment* vol. 2001 (2001).

72. Suh, B. C. & Hille, B. Regulation of ion channels by phosphatidylinositol 4,5-bisphosphate. *Current Opinion in Neurobiology* vol. 15 370–378 (2005).

73. Suh, B. C. & Hille, B. Regulation of KCNQ channels by manipulation of phosphoinositides. in *Journal of Physiology* vol. 582 911–916 (2007).

74. Hajnóczky, G., Robb-Gaspers, L. D., Seitz, M. B. & Thomas, A. P. Decoding of cytosolic calcium oscillations in the mitochondria. *Cell* **82**, 415–424 (1995).

75. Orrenius, S., Zhivotovsky, B. & Nicotera, P. Regulation of cell death: The calcium-apoptosis link. *Nature Reviews Molecular Cell Biology* vol. 4 552–565 (2003).

76. Hansford, R. G. Physiological role of mitochondrial Ca2+ transport. *J. Bioenerg. Biomembr.* **26**, 495–508 (1994).

77. Brand, M. D. Mitochondrial generation of superoxide and hydrogen peroxide as the source of mitochondrial redox signaling. *Free Radical Biology and Medicine* vol. 100 14–

31 (2016).

78. Gordeeva, A. V., Zvyagilskaya, R. A. & Labas, Y. A. Cross-Talk between Reactive Oxygen Species and Calcium in Living Cells. *Biochemistry (Moscow)* vol. 68 1077–1080 (2003).

79. Chinopoulos, C. & Adam-Vizi, V. Calcium, mitochondria and oxidative stress in neuronal pathology: Novel aspects of an enduring theme. *FEBS Journal* vol. 273 433–450 (2006).

80. Chaudhari, N., Talwar, P., Parimisetty, A., d'Hellencourt, C. L. & Ravanan, P. A molecular web: Endoplasmic reticulum stress, inflammation, and oxidative stress. *Frontiers in Cellular Neuroscience* vol. 8 (2014).

81. Takeshima, T., Kuroda, S. & Yumura, Y. Reactive Oxygen Species and Sperm Cells. in *Reactive Oxygen Species (ROS) in Living Cells* (InTech, 2018). doi:10.5772/intechopen.73037.

82. Sena, L. A. & Chandel, N. S. Physiological roles of mitochondrial reactive oxygen species. *Molecular Cell* vol. 48 158–167 (2012).

83. Circu, M. L. & Aw, T. Y. Reactive oxygen species, cellular redox systems, and apoptosis. *Free Radical Biology and Medicine* vol. 48 749–762 (2010).

84. Cornwall, G. A. Role of Posttranslational Protein Modifications in Epididymal Sperm Maturation and Extracellular Quality Control. in 159–180 (Springer, New York, NY, 2014). doi:10.1007/978-1-4939-0817-2_8.

85. Zhang, J. *et al.* ROS and ROS-Mediated Cellular Signaling. *Oxid. Med. Cell. Longev.* **2016**, (2016).

86. Yamagishi, S. I. *et al.* Leptin Induces Mitochondrial Superoxide Production and Monocyte Chemoattractant Protein-1 Expression in Aortic Endothelial Cells by Increasing Fatty Acid Oxidation via Protein Kinase A. *J. Biol. Chem.* **276**, 25096–25100 (2001).

87. Urner, F. & Sakkas, D. Protein phosphorylation in mammalian spermatozoa. *Reproduction* **125**, 17–26 (2003).

88. Rivlin, J., Mendel, J., Rubinstein, S., Etkovitz, N. & Breitbart, H. Role of Hydrogen Peroxide in Sperm Capacitation and Acrosome Reaction1. *Biol. Reprod.* **70**, 518–522 (2004).

89. Kodama, H., Kuribayashi, Y. & Gagnon, C. Effect of sperm lipid peroxidation on fertilization. *J. Androl.* **17**, 151–157 (1996).

90. de Lamirande, E. & O'Flaherty, C. Sperm activation: Role of reactive oxygen species and kinases. *Biochimica et Biophysica Acta - Proteins and Proteomics* vol. 1784 106–115 (2008).

91. Ochsendorf, F. R. *et al.* Chemiluminescence in semen of infertile men. *Andrologia* **26**, 289–293 (1994).

92. De Lamirande, E., Jiang, H., Zini, A., Kodama, H. & Gagnon, C. Reactive oxygen species and sperm physiology. *Rev. Reprod.* **2**, 48–54 (1997).

93. Aitken, R. J. *et al.* Relative Impact of Oxidative Stress on the Functional Competence and Genomic Integrity of Human Spermatozoa1. *Biol. Reprod.* **59**, 1037–1046 (1998).

94. Jones, R., Mann, T. & Sherins, R. Peroxidative breakdown of phospholipids in human spermatozoa, spermicidal properties of fatty acid peroxides, and protective action of seminal plasma. *Fertil. Steril.* **31**, 531–537 (1979).

95. Aitken, R. J., Wingate, J. K., De Iuliis, G. N., Koppers, A. J. & Mclaughlin, E. A. Cis-Unsaturated Fatty Acids Stimulate Reactive Oxygen Species Generation and Lipid Peroxidation in Human Spermatozoa. **91**, 4154–4163 (2006).

96. Iwasaki, A. & Gagnon, C. Formation of reactive oxygen species in spermatozoa of infertile patients. *Fertil. Steril.* **57**, 409–416 (1992).

97. Agarwal, A., Said, T. M., Bedaiwy, M. A., Banerjee, J. & Alvarez, J. G. Oxidative stress in an assisted reproductive techniques setting. *Fertil. Steril.* **86**, 503–512 (2006).

98. Takeshima, T. *et al.* Inverse correlation between reactive oxygen species in unwashed semen and sperm motion parameters as measured by a computer-assisted semen analyzer. *Asian J. Androl.* **19**, 350 (2017).

99. Henkel, R. R. Leukocytes and oxidative stress: Dilemma for sperm function and male fertility. *Asian Journal of Andrology* vol. 13 43–52 (2011).

100. Turrens, J. F. Mitochondrial formation of reactive oxygen species. *Journal of Physiology* vol. 552 335–344 (2003).

101. Williams, A. C. & Ford, W. C. L. Functional Significance of the Pentose Phosphate Pathway and Glutathione Reductase in the Antioxidant Defenses of Human Sperm1. *Biol. Reprod.* **71**, 1309–1316 (2004).

102. Fedder, J., Askjaer, S. A. & Hjort, T. Nonspermatozoal cells in semen: Relationship to other semen parameters and fertility status of the couple. *Syst. Biol. Reprod. Med.* **31**, 95–103 (1993).

103. Aitken, R. J. & Clarkson, J. S. Cellular basis of defective sperm function and its association with the genesis of reactive oxygen species by human spermatozoa. *J. Reprod. Fertil.* **81**, 459–69 (1987).

104. Sharma, R. K., Pasqualotto, F. F., Nelson, D. R., Thomas, A. J. & Agarwal, A. Relationship between seminal white blood cell counts and oxidative stress in men treated at an infertility clinic. *J. Androl.* **22**, 575–583 (2001).

105. Sakkas, D., Seli, E., Bizzaro, D., Tarozzi, N. & Manicardi, G. C. Abnormal spermatozoa in the ejaculated: Abortive apoptosis and faulty nuclear remodelling during spermatogenesis. *Reprod. Biomed. Online* **7**, 428–432 (2003).

106. Agarwal, A. & Allamaneni, S. S. R. Role of free radicals in female reproductive diseases and assisted reproduction. *Reproductive BioMedicine Online* vol. 9 338–347 (2004).

107. Bedaiwy, M. A. Prediction of endometriosis with serum and peritoneal fluid markers: a prospective controlled trial. *Hum. Reprod.* **17**, 426–431 (2002).

108. Levine, H. *et al.* Temporal trends in sperm count: A systematic review and meta-regression analysis. *Hum. Reprod. Update* **23**, 646–659 (2017).

109. Rehman, S. *et al.* Endocrine disrupting chemicals and impact on male reproductive health. *Translational Andrology and Urology* vol. 7 490–503 (2018).

110. vom Saal, F. S., Parmigiani, S., Palanza, P. L., Everett, L. G. & Ragaini, R. The plastic world: Sources, amounts, ecological impacts and effects on development, reproduction, brain and behavior in aquatic and terrestrial animals and humans. *Environmental Research* vol. 108 127–130 (2008).

111. Gore, A. C. *et al.* EDC-2: The Endocrine Society's Second Scientific Statement on Endocrine-Disrupting Chemicals. *Endocrine Reviews* vol. 36 1–150 (2015).

112. Rissman, E. F. & Adli, M. Minireview: Transgenerational epigenetic inheritance: Focus on endocrine disrupting compounds. *Endocrinology* vol. 155 2770–2780 (2014).

113. Diamanti-Kandarakis, E. *et al.* Endocrine-disrupting chemicals: An Endocrine Society scientific statement. *Endocrine Reviews* vol. 30 293–342 (2009).

114. Meyer, J. N. *et al.* Mitochondria as a target of environmental toxicants. *Toxicological Sciences* vol. 134 1–17 (2013).

115. Nadal, A., Quesada, I., Tudurí, E., Nogueiras, R. & Alonso-Magdalena, P. Endocrine-disrupting chemicals and the regulation of energy balance. *Nature Reviews Endocrinology* vol. 13 536–546 (2017).

Chapter II

Phosphatidylinositol-4,5-Bisphosphate is an Endogenous Activator of the Mitochondrial Calcium Uniporter

Liliya Gabelev Khasin[1], Monika Haoui[2], Alexis Traynor-Kaplan[3] and Polina V. Lishko[1,2*]

[1]Department of Molecular and Cell Biology, University of California, Berkeley, CA 94720

[2]Graduate Group in Endocrinology, University of California, Berkeley, CA 94720

[3]ATK Innovation, Analytics and Discovery, North Bend, WA 98045, USA

5. Abstract

Phosphatidylinositol-4,5-bisphosphate (PIP2) is a major lipid signaling molecule known to regulate various ion transporters and ion channels in the plasma membrane. However, no comprehensive studies have been performed to test the presence and physiological significance of PIP2 in mitochondrial physiology, particularly whether it can affect the function of mitochondrial ion channels. The principal calcium channel of the inner mitochondrial membrane (IMM) is the mitochondrial calcium uniporter (MCU), an essential component of mitochondrial calcium uptake with few known endogenous regulators. Here, by combining mass spectrometry analysis and mitochondrial electrophysiology, we show that PIP2 is abundant in mitochondrial membranes and it potentiates MCU calcium current. Specifically, application of 20 μM of PIP2 water-soluble analog, phosphatidylinositol-4, 5- dioctanoyl bisphosphate, to the matrix face of the inner mitochondrial membrane was found to cause an increase in the amplitude of the MCU calcium currents recorded from murine kidney, liver, and COS7 mitochondria. Moreover, we found that an application of the PIP2 binding protein that scavenges PIP2 from the IMM inhibits the MCU current by 30%. Also, PIP2 analog did not induce any calcium currents in MCU-deficient mitochondria, confirming the specificity of PIP2 effect. Thus, PIP2 is emerging as an important component of mitochondrial membranes, which serves as an endogenous regulator of mitochondrial calcium homeostasis.

5.1 Introduction

Mitochondrial Ca2+ uptake is an essential regulator of cellular physiology. It controls the rate of respiration and ATP production, shapes cytosolic Ca2+ signaling, regulates cellular proliferation as well as gene expression and protein folding, and initiates apoptosis upon mitochondrial Ca2+ overload [1–3] . Cytosolic Ca2+ influx into the mitochondrial matrix is carried primarily by the mitochondrial Ca2+ uniporter (MCU) [4–6]. MCU is a Ca2+- selective ion channel that resides in the inner mitochondrial membrane (IMM) [7] and is part of a macromolecular complex known as the MCU complex. The latter includes the channel-forming subunit MCU and its auxiliary regulatory subunits MICU1, MICU2, MCUb, EMRE, and MCUR1[8–13]. Besides the aforementioned auxiliary subunits, MCU activity is also controlled by a transcriptional and post-

transcriptional modification that affects protein expression. Also, nucleotides and anions regulate MCU by generating a stronger driving force for calcium uptake. In addition, there are two endogenous, post-translational regulators of mitochondrial calcium uptake; mitochondrial reactive oxygen species (ROS) and Calmodulin kinase II [14,15] . These regulators oxidize and phosphorylate residues on MCU, respectively. Here we show that the bioactive phospholipid-phosphatidylinositol 4,5-bisphosphate (PIP2) is yet another endogenous regulator of MCU.

PIP2 is an anionic lipid found in the inner leaflet of the plasma membrane [16] . Although the majority of cellular PIP2 is situated in the plasma membrane, pools of PIP2 are also found in organellar membranes, and previous studies have shown PIP2 as a component of the mitochondrial outer membrane [17]. PIP2 is a direct regulator of various plasma membrane ion channels and transporters, such as voltage-gated K+ and Ca2+ channels, specific TRP channels, Na+-Ca2+ exchanger, Ca2+ ATPase and more [18–22]. PIP2 is a versatile regulator; for some ion channels, it serves as a positive regulator, whereas for others, it inhibits the ion channel's activity. Phosphoinositides appear to play a similar regulatory role in organellar membranes. One example is the lysosomal TRPML1 channel, which is negatively regulated by PI(4,5)P2 [23]. Whether mitochondrial PIP2 can also control mitochondrial ion channels, particularly the MCU, was unknown.

Here, by applying the patch-clamp technique to mitochondrial inner membranes vesicles, known as mitoplasts, isolated from murine kidney, liver, heart, and COS7 cells, we showed that PIP2 potentiates calcium influx through the MCU. Moreover, our mass spectrometry analysis detected large concentrations of PIP2 present in the mitochondrial membranes. These results revealed that PIP2 is an important component of the mitochondrial membranes and serves as an endogenous activator of calcium uptake by MCU.

5.2 Results

Mitochondrial PIP2 concentrations are comparable to the levels of PIP2 in the plasma membrane. To reveal the presence of PIP2 in the mitochondrial membranes, we isolated lipids from purified murine kidney and liver mitochondria, followed by PIP2 detection by electrospray ionization mass spectrometry. These experiments resulted in the detection of thirteen different molecular species of PIP2 and nine different molecular species of Cardiolipin (CL) in nanogram quantities as calculated using standard curves (Figure 1A-B, supplemental figures 1 and 2). The detection of CL is an essential step in this procedure, as it serves as a hallmark of mitochondrial lipid content [24–28] and is used for normalization purposes. It was previously reported that 1 µg of heart mitochondria contains ~ 72 ng of CL [29] . Therefore, we used this number as a proxy for the mitochondrial content in our samples.

To account for any loss of lipids during multiple steps of sample preparation, we spiked the samples with internal standards of PIP2 and CL before lipid extraction. The average amount of CL per kidney sample detected by mass spectrometry was 1,337,496 ng, while the average amount of CL per liver sample was 138,146 ng. Therefore, based on the aforementioned ratio of 1 µg mitochondria: 72 ng of CL, the kidney sample contained ~ 18,576 µg of mitochondria, while the liver samples contained 1,919 µg of mitochondria. Since CL makes up 14-20 % of all phospholipids in the mitochondrial membrane [30], it means that 1 µg of mitochondria holds ~ 360 ng of phospholipids. Therefore, on average, mitochondria isolated from the kidney contained 6,687,480 ng of phospholipids. The liver mitochondria had, on average, 690,728 ng of phospholipids. Since the amount of phospholipids per µg of mitochondria is known, and we have

calculated the amount of mitochondria, PIP2, and CL per sample, we could determine the ratio between PIP2 and mitochondrial phospholipids. As the detected amount of PIP2 in the kidney was 74,970 ng, PIP2 comprises 1.12% of all mitochondrial phospholipids and therefore is present in a 1:100 ratio. In the liver, the detected amount of PIP2 was 6,619 ng, which constitutes 0.96 % of all mitochondrial phospholipids, resulting in a similar 1:100 ratio. Overall, these results indicate that not only is PIP2 present in liver and kidney mitochondria, but its concentration in these organelles is comparable to the levels of PIP2 found in the plasma membrane [30].

PIP2 regulates MCU Ca2+ uptake. PIP2 is known to regulate a wide variety of ion channels and transporters. Also, previous studies implicated the involvement of PIP2 in the regulation of mitochondrial calcium uptake [17,31]. Since mitochondrial calcium dynamics is mainly governed by the mitochondrial calcium uniporter (MCU), we have tested whether PIP2 can influence MCU function. Since the endogenous PIP2 molecules are composed of long- stearoyl/archidonyl side chains, it makes the molecule extremely hydrophobic and, therefore, unsuitable for dissolution in aqueous solutions required for electrophysiological experiments. Therefore, to explore the effect of PIP2 on MCU, we have used a soluble analog dioctanoyl glycerol- PIP2 (diC8- PIP2), which is commonly used for such purposes [32] and could be easily applied and washed out . To record calcium currents carried by the MCU, we utilized a state-of-the-art mitochondrial patch-clamp technique [33]. It allows a direct recording of MCU activity from isolated mitochondrial inner membranes (IMM), also known as mitoplasts. Application of 20 μM diC8- PIP2 to the matrix face of the mitoplasts significantly increased the amplitude of the MCU current. Calcium current potentiation was observed in the mitochondria obtained from the COS7 cells and mitochondria isolated from murine kidneys and livers (Figure 2A-D, G-H). However, the diC8- PIP2 did not affect MCU activity in heart mitochondria (Figure 2E-F). MCU currents were elicited using voltage ramp protocol from −160 mV to +80mV with the holding potential of 0 mV. MCU currents were measured at -160mV, and MCU current densities were calculated by normalizing the former currents on the corresponding capacitance of the mitoplast, as shown in supplemental table 1. These results confirmed that the PIP2 analog could effectively potentiate MCU currents recorded from the liver, kidney, and COS7 mitoplasts.

PIP2 binding protein inhibits calcium uptake by the MCU. To further evaluate the effect of PIP2 on MCU activity, we applied PIP2 binding protein (PBP10) to the bath solution, which mimics the intermembrane surface of the mitoplasts. PBP10 is a small hydrophobic peptide derived from the gelsolin PIP2-binding site, which can easily cross membranes and sequester endogenous PIP2 [34]. Application of 20 μM PBP10 inhibited the calcium uptake by the MCU in COS7 mitoplasts as well as by murine liver and kidney mitoplasts (Figure 3A-F). After a washout period, the MCU current was fully restored. MCU's current densities were measured as described above at −160 mV and are shown in supplemental table 2. This data confirms that PIP2 sequestering from the mitoplast membrane can diminish MCU currents; therefore, PIP2 is present in the inner mitochondrial membrane and is required for the full extent of MCU activity.

PIP2 effect is specific to MCU. In order to exclude any non-MCU contribution to the observed calcium uptake upon addition of PIP2 in the recording pipette, MCU calcium currents were recorded from both wild type and MCU knock-out (KO) murine mitochondria (Figure 4A-B). MCU's current densities elicited with diC8- PIP2 added to the matrix side of the mitoplasts were

compared. Genetic deletion of MCU results in a complete loss of Ca2+ uptake carried out by the uniporter. Thus, diC8- PIP2 should not affect the calcium uptake unless another mechanism is involved. As expected, the application of 20 μM diC8- PIP2 did not trigger any calcium uptake in MCU-KO mitoplasts isolated from kidney mitochondria. Therefore, we have concluded that mitochondrial PIP2 regulates calcium uptake, specifically via the MCU mechanism.

5.3 Discussion

The physiological importance of the plasma membrane pool of PIP2 is well documented. There it participates in a plethora of physiological functions such as cytoskeleton dynamics, endocytosis, and the regulation of ion channels and transporters [35,36]. Over the last decade, it became increasingly clear that PIP2 is also found in the membranes of intracellular organelles, such as mitochondria. Specifically, PIP2 presence and physiological importance in mitochondrial function is supported by (a) mitochondrial localization of phospholipase C (PLC-δ1), an enzyme specifically hydrolyzes PIP2 [31]; (b) detection of phosphoinositides-modifying enzymes such as kinases and phosphatases in the mitochondrial matrix [37]; (c) detection of PIP2 in the mitochondrial membranes using immunogold labeling [17]; (d) PIP2 presence in mitochondria as confirmed by the electron microscopy studies using a specific PIP2 probe PLCδ-PH [17,38] ; (e) finally, PIP2 elimination by either phosphatases or its masking with PIP2 binding (PH) domains leads to mitochondrial degradation [39]. It has been proposed that mitochondrial PIP2 is required for mitochondrial integrity [39] and plays a regulatory role in maintaining calcium homeostasis [31]. However, the molecular nature of the PIP2- dependent calcium regulation has not been determined.

Mitochondrial calcium uptake is essential for the cellular and mitochondrial function. The cellular energetic demands are tightly coupled to mitochondrial Ca2+ levels [40]. Ca2+ in the mitochondrial matrix is a 'multisite' activator; it directly influences oxidative phosphorylation by activating key enzymes of the Krebs Cycle, the electron transport chain [4,41,42], and the F_1–F_O ATP synthase [43,44]. Also, mitochondrial Ca2+ uptake functions as a cytosolic Ca2+ buffer by removing calcium excess from the cytoplasm and, hence, shaping the spatiotemporal calcium signals within the cell[45]. Excessive mitochondrial Ca2+ uptake can lead to destructive processes within the cell and initiate programmed cellular death [46].

Mitochondrial calcium uptake is primarily controlled by the mitochondrial calcium uniporter (MCU). To date, few endogenous MCU regulators have been identified, including Ca2+, mitochondrial reactive oxygen species (ROS), Calmodulin kinase II and nucleotides [14,15]. Since mitochondrial calcium uptake is regulated by the MCU and has been shown to depend on PIP2, we explored whether PIP2 can influence MCU activity.

Using a targeted lipid mass spectrometry analysis, we were able to detect thirteen PIP2 species in the mitochondrial membranes isolated from murine kidney and liver tissues (Supplemental figure 2). This finding supports the previous reports on the physiological presence of PIP2 in the mitochondria [17,31]. Additionally, the direct measurements of MCU currents using the mitochondria patch-clamp method showed that PIP2 analog potentiates calcium currents specifically via the MCU mechanism. The potentiation was observed in mitochondria obtained from COS7 cells, as well as from mitochondria isolated from murine kidney and liver. However, the PIP2 analog had no effect on MCU activity in murine heart mitochondria. This is most likely due to tissue-specific expression of the Ca2+-sensing regulator MICU1. MICU1 plays a dual role in MCU regulation: at low calcium concentrations, MICU1 acts as the gatekeeper, whereas at

high calcium, it increases calcium uptake [47]. It had been previously reported that heart mitochondria have a low expression of MICU1 compared to liver and kidney mitochondria [47,48]. The low expression of MICU1 in cardiac mitochondria may lead to a reduced capacity to uptake calcium in the presence or absence of PIP2.

The removal of PIP2 with PIP2 binding protein 10 (PBP10), led to a decrease in calcium current amplitude. This suggested that PIP2 interacts with the MCU channel. The recovery of current requires unmasking of the PIP2 or a de-novo synthesis of PIP2. Interestingly, previous studies indicate that the functional enzymes involved in PIP2 synthesis are indeed present in mitochondria [49]. We further confirmed that the observed effect is specific to MCU by utilizing MCU knock-out mice. Genetic ablation of MCU completely prevents Ca2+ uptake by somatic mitochondria [50]. The results of this study show that PIP2 is present in the mitochondrial membrane, where it regulates calcium uptake via enhancing the function of the mitochondrial calcium uniporter. These data broaden our understanding of the function of phosphoinositides in the intracellular organelles and their function as regulators of intracellular calcium signaling.

5.4 Methods

Isolation of mitochondria and mitoplasts for electrophysiology. Mitoplasts were prepared as previously described [33] from the COS7 cell line as well as the following murine tissues: kidney, liver, and heart. Briefly, for tissue isolation, wild-type BL6 mice were sacrificed by CO2 asphyxiation followed by cervical dislocation. The selected mouse tissue was isolated, rinsed, and homogenized in ice-cold medium containing 250 mM sucrose, 5 mM HEPES, and 1 mM EGTA (pH adjusted to 7.2 with 1M KOH), using six slow strokes of Teflon pestle rotating at 280 rotations per minute. The homogenate was then centrifuged at 700 g for 10 min to pellet nuclei and cellular debris. The supernatant was subsequently centrifuged at 8,500 g for 10 min to collect mitochondria. The mitochondrial pellet was resuspended and incubated for 15 min in a solution containing 140 mM sucrose, 440 mM D-mannitol, 5 mM HEPES, and 1 mM EGTA (pH adjusted to 7.2 with 1M KOH). At the end of the incubation, mitochondria were subjected to a French press at 2,000 psi to rupture the outer membrane and produce mitoplasts. The mitoplasts were then pelleted at 10,500 g for 10 min. The supernatant was discarded, and the mitoplast pellet was resuspended in a solution containing 750 mM KCl, 100 mM HEPES, and 1 mM EGTA (pH adjusted to 7.3 with 1M KOH). All mitochondria handling was done at 0–4 °C and stored on ice for 3-5 hours. Immediately before mitochondrial patch-clamp, 15–50 µL of the mitoplast suspension was added to 500 µL solution containing 150 mM KCl, 10 mM HEPES, and 1 mM EGTA (pH adjusted to 7.0 with 1M KOH) and plated on 5 mm coverslips pretreated with 0.1% gelatin to reduce mitoplast adhesion.

Patch-clamp recording. Mitoplasts used for patch-clamp experiments typically had membrane capacitances of 0.3–1 pF. Giga-ohm seals were formed in the bath solution containing 150 mM KCl, 10 mM HEPES, and 1 mM EGTA, pH 7 (adjusted with Trizma® base). A 3M KCl agar salt bridge was used as the bath reference electrode. Voltage steps of 300–550 mV and 5-15 ms were applied to obtain the whole-mitoplast configuration, as monitored by the appearance of capacitance transients. The access resistance and membrane capacitance of mitoplasts were determined with the Membrane Test tool of pClamp 10 (Molecular Devices). Mitoplasts were stimulated every 5s. Pipettes were filled with 110 mM Na-gluconate, 40 mM HEPES, 1.5 mM EGTA, and 2 mM NaCl (pH adjusted to 7.0 with NaOH, tonicity adjusted to ~330 mmol/kg with

sucrose). Typically, pipettes had resistances of 25–50 MΩ, and the access resistance was 40–100 MΩ. Whole-mitoplast MCU current was recorded in the bath solution containing 150 mM HEPES and 80 mM Sucrose,0.5 mM CaCl2 (pH adjusted to 7.0 with Trizma® base, tonicity adjusted to ~300 mmol/kg with sucrose). Current amplitudes for histograms were measured within 5 ms after stepping the membrane from 0 to −160 mV. All experiments were performed under continuous perfusion of the bath solution.

Whole-mitoplast control currents were recorded in a bath solution (HEPES/Tris solution) containing 150 mM HEPES and 1 mM EGTA (pH adjusted to 7.0 with Tris-base, tonicity adjusted to ~300 mmol/kg with sucrose). To record whole-mitoplast MCU Ca2+ currents, a bath solution containing 0.5 mM CaCl2 in a HEPES/Tris solution was used. To analyze the effect of PI(4,5)P2 on MCU Ca2+ currents, PIP2 was added to the pipette solution at a final concentration of 20 μM. DiC8-PIP2 (Echelon Biosciences) was solubilized in water as a 2.5 mM stock, frozen at −80°C, and used the same day it was diluted from the stock. To show current inhibition caused by PI(4,5)P2 depletion, PIP2 binding protein (PBP) was added to the bath solution at a final concentration of 20 μM.

To ensure that the observed effect of PIP2 is indeed on MCU, mitoplasts were isolated from mice deficient for MCU protein. Currents were recorded as above in the presence and absence of diC8- PIP2.

Mitochondria extraction and isolation for mass spectrometry experiments. Mitochondria were extracted from murine kidney and liver tissue. Isolation of pure mitochondria was done with anti-TOM22 Microbeads (MACS Miltenyi Biotec), as described in [51] with a few modifications. After the tissue was dissected out, it was rinsed and homogenized in an ice-cold medium containing 250 mM sucrose, 10 mM HEPES, and 1 mM EGTA (pH adjusted to 7.2 with Trizma® base), using six slow strokes of Teflon pestle rotating at 280 revolutions per minute. The homogenate was then centrifuged at 700 g for 10 min to pellet nuclei and cellular debris. The supernatant was collected and pelleted at 8,500 g for 10. The pellet was then resuspended in 1 mL of lysis buffer provided in the kit + 9 mL of 1X ice-cold separation buffer. 50 μL of anti-TOM22 Microbeads were added to the suspension to magnetically label mitochondria. The monoclonal Anti-TOM22 antibody specifically binds to the translocase of outer mitochondrial membrane 22 (TOM22) of mouse mitochondria. After 60 minutes of incubation at 4 °C, the labeled mitochondria were loaded onto a MACS Column, which was placed in the magnetic field of a MACS Separator. The magnetically labeled mitochondria were retained within the column. The column was then washed three times to wash out the unlabeled organelles and cell components. Then, the column was removed from the magnetic field, and the magnetically retained mitochondria were eluted. Immediately after elution, we proceeded with lipid extraction for mass spectrometry.

Lipid extraction. The mitochondrial pellet was resuspended in PBS and transferred to a glass tube. Subsequently, the tube was centrifuged at 8500 g. The supernatant was discarded, and the pellet was resuspended in 0.5 M TCA. The suspension was then transferred into 2 mL polypropylene tubes (ultra-hydrophobic DNA Lo-Bind, Eppendorf), vortexed 30 seconds, and incubated on ice for 10 min. The TCA-treated sample was then centrifuged at 20.000 x g for 3 min at 4 ° C. The supernatant was carefully removed without disturbing the pellet and 1 mL of 5% (w/v) TCA with 10 mM EDTA were added to the pellet, vortexed for 30 seconds and, centrifuged at 20.000 x g for 3 min at 4℃. The supernatant was removed, and internal lipid

standards were added to the pellet as follows: 50 ng of cardiolipin and 20ng of PIP2. Subsequently 670 µL of ice-cold chloroform: methanol:12.1 M HCl, 80/40/1, v/v/v was added, and the sample was vigorously vortexed for 2-5 min. The sample was then incubated on ice for 10 min. Next, 650 µL of ice-cold chloroform was added to the tube and vortexed for an additional 5 min. 300 µL of 1 M HCl was added to the suspension. The suspension was vortexed for 2 min, and centrifuged at 10,000 x g for 5 min at 4 degrees C. The lower phase was then collected into a 2 mL fresh tube and 990 µL of the lower phase was added to the remaining upper phase and then vortexed again for 2 min, and centrifuged at 10,000 x g for 5 min at 4℃. The lower phase was collected and combined with the previously collected lower phase. The combined lower phases were evaporated to dryness under nitrogen gas and stored at -80 °C.

Standard curves were made by spiking TCA precipitates with standardized Cardiolipin Mix I (Avanti):14:1(3)-15:1 CA 15:0(3)-16:1 CA 22:1(3)-14:1 CA 24:1(3)-14:1 CA and PI(4,5)P2 17:0-20:4. Four different concentrations were used for the standard curve generation. Cardiolipin: 10 ng, 50 ng, 300 ng, and 700 ng and PIP2: 10 ng, 20 ng, 50 ng, and 200 ng.

Mass Spectrometry. For the measurement of phosphoinositides, the dried lipid extracts were methylated with trimethylsilyl diazomethane and the methylated phosphoinositide lipid derivatives measured using UPLC/ESI-MS/MS as described previously [52]. For quantitative analyses, the effluent was monitored by a Waters XEVO TQ-S MS/MS using multiple reaction monitoring (MRM) and positive ion mode. For cardiolipin analysis, an aliquot of the methylated extracts resuspended in methanol was injected over a Waters Acquity UPLC BEH C8 column (1.7 µm, 2.1x 50 mm). The mobile phase consisted of a 27.3 min gradient initiated with 10 mM formic acid in water (A)/ 10 mM formic acid in acetonitrile/methanol/isopropanol (55/30/15) (B); A/B (33/67) delivered at a flow rate of 0.3 ml/min by a Waters Acquity I-Class UPLC. Initial conditions were held for 2 min, then increased to 90% B at 3 min, where it was held for the next 11 min at which time it was increased to 100% B and held for an additional 10 min prior to equilibration to starting conditions where it was maintained for another 3 min prior to the end of the run. The effluent was monitored by a Waters XEVO TQ-S MS/MS in multiple reactions.

Quantitation of the different molecular species of CL and PIP2. The nanomole amounts of a single molecular species of PIP2 and CL were calculated by first determining the ratio of the peak area of the selected molecular species to the internal standard. Then, the slope and intercept of the standard curve were determined. By using the formula $y = mx + b$, where y is the ratio, b is the intercept, m is the slope, and x is the nanomoles of the molecular species.

Genotyping. All MCU mice were genotyped using a PCR assay on-ear DNA with the forward primer: GT F2 - 5'-GGAGTTAAGTCATGAGCTGCTAT-3' and reverse primers: GT R2 - 5' - CTGGCTTAGTTGGCAGAGTTC -3', V76R - 5' - CCAATAAACCCTCTTGCAGTTGC -3'. The PCR conditions were as previously reported [53]. PCR products were analyzed on 1% agarose gel run at 100 V for 60 min with Tris-acetate -EDTA running buffer with 1X GelRedTM Nucleic Acid Gel Stain (Biotium, Fremont, CA, USA)

Statistical analyses. For statistical analyses used in the manuscript the Clampfit 10.3 (Molecular Devices, Sunnyvale, CA, USA), OriginPro 8.6 (OriginLab Corp., Northampton, MA, USA) and GraphPad Prism 5 software (GraphPad Software, Inc., La Jolla, CA) were used. Unpaired t-test was used to determine current potentiation by PIP2, statistical significance for $p \leq 0.05$ as the

limit. Paired t-test was used for determining current inhibition by PBP10. All results are shown with the standard error of the mean. The significance of changes is indicated as follows: * $p \leq 0.05$, ** $p \leq 0.01$, *** $p \leq 0.001$

Authors' contributions. LGK and PVL conceived the project, designed the experiments, and wrote the manuscript. LGK performed all studies, data acquisition, and analysis for the manuscript. MH assisted with lipid extraction for mass spectrometry studies. ATK conducted the mass spectrometry. All authors discussed the results and commented on the manuscript.

Declaration of Interests. *The authors declare that the research was conducted in the absence of any commercial or financial relationships that could be construed as a potential conflict of interest*.

5.5 Figures

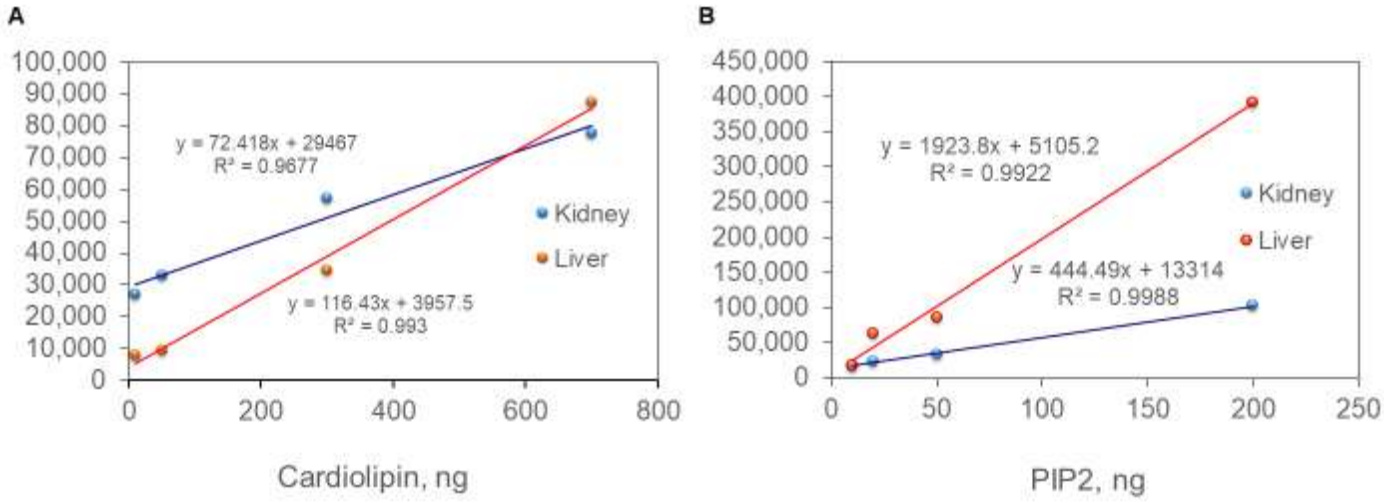

Figure 1. Standard curves. **A**. Standard curve for CL generated with standardized CL mix. Four different internal standards (IS) concentrations were used for the generation of the standard curve: 10 ng, 50 ng, 300 ng and 700 ng. **B.** Standard curve for PIP2 with synthetic PIP2 as IS. Standardized PIP2 was added at four different concentrations 10 ng, 20 ng, 30 ng and 50 ng, and subsequently extracted and analyzed by MS.

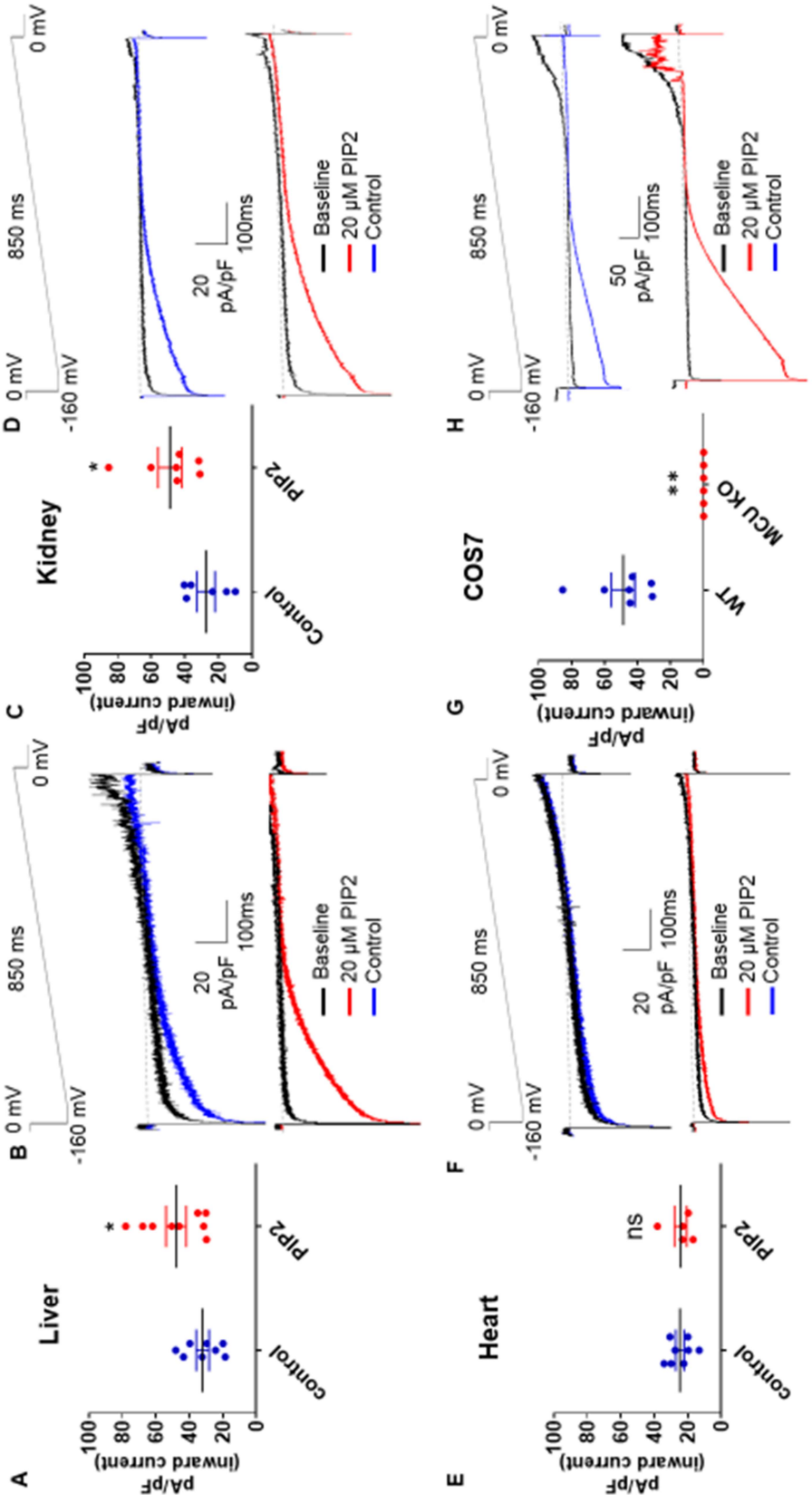
A
Liver
pA/pF (inward current)
control
PIP2
*
B
0 mV
-160 mV
850 ms
0 mV
20 pA/pF
100ms
Baseline
20 μM PIP2
Control
C
Kidney
pA/pF (inward current)
Control
PIP2
*
D
0 mV
-160 mV
850 ms
0 mV
20 pA/pF
100ms
Baseline
20 μM PIP2
Control
E
Heart
pA/pF (inward current)
control
PIP2
ns
F
0 mV
-160 mV
850 ms
0 mV
20 pA/pF
100ms
Baseline
20 μM PIP2
Control
G
COS7
pA/pF (inward current)
WT
MCU KO
**
H
0 mV
-160 mV
850 ms
0 mV
50 pA/pF
100ms
Baseline
20 μM PIP2
Control

Figure 2. PIP2 potentiates MCU Ca2+ uptake. Whole-mitoplast current recorded without (blue traces) and with (red traces) 20 μM PIP2 in the pipette solution. Currents were elicited by a voltage-ramp protocol (shown above) Whole-mitoplast MCU current was normalized to the membrane capacitance (Cm) in all tested mitoplasts. A. The measured inward calcium current density via the MCU in mitoplasts extracted from murine liver. B Representative calcium traces in liver mitoplasts in the absence of PIP2 (control- blue) and in the in the presence of 20 μM PIP2 in the pipette solution. C. The measured inward calcium current in mitoplasts extracted from murine kidney. D. Representative calcium traces in kidney mitoplasts. Control currents in blue, measure current in the presence of 20 μM PIP2, in red. E. The measured inward calcium current in mitoplasts extracted from murine heart. F. Representative calcium traces in heart mitoplasts. Control currents in blue, PIP2 currents, in red. G. The measured inward calcium current in mitoplasts extracted from COS7 cells. H. Representative calcium traces in COS7 mitoplasts. Control currents in blue, PIP2 currents, in red. Data are means +/− S.E.M. Asterisk indicates a statistical difference between control currents and calcium currents in the presence of PIP2. * ($P<0.05$), *** ($P<0.01$)

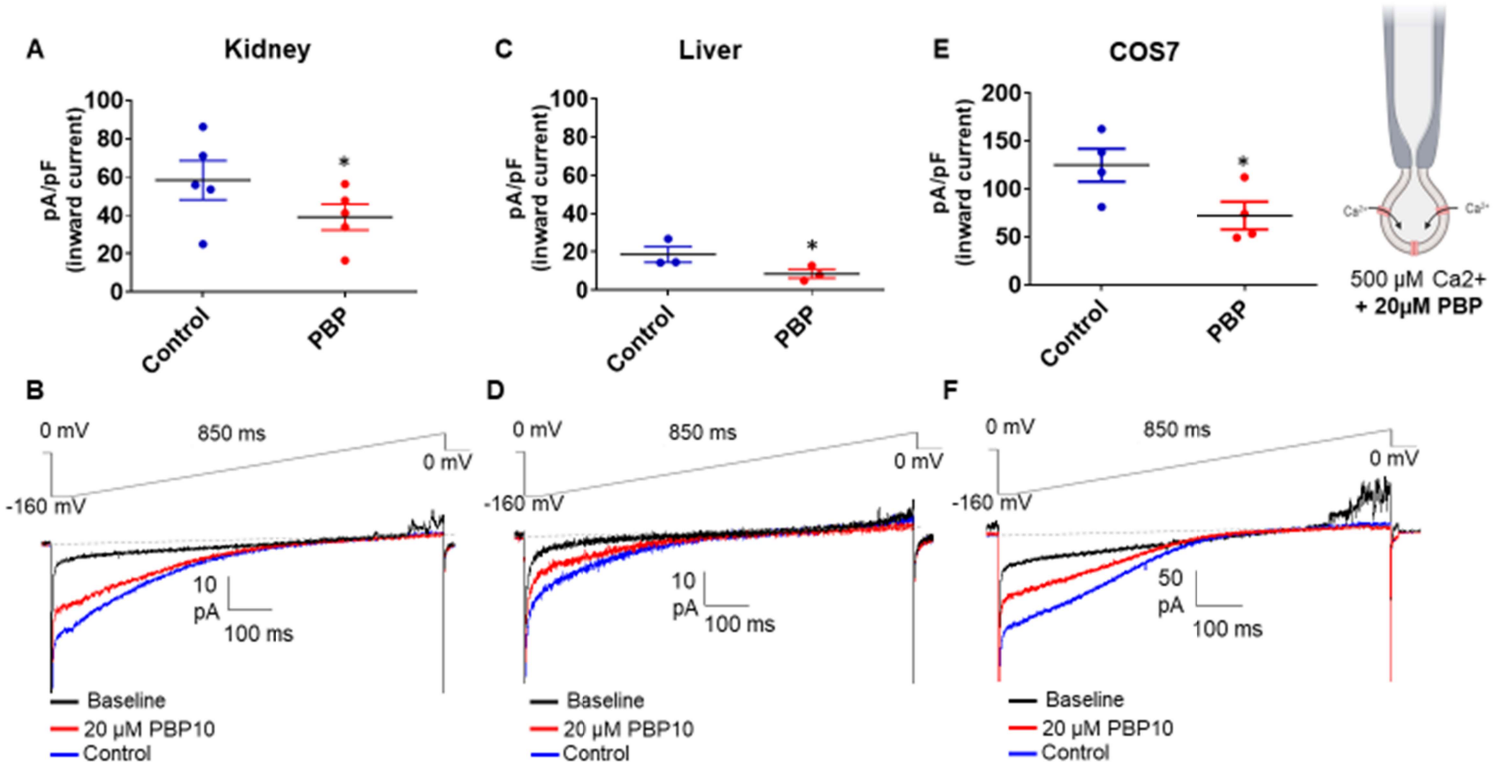
A
Kidney
pA/pF (inward current)
100
80
60
40
20
0
Control
PBP
*
C
Liver
pA/pF (inward current)
100
80
60
40
20
0
Control
PBP
*
E
COS7
pA/pF (inward current)
200
150
100
50
0
Control
PBP
*
500 µM Ca2+
+ 20µM PBP
B
0 mV
850 ms
0 mV
-160 mV
10
pA
100 ms
Baseline
20 µM PBP10
Control
D
0 mV
850 ms
0 mV
-160 mV
10
pA
100 ms
Baseline
20 µM PBP10
Control
F
0 mV
850 ms
0 mV
-160 mV
50
pA
100 ms
Baseline
20 µM PBP10
Control

Figure 3. PIP2 binding protein inhibits calcium uptake by the MCU. Whole-mitoplast current recorded without (blue traces) and with (red traces) 20 μM PBP in the bath solution. Baseline current recorded in calcium free bath solution (HT), in black. Currents were elicited by a voltage-ramp protocol (shown above) Whole-mitoplast MCU current was normalized to the membrane capacitance (Cm) in all tested mitoplasts. **A**. The measured inward calcium current density via the MCU in mitoplasts extracted from murine kidney in the absence and presence of PBP. **B** Representative calcium traces in kidney mitoplasts in the absence of PBP (control- blue) and in the in the presence of 20 μM PIP2 in the bath solution. **C**. The measured inward calcium current in mitoplasts extracted from murine liver. **D**. Representative calcium traces in liver mitoplasts. **E**. The measured inward calcium current in mitoplasts extracted from COS7 cells. **F**. Representative calcium traces in COS7 mitoplasts. Data are means +/− S.E.M. Asterisk indicates a statistical difference between control currents and calcium currents in the presence of PIP2. * ($P<0.05$). Picture in inset, glass pipette attached to a mitoplast in a bath solution containing 20 μM PBP

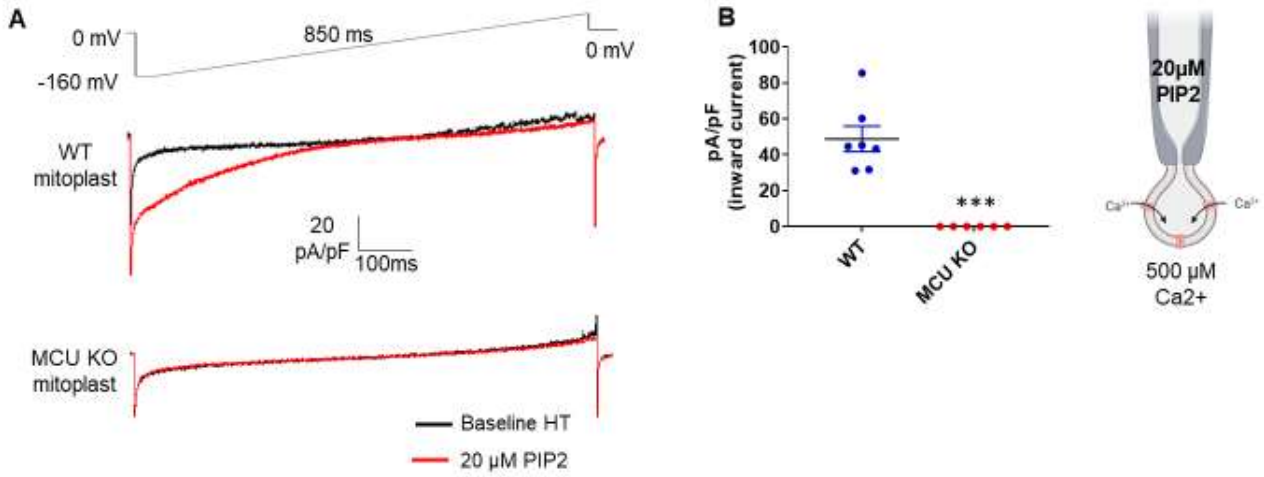

Figure 4. PIP2 effect is specific to MCU. **A.** Representative traces of whole-mitoplast currents recorded from wild type and MCU KO mitoplasts in the presence of 20 µM PIP2 in the pipette solution. Baseline current recorded in calcium free bath solution (HT) in black. No calcium uptake in MCU-KO mitoplasts was detected. **B.** The measured inward calcium current density, in the presence of 20 µM PIP2 in the pipette solution, as measured from mitoplasts extracted from wild-type and MCU-KO murine kidney. Picture in inset, glass pipette filled with 20 µM PIP2 inside solution, attached to a mitoplast in a bath solution containing 500 µM calcium.

	Liver	Kidney	Heart	Cos7
Control (pA/pF)	32.05±3.87, n=8	27.42±5.33, n=6	24.7±2.48, n=8	137.5±12.6, n=4
20 µM PIP2 (pA/pF)	47.89±5.9, n=9	48.8±7.14, n=7	24.24±3.68, n=5	258±2.6, n=4

Supplementary table 1. PIP2 analog potentiates MCU currents. MCU currents in the presence and absence of 20 µM PIP2 analog in the pipette solution as measured at -160 mV. MCU current densities were calculated by normalizing the measured currents to the corresponding capacitance of the mitoplast

	Liver	Kidney	Cos7
Control (pA/pF)	18.6±4.09 , n=3	58.3±10.2, n=5	124.7±17.24, n=4
20 µM PBP10 (pA/pF)	8.56 ±2.29, n=3	39.1 ±6.7 , n=7	71.98±14.43, n=4

Supplementary table 2. PBP10 analog inhibits MCU currents. MCU currents in the presence and absence of 20 µM PBP10 in the bath solution as measured at -160 mV. MCU current densities were calculated by normalizing the measured currents to the corresponding capacitance of the mitoplast

Supplemental Figure 1

Nanograms of cardiolipin species based on the standard curve									
	62:0	66:0	66:1	68:1	70:4	72:0	72:3	72:4	72:6
Liver									
1	193.2581	137.755	2815.209	29226.45	7814.323	28177.2	5463.697	31511.0396	5417.636405
2	212.2093	145.3365	3026.642	26509.74	9430.921	32622.69	5371.842	34344.4687	5342.670321
3	192.8507	57.26076	1080.742	22445.04	3738.486	132987.4	12022.57	32575.2407	11895.37473
4	146.6671	248.2673	4637.869	30227.99	9048.674	25898.63	4659.535	28554.0757	4404.253778
Kidney									
1	11325.32	3103.057	53914.75	337391.7	413491.7	198781.9	91245.21	357068.424	104075.9326
2	14538.07	2920.336	47968.28	227785.4	325823.5	172738.3	58625.24	270031.803	92582.04605
3	9694.81	2421.88	39668.38	234238.6	339855.6	143709.4	61405.43	305205.691	82110.87237
4	12324.18	2642.967	51787.72	219454.3	377710.1	190593.7	62635.52	331588.441	99527.35095

Supplemental Figure 2

			Nanograms of PIP2 per species based on the standard curve										
	34:0	34:1	34:2	36:1	36:2	36:3	36:4	38:2	38:3	38:4	38:5	40:4	40:5
Liver													
1	0	5.523707	20.55963	10.54532	78.49841	17.832695	40.11848	22.56359	3794.15	4218.771	556.90469	21.02186	19.40671
2	0	7.269179	18.09838	18.42253	122.2127	14.941095	29.42109	31.1187	5188.607	5627.128	525.90986	33.71899	25.13268
3	0	1.354327	6.584591	4.371198	49.94103	11.650606	21.72185	13.53657	133.35	461.6218	35.508468	4.290319	7.598552
4	0	3.76096	13.93346	6.259246	30.54528	16.4642	37.81406	17.18549	1945.391	2830.231	377.77871	0	8.098671
Kidney													
1	826.4955	463.4421	102.0117	2058.139	3400.844	77.47796	221.8462	1003.613	18802.7	66198.38	3168.8864	224.7903	271.9572
2	927.4436	490.0044	160.4912	1632.878	3295.672	104.57876	298.2432	938.868	20399.89	64703.81	3765.9614	177.5051	381.3252
3	1025.275	796.6091	112.7505	2318.549	3647.66	120.22438	352.91	1130.135	11353.64	36656.6	1933.7663	271.8434	442.9796
4	1275.074	530.7059	149.9697	1922.878	4260.003	107.20446	295.3028	1218.336	8722.357	24805.77	1656.8015	230.0154	444.9651

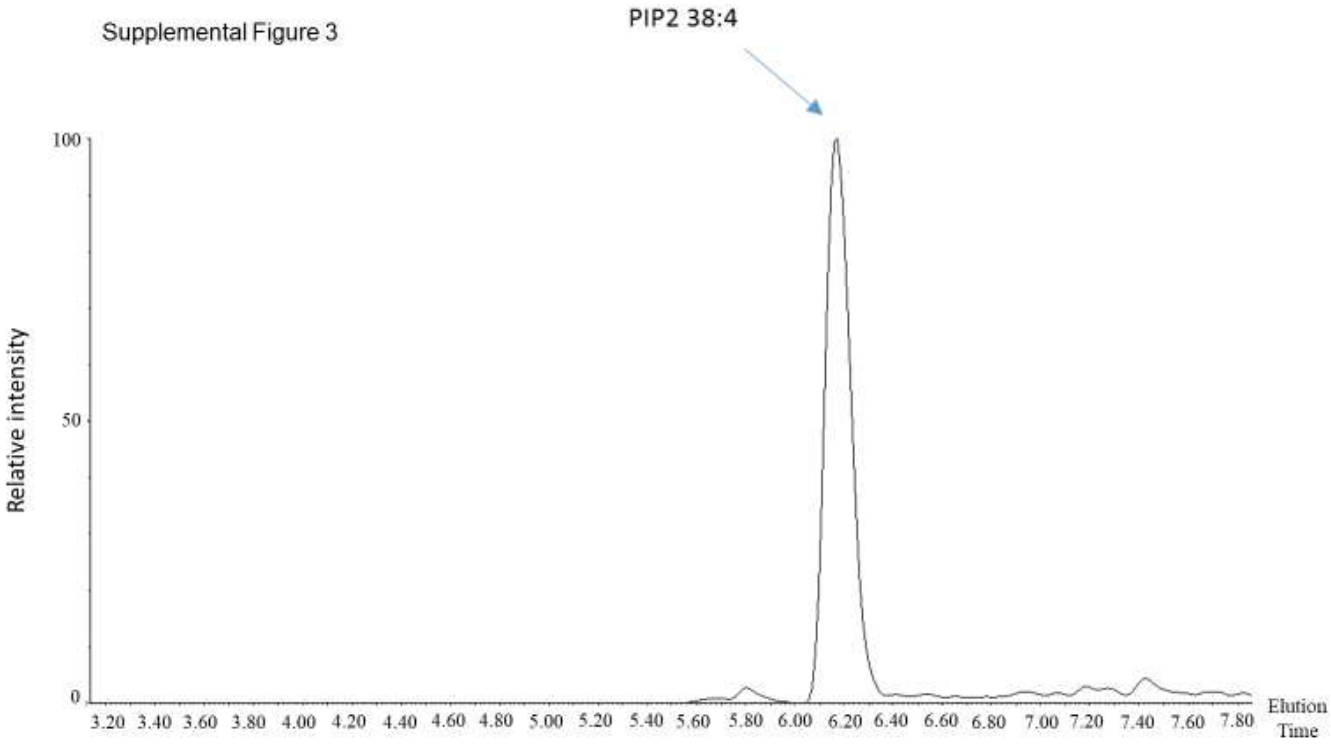

Detection of PIP2 species in mitochondrial membranes. Electrospray ionization mass spectrometry in multiple reaction monitoring mode detected thirteen different species of PIP2. Representative chromatogram of one of the most abundant species of PIP2, 38:4, in the mitochondrial membranes.

5.6 References

1. Duchen, M. R., Verkhratsky, A. & Muallem, S. Mitochondria and calcium in health and disease. *Cell Calcium* vol. 44 1–5 (2008).
2. Giacomello, M., Drago, I., Pizzo, P. & Pozzan, T. Mitochondrial Ca2+ as a key regulator of cell life and death. *Cell Death and Differentiation* vol. 14 1267–1274 (2007).
3. Orrenius, S., Gogvadze, V. & Zhivotovsky, B. Calcium and mitochondria in the regulation of cell death. *Biochemical and Biophysical Research Communications* vol. 460 72–81 (2015).
4. Rizzuto, R., Bernardi, P. & Pozzan, T. Mitochondria as all-round players of the calcium game. *Journal of Physiology* vol. 529 37–47 (2000).
5. Carafoli, E. Intracellular Calcium Homeostasis. *Annu. Rev. Biochem.* **56**, 395–433 (1987).
6. Gunter, T. E. & Pfeiffer, D. R. Mechanisms by which mitochondria transport calcium. *American Journal of Physiology - Cell Physiology* vol. 258 (1990).
7. Mishra, J. *et al.* The mitochondrial Ca2+ uniporter: Structure, function, and pharmacology. in *Handbook of Experimental Pharmacology* vol. 240 129 (Springer New York LLC, 2017).
8. Baughman, J. M. *et al.* Integrative genomics identifies MCU as an essential component of the mitochondrial calcium uniporter. *Nature* **476**, 341–345 (2011).
9. Perocchi, F. *et al.* MICU1 encodes a mitochondrial EF hand protein required for Ca2+ uptake. *Nature* **467**, 291–296 (2010).
10. Mallilankaraman, K. *et al.* MCUR1 is an essential component of mitochondrial Ca2+ uptake that regulates cellular metabolism. *Nat. Cell Biol.* **14**, 1336–1343 (2012).
11. Sancak, Y. *et al.* EMRE is an essential component of the mitochondrial calcium uniporter complex. *Science (80-.).* **342**, 1379–1382 (2013).
12. Plovanich, M. *et al.* MICU2, a Paralog of MICU1, Resides within the Mitochondrial Uniporter Complex to Regulate Calcium Handling. *PLoS One* **8**, (2013).
13. Raffaello, A. *et al.* The mitochondrial calcium uniporter is a multimer that can include a dominant-negative pore-forming subunit. *EMBO J.* **32**, 2362–2376 (2013).
14. Tomar, D. *et al.* Mitochondrial Ca 2 + Uniporter Is a Mitochondrial Luminal Redox Sensor that Augments MCU Channel Article Mitochondrial Ca 2 + Uniporter Is a Mitochondrial Luminal Redox Sensor that Augments MCU Channel Activity. *Mol. Cell* **65**, 1–15 (2017).
15. Joiner, M. L. A. *et al.* CaMKII determines mitochondrial stress responses in heart. *Nature* **491**, 269–273 (2012).
16. McLaughlin, S., Wang, J., Gambhir, A. & Murray, D. PIP2 and proteins: Interactions,

organization, and information flow. *Annual Review of Biophysics and Biomolecular Structure* vol. 31 151–175 (2002).

17. Watt, S. A., Kular, G., Fleming, I. N., Downes, C. P. & Lucocq, J. M. Subcellular localization of phosphatidylinositol 4,5-bisphosphate using the pleckstrin homology domain of phospholipase C δ1. *Biochem. J.* **363**, 657–666 (2002).

18. Kruse, M., Hammond, G. R. V. & Hille, B. Regulation of voltage-gated potassium channels by PI(4,5)P2. *J. Gen. Physiol.* **140**, 189–205 (2012).

19. Wu, L., Bauer, C. S., Zhen, X. guang, Xie, C. & Yang, J. Dual regulation of voltage-gated calcium channels by PtdIns(4, 5)P2. *Nature* **419**, 947–952 (2002).

20. Rohacs, T. Phosphoinositide regulation of TRP channels. *Handb. Exp. Pharmacol.* **223**, 1143–1176 (2014).

21. Yaradanakul, A. *et al.* Dual control of cardiac Na+-Ca2+ exchange by PIP2: Electrophysiological analysis of direct and indirect mechanisms. *J. Physiol.* **582**, 991–1010 (2007).

22. Penniston, J. T. *et al.* Apart from its known function, the plasma membrane Ca2+atpase can regulate Ca2+ signaling by controlling phosphatidylinositol 4,5-bisphosphate levels. *J. Cell Sci.* **127**, 72–84 (2014).

23. Dong, X. P. *et al.* PI(3,5)P2 controls membrane trafficking by direct activation of mucolipin Ca2+ release channels in the endolysosome. *Nat. Commun.* **1**, (2010).

24. Daum, G. & Vance, J. E. Import of lipids into mitochondria. *Progress in Lipid Research* vol. 36 103–130 (1997).

25. Mileykovskaya, E., Zhang, M. & Dowhan, W. Cardiolipin in energy transducing membranes. *Biochem.* **70**, 154–158 (2005).

26. Joshi, A. S., Zhou, J., Gohil, V. M., Chen, S. & Greenberg, M. L. Cellular functions of cardiolipin in yeast. *Biochimica et Biophysica Acta - Molecular Cell Research* vol. 1793 212–218 (2009).

27. Davidson, J. B. & Stanacev, N. Z. Biosynthesis of cardiolipin in mitochondria isolated from guinea pig liver. *Biochem. Biophys. Res. Commun.* **42**, 1191–1199 (1971).

28. Zinser, E. *et al.* Phospholipid synthesis and lipid composition of subcellular membranes in the unicellular eukaryote Saccharomyces cerevisiae. *J. Bacteriol.* **173**, 2026–2034 (1991).

29. Kim, J. & Hoppel, C. L. Comprehensive approach to the quantitative analysis of mitochondrial phospholipids by HPLC-MS. *J. Chromatogr. B Anal. Technol. Biomed. Life Sci.* **912**, 105–114 (2013).

30. Paradies, G., Paradies, V., De Benedictis, V., Ruggiero, F. M. & Petrosillo, G. Functional role of cardiolipin in mitochondrial bioenergetics. *Biochimica et Biophysica Acta - Bioenergetics* vol. 1837 408–417 (2014).

31. Knox, C. D. *et al.* Novel role of phospholipase C-δ1: Regulation of liver mitochondrial Ca2+ uptake. *Am. J. Physiol. - Gastrointest. Liver Physiol.* **287**, (2004).

32. Rodriguez-Menchaca, A. A. *et al.* PIP 2 controls voltage-sensor movement and pore opening of Kv channels through the S4-S5 linker. **109**, 14299 (2012).

33. Kirichok, Y., Krapivinsky, G. & Clapham, D. E. The mitochondrial calcium uniporter is a highly selective ion channel. *Nature* **427**, 360–364 (2004).

34. Liepiņa, I., Czaplewski, C., Janmey, P. & Liwo, A. Molecular dynamics study of a gelsolin-derived peptide binding to a lipid bilayer containing phosphatidylinositol 4,5-bisphosphate. *Biopolym. - Pept. Sci. Sect.* **71**, 49–70 (2003).

35. Balla, T. Phosphoinositides: Tiny lipids with giant impact on cell regulation. *Physiological Reviews* vol. 93 1019–1137 (2013).

36. Di Paolo, G. & De Camilli, P. Phosphoinositides in cell regulation and membrane dynamics. *Nature* vol. 443 651–657 (2006).

37. Schon, E. A. Appendix 5. Gene Products Present in Mitochondria of Yeast and Animal Cells. *Methods in Cell Biology* vol. 80 835–876 (2007).

38. Lemmon, M. A. & Ferguson, K. M. Signal-dependent membrane targeting by pleckstrin homology (PH) domains. *Biochemical Journal* vol. 350 1–18 (2000).

39. Rosivatz, E. & Woscholski, R. Removal or masking of phosphatidylinositol(4,5)bisphosphate from the outer mitochondrial membrane causes mitochondrial fragmentation. *Cell. Signal.* **23**, 478–486 (2011).

40. Lehninger, A. L., Carafoli, E. & Rossi, C. S. Energy-Linked Ion Movements in Mitochondrial Systems. in *Advances in Enzymology and Related Areas of Molecular Biology* vol. 29 259–320 (wiley, 2006).

41. Tarasov, A. I., Griffiths, E. J. & Rutter, G. A. Regulation of ATP production by mitochondrial Ca2+. *Cell Calcium* **52**, 28–35 (2012).

42. Maechler, P. & Wollheim, C. B. Mitochondrial signals in glucose-stimulated insulin secretion in the beta cell. *Journal of Physiology* vol. 529 49–56 (2000).

43. Hubbard, M. J. & McHugh, N. J. Mitochondrial ATP synthase F1-β-subunit is a calcium-binding protein. *FEBS Lett.* **391**, 323–329 (1996).

44. Boerries, M. *et al.* Ca2+-Dependent Interaction of S100A1 with F1-ATPase Leads to an Increased ATP Content in Cardiomyocytes. *Mol. Cell. Biol.* **27**, 4365–4373 (2007).

45. Duchen, M. R. Mitochondria and calcium: From cell signalling to cell death. *Journal of Physiology* vol. 529 57–68 (2000).

46. Ichas, F. & Mazat, J. P. From calcium signaling to cell death: Two conformations for the mitochondrial permeability transition pore. Switching from low- to high-conductance state. *Biochim. Biophys. Acta - Bioenerg.* **1366**, 33–50 (1998).

47. Liu, J. C. *et al.* MICU1 Serves as a Molecular Gatekeeper to Prevent In Vivo Mitochondrial Calcium Overload. *Cell Rep.* **16**, 1561–1573 (2016).

48. Paillard, M. *et al.* Tissue-Specific Mitochondrial Decoding of Cytoplasmic Ca2+ Signals

Is Controlled by the Stoichiometry of MICU1/2 and MCU. *Cell Rep.* **18**, 2291–2300 (2017).

49. Nemoto, Y. & De Camilli, P. Recruitment of an alternatively spliced form of synaptojanin 2 to mitochondria by the interaction with the PDZ domain of a mitochondrial outer membrane protein. *EMBO J.* **18**, 2991–3006 (1999).

50. Pan, X. *et al.* The Physiological Role of Mitochondrial Calcium Revealed by Mice Lacking the Mitochondrial Calcium Uniporter. *Nat. Cell Biol.* **15**, 1464–1472 (2013).

51. Hornig-Do, H. T. *et al.* Isolation of functional pure mitochondria by superparamagnetic microbeads. *Anal. Biochem.* **389**, 1–5 (2009).

52. Traynor-Kaplan, A. *et al.* Fatty-acyl chain profiles of cellular phosphoinositides. *Biochim. Biophys. Acta - Mol. Cell Biol. Lipids* **1862**, 513–522 (2017).

53. Hamilton, J. *et al.* Deletion of mitochondrial calcium uniporter incompletely inhibits calcium uptake and induction of the permeability transition pore in brain mitochondria. *J. Biol. Chem.* **293**, 15652–15663 (2018).

Chapter III

The impact of di-2-ethylhexyl phthalate on sperm fertility

Liliya Gabelev Khasin[1], John Della Rosa[1,2], Natalie Petersen[1], Jacob Moeller[5], Lance J. Kriegsfeld[3,4,5,6], and Polina V. Lishko[1,5*]

[1]Department of Molecular and Cell Biology, University of California, Berkeley, CA 94720
[2]Department of Chemistry, University of California, Berkeley, CA 94720
[3]Department of Psychology, University of California, Berkeley, CA 94720
[4]Department of Integrative Biology, University of California, Berkeley, CA 94720
[5]Graduate Group in Endocrinology, University of California, Berkeley, CA 94720
[6]The Helen Wills Neuroscience Institute, University of California, Berkeley, CA 94720

6. Abstract

A growing number of studies point to reduced fertility upon chronic exposure to endocrine-disrupting chemicals (EDCs) such as phthalates and plasticizers. These toxins are ubiquitous and are often found in food and beverage containers, medical devices, as well as in common household and personal care items. Animal studies with EDCs, such as phthalates and bisphenol A have shown a dose-dependent decrease in fertility and embryo toxicity upon chronic exposure. However, limited research has been conducted on the acute effects of these EDCs on male fertility. Here we used a murine model to test the acute effects of four ubiquitous environmental toxins: bisphenol A (BPA), di-2-ethylhexyl phthalate (DEHP), diethyl phthalate (DEP), and dimethyl phthalate (DMP) on sperm fertilizing ability and pre-implantation embryo development. The most potent of these toxins, di-2-ethylhexyl phthalate (DEHP), was further evaluated for its effect on sperm ion channel activity, capacitation status, acrosome reaction and generation of reactive oxygen species (ROS). DEHP demonstrated a profound hazardous effect on sperm fertility by producing an altered capacitation profile, impairing the acrosome reaction, and interestingly, also increasing ROS production. These results indicate that in addition to its known chronic impact on reproductive potential, DEHP also imposes acute and profound damage to spermatozoa, and thus, represents a significant risk to male fertility.

6.1 Introduction

Phthalates and plasticizers are synthetic chemicals that are utilized to make plastic more flexible. They are known to act as endocrine-disrupting chemicals (EDC) [1,2], which are ubiquitous in food and beverage containers, as well as coatings of pills, medical tubing [3,4] and plastic packaging [5]. Phthalates and plasticizers are bound to plastic polymers by non-covalent bonds, and thus, easily leak into the environment [6]. The main routes of exposure to these substances are ingestion, inhalation, dermal absorption, or intravenous medication administration [4,7]. Consequently, the vast majority of the population is exposed to these toxins on a daily basis.

Low micromolar concentrations of certain EDCs in human urine, sweat and plasma have been associated with an increased rate of miscarriages and compromised male and female fertility [8–17].

In the present study, we evaluated the reproductive outcomes of acute exposure to four omnipresent EDCs - Bisphenol A (BPA), dimethyl phthalate (DMP), diethyl phthalate (DEP) and Di-ethyl hexyl phthalate (DEHP). BPA, a plasticizer manufactured in large volumes for the production of polycarbonate plastics and epoxy resins, is used to line food and beverage storage containers, coat water supply pipes and is also a component of dental fillings. The aforementioned exposure routes lead to detectable levels of BPA in human serum [18], urine [19,20], adipose tissue [21] and breast milk [22]. Numerous studies have shown that chronic exposure to BPA alters fertility in both males and females [23,24].

Phthalates are similarly produced in large volumes and are used as plasticizing agents. Phthalates can be grouped into two broad categories: low-molecular-weight and high-molecular-weight phthalates. The low-molecular-weight phthalates, such as DEP and DMP, are commonly found in cosmetics and personal care products, respectively. Specifically, DEP is utilized as a solvent and a fixative in fragrances. Studies have shown that chronic exposure to DEP may lead to multigenerational effects on reproductive health in both male and female rats [25]. The second most common low-molecular-weight phthalate is DMP. DMP is used primarily as an insect repellent, resulting in extensive exposure due to generous application to exposed skin and clothing. A recent study in mice found that chronic exposure to DMP triggers changes in the levels of serum hormone that lead to increased rates of ovarian granulosa cell death [26].

The high-molecular-weight phthalates, such as Di-ethyl hexyl phthalate (DEHP), are used in construction materials and numerous polyvinyl chloride (PVC) products. DEHP is one of the most commonly used phthalates [27] and is of primary interest regarding its disrupting impact on fertility. In fact, 98% of the US population test positive for DEHP and its metabolites [28,29]. Despite numerous reports on its toxicity, DEHP is still widely used in consumer products and in a number of medical devices, such as blood bags, infusion tubes, nasogastric tubes, peritoneal dialysis bags, and urological catheters. Patients who undergo frequent hemodialysis, catheterization or massive blood transfusions are at particular risk for DEHP toxicity and are exposed to doses as high as 168 mg/day [30]. Several human studies have demonstrated the profound effects of prolonged exposure to DEHP on both male and female fertility [9,31,32]

The majority of studies on EDC's impact on reproductive health, including those mentioned above, evaluated the toxic effects of chronic exposure to phthalates and plasticizers. However, little is known about the reproductive outcomes of short exposure to such EDCs.

In the present study, we assessed the effects of acute exposure to BPA, DMP, DEP and DEHP. Out of the four EDCs tested, DEHP demonstrated the strongest effect on male fertility by significantly altering the maturation process sperm undergoes, also known as capacitation, as well as inhibiting acrosome reaction, and triggering excessive reactive oxygen species (ROS) production. Altogether these changes led to sperm inability to fertilize eggs. These results suggest that DEHP can directly affect sperm fertility and is therefore detrimental to male reproductive health.

6.2 Results

Murine embryo development is impacted by DMP, BPA, DEP, and DEHP.

Exposure to phthalates could either damage sperm directly or impair pre-implantation embryo development after fertilization occurs. To test the susceptibility of pre-implanted embryos to DEHP, DMP, DEP, and BPA, naturally derived zygotes were harvested and subjected to 0, 1, 2, and 10 μM of each EDC as outlined in the methods section. The ability of the pre-implantation embryo to progress towards the blastocyst stage was recorded on day 5 post-fertilization (Figure 1 and Supplemental Figure 1), and the respective survival rate was calculated as described in methods. While all four tested compounds did not affect pre-implantation development at the lower concentrations (up to 2 μM), we found that at 10 μM, all four chemicals effectively prevented blastocyst formation ($p<0.05$; Figure 1A-H and Supplemental Tables 1A-1D). All controls have been performed with either vehicle control (0.1% ethanol) or EDC-free media. No significant differences were observed among control conditions (Supplemental Table 2).

In vitro fertilization is affected by DEHP

To explore the direct effect of DEHP, DMP, DEP, and BPA on sperm fertilizing ability, *in vitro* fertilization (IVF) assays were carried out. Mouse sperm were capacitated in phthalate-supplemented media as described in methods by exposing sperm to different concentrations (0 μM, 1 μM, 2 μM, and 10 μM) of EDCs, and 60-90 minutes post-exposure, sperm was introduced to healthy murine eggs. The fertilization rate was calculated and presented as the percentage of embryos that reached the morula or blastula stage on day 5 post-fertilization ($p<0.05$; Figure 2A-H, Supplemental Figure 2 and Supplemental Tables 3A-3D). As shown in Figure 2, all tested concentrations of DEP and DMP did not produce any effect on sperm fertilizing ability and subsequent blastocyst formation, while 10 μM BPA had a minimal, but not a statistically significant impact on early embryo development (Figure 2C-D and Supplemental Figure 2). The most damaging effect to blastocyst formation was observed with DEHP (Figure 2G-H). While spermatozoa retained their fertilization potential at 1 μM, a significant decrease in embryo progression to blastulae was found already at 2 μM (74.95 ± 5.459 % in control vs. 47.68 ± 9.68 % in 2 μM). Moreover, at 10 μM of DEHP, almost no blastocyst formation was observed (Figure 2G-H). All controls have been done with either 0.1% ethanol as a vehicle control or EDC-free media, and no significant differences were detected between the control conditions (Supplemental Table 4).

DEHP prevents fertilization

The acute exposure to DEHP may either affect sperm ability to fertilize the egg or may permit fertilization but subsequently inhibit the zygotic division. To distinguish between these two scenarios, sperm fertility was assessed by recording pronuclei formation 9 hours post IVF. As shown in Figure 3, in the presence of 10 μM DEHP, a 92.76% reduction in pronuclei formation was detected compared to untreated control. Values were calculated based on pooled data from three independent experiments and represent a total of 19 zygotes out of 25 eggs in the control conditions, versus 2 zygotes out of 36 eggs in the presence of DEHP (Supplemental Table 5). These results indicate that even short exposure to DEHP modifies sperm physiology making spermatozoa unable to penetrate the zona pellucida.

Murine CatSper is not affected by DEHP

Since DEHP has demonstrated the most substantial effect on sperm fertility among all tested EDCs, we further explored which sperm functions were directly affected by exposure to this phthalate. Once deposited inside the female reproductive tract, mammalian spermatozoa must undergo a final maturation step, i.e., capacitation, to become competent to fertilize the egg [33,34]. This process results in the removal of non-covalently attached glycoproteins, depletion of cholesterol, and other steroids [35], as well as the removal of adherent seminal plasma proteins [36]. These physiological changes alter sperm membrane potential and make the cell competent to undergo a change in motility, known as hyperactivation, trigger the acrosome reaction and prepare spermatozoa for fertilization. Hyperactivation is characterized by calcium influx into the sperm flagellum via the calcium channel- CatSper [37,38] and is defined as an asymmetrical flagellar beat that is required for penetration through the viscous luminal fluids of the female reproductive tract and the protective vestments of the egg. CatSper deficiency, as well as its suppression by environmental toxins, has been previously linked to male infertility [37,39–41]. To investigate whether murine CatSper is also affected by DEHP, we used murine sperm patch-clamp technique [42]. As shown in Supplemental Figure 3A-3B, the application of 10μM DEHP did not alter CatSper currents. Since previous studies on several EDCs reported that phthalates impact human CatSper at micromolar concentrations [41], we also tested DEHP at a higher dose (Supplemental Figure 3A-3B). However, at either 10 μM or 100 μM concentration, no significant changes in monovalent CatSper currents were observed. This indicates that DEHP affects sperm cells through a CatSper-independent mechanism.

DEHP alters sperm capacitation and ROS production

Another hallmark of capacitation is the phosphorylation of sperm proteins on tyrosine residues [43,44]. Previous reports on the capacitation of murine sperm demonstrate a time-dependent increase in the phosphorylation of tyrosine residues in proteins with the molecular weight of 40 kDa-170 kDa [44–47]. This modification allows sperm to hyperactivate, undergo the acrosome reaction and interact with the zona pellucida [46,48]. To test the effect of DEHP on sperm tyrosine phosphorylation, caudal epididymal spermatozoa were incubated in a capacitating medium containing either 10 μM DEHP or vehicle control. Subsequently, tyrosine phosphorylation was assessed by a western blot using a monoclonal anti-phosphotyrosine antibody (anti-PY) (EMD Millipore). As shown in Figure 4A-B, DEHP markedly alters sperm capacitation-associated tyrosine phosphorylation kinetics, by expediting the process within the first 60 minutes of exposure, followed by a complete reversal after 120 minutes of incubation. Specifically, at the 60-minute time point, a 150% increase in the global tyrosine phosphorylation was detected in DEHP treated spermatozoa in comparison to the control condition. As capacitation progressed, the detected levels of the global tyrosine phosphorylation increased in the control samples. However, in the DEHP treated samples, the levels of detected phosphotyrosine significantly dropped. Specifically, at the 120-minute time point, the detected levels of phosphoproteins were 59% lower in the control. The most striking changes in phosphorylation were observed at the regions that correspond to 75 kDa, 95 kDa, 170 kDa, and 270 kDa (Supplementary Figure 4). The 75 kDa, 95 kDa, and 170 kDa molecular weight proteins were previously reported to have important roles in sperm fertility [46,47]. In addition, immunocytochemistry experiments using the same anti-PY antibody, revealed that the increased protein phosphorylation caused by DEHP is primarily localized to the mid-piece region of sperm (Figure 4C). According to previous reports, during the normal capacitation process, the sperm

midpiece is undergoing more robust tyrosine phosphorylation in comparison to other parts of the flagellum [49], and it appears that DEHP exacerbates this process. To further assess the global changes in sperm tyrosine phosphorylation induced by DEHP, flow cytometry analysis was performed using anti-PY labeled with CF647 dye (Biotium). As shown in Figure 4D, a significant increase in overall fluorescence was observed in DEHP treated cells resulting in 1.5±0.2- fold increase in global fluorescence.

The mid-piece region of sperm flagellum harbors mitochondria- an organelle known to generate reactive oxygen species (ROS). Interestingly, DEHP increases ROS generation in various cells and tissues, including hepatocytes, adipocytes, and testis [50–52]. However, DEHP's ability to alter sperm ROS production has not been studied. To detect ROS production, a chemiluminescence assay was employed, a commonly described technique to detect ROS in semen [53–55]. The levels of ROS production were assessed in caudal sperm capacitated in the presence or absence of 10 μM and 100 μM DEHP after 60 minutes of exposure. A significant increase in ROS production was detected in all treated samples in comparison to vehicle-treated controls (Figure 5A). We found that already at 10 μM of DEHP, a maximal ROS production was achieved, and no further increase was detected at 100 μM. Since excessive ROS production is known to be cytotoxic to sperm, exposure to DEHP may lead to impaired sperm fertilizing capacity.

The acrosome reaction in capacitated spermatozoa is inhibited by DEHP

The acrosome reaction is the fusion of the sperm plasma membrane with the outer acrosomal membrane. It is vital for fertilization, as only acrosome-reacted spermatozoa can fuse with the egg [56]. According to previous reports, increased levels of ROS production result in excessive peroxidation of the sperm acrosomal membrane [57], impairing acrosomal exocytosis and sperm-egg fusion [58–60]. While there is a debate over the physiological triggers for the acrosome reaction and the exact site of acrosomal exocytosis, it is well accepted that the acrosome reaction is required for sperm fertility. Therefore, we have explored whether DEHP can alter the spontaneous acrosome reaction. We found that incubation with 10 μM DEHP, decreased the percentage of spontaneous acrosome reaction. In control samples, the detected rates of acrosome reacted cells were 20.95 ±0.62 %, whereas in DEHP treated samples, the rates dropped to 8.28 ±1.24 % (Figure 5B-D).

To summarize, these results indicate that acute DEHP exposure stimulates excessive ROS production in sperm, as well as trigger altered tyrosine phosphorylation and inhibits the acrosome reaction. Consequently, these changes negatively affect sperm physiology and impact their fertility.

6.3 Discussion

Exposure to EDCs poses a significant risk to reproductive health and fetal development [61,62]. In this study, we assessed the effects of acute exposure to four omnipresent EDC's - BPA, DEHP, DMP, and DEP on sperm fertility and early embryo development. While it is well documented that chronic exposure to these compounds can affect both male and female fertility [16,63–66], the effects of short exposure are less clear. To assess the impact of the chosen EDCs on sperm fertility and pre-implantation embryo development, we employed in-vitro embryo development and IVF studies. Of all tested EDC's DEHP had the most profound impact on fertilization and sperm fertility. While it is known that chronic exposure to DEHP impairs sperm

motility and chromatin DNA stability [31,67], its acute effect on sperm fertilizing capacity has not been elucidated. Here, we sought to investigate the impact of short exposure to DEHP on sperm fertility and the mechanisms by which this EDC exhorts its effects.

Upon absorption, DEHP is distributed throughout the body by the circulatory system. The majority of DEHP is quickly hydrolyzed by the liver into various metabolites, which have been linked to altered fertility and DNA damage in sperm [20]. However, a portion of DEHP is stored un-metabolized in the adipose tissue- which acts as a reservoir for lipophilic EDCs [68,69]. Hormonal and neuronal signals regulating the fat tissue can trigger an abrupt release of lipophilic EDCs to the systemic circulation [69]. There are two main ways in which sperm can encounter un-metabolized DEHP: via abrupt release from adipose tissue or through release from medical devices, such as a urological catheter- making unmetabolized DEHP a prominent threat to sperm fertility.

DEHP exposure has been previously linked to increased ROS production in somatic cells and oocytes [63,70–72]. However, its impact on ROS overproduction in sperm was not elucidated. Here we show that acute exposure to DEHP triggers excessive ROS generation, leading to oxidative damage and ultimately sperm infertility.

While minor ROS generation naturally takes place during early sperm capacitation, this process must be tightly regulated. Mild ROS production triggers an increase in intracellular cAMP, resulting in the activation of Protein Kinase A (PKA). PKA, in turn, carries out a series of controlled tyrosine phosphorylation events in a time-dependent manner. [73,74]. Interestingly, certain EDCs such as BPA have been shown to up-regulate PKA's activity leading to an altered phosphorylation pattern downstream of PKA [75]. Since mature spermatozoa are transcriptionally and translationally silent cells, post-translational protein modifications such as tyrosine phosphorylation play an essential role in sperm maturation process and their ability to fertilize an egg [46]. Unwarranted ROS production leads to over-phosphorylation which significantly alters the maturation process of sperm [76,77]. Moreover, an excess of ROS is cytotoxic to sperm due to their limited antioxidant capacity and their high content of polyunsaturated long-chain fatty acids in the plasma membrane [58,78,79].

DEHP-treated sperm cells had altered capacitation with aberrantly fast tyrosine phosphorylation within the first 60 minutes of capacitation. This differs from the gradual increasing protein phosphorylation pattern that was observed in the control condition and previously reported in the literature [80,81]. The detected increase in tyrosine phosphorylation was localized primarily to the mid-piece region of sperm, the flagellar compartment where mitochondria are located. Mitochondrial respiration produces a significant amount of ROS, this process, if unregulated, can damage sperm genomic DNA, lipid and protein structures, and subsequently impair sperm integrity and fertility. Previous reports show that DEHP exposed oocytes and somatic cells produce an excessive amount of ROS via mitochondrial-derived ROS [63,82,83]. However, it has not been shown that DEHP affects spermatozoa in a similar manner. In fact, several EDCs were suggested to affect sperm fertility via CatSper-related mechanism [41]. Here, we show that while murine CatSper was not sensitive to DEHP exposure, this phthalate indeed triggers excessive ROS production and subsequently impairs sperm fertility.

An additional effect of excessive oxidative stress on spermatozoa is lipid peroxidation. Spermatozoa are extremely susceptible to lipid peroxidation due to their high concentration of long- chain polyunsaturated fatty acids [58,78,79,84,85]. Alteration of the lipid structure due to peroxidation in sperm leads to a decrease in membrane fluidity [57,86–88] causing decreased motility and altered acrosome reaction [57–60]. The acrosome reaction is an important step during

fertilization in order to expose sperm-egg recognition elements [89]. Murine sperm begin to undergo the acrosome reaction in the upper isthmus [90], the part of the oviduct that connects the uterine with the ampulla. Thus, mouse fertile sperm are acrosome-reacted prior to reaching the ampulla, the site of fertilization and before encountering the eggs [91]. In fact, most acrosome-intact spermatozoa are unable to fertilize the egg and swim away from the zona pellucida [91]. Thus, sperm ability to undergo the AR at the end of capacitation is highly important for sperm fertility [92]. Here we find that DEHP significantly inhibits the acrosome reaction in capacitated sperm. As a result, DEHP-exposed sperm were largely acrosome-intact and therefore unable to fertilize murine eggs. This explains the reduced levels of fertilization that were observed in IVF and the absence of pronuclei formation. These results indicate that, in addition to its chronic impact on reproductive potential, DEHP also imposes acute damage to sperm by affecting its ability to fertilize and thereby represent a risk to male fertility.

6.4 Methods

Ethical statements and animal care. All experiments were performed in accordance with NIH Guidelines for Animal Research and approved by UC Berkeley Animal Care and Use Committee (AUP 2015-07-7742), with every effort made to minimize suffering for the animals. C57BL6 mice were purchased from Jackson Laboratory, Bar Harbor, Maine or Harlan Laboratories (Indianapolis, IN). The mice were kept in a room in a room with controlled light (14 hours light, 10 hours darkness) and temperature (23 ± 0.5°C); 50–60% humidity. The mice were fed a standard chow diet (PicoLab Rodent diet 20, LabDiet, 5053) and hyper-chlorinated water *ad libitum*. BPA, DEHP, DMP, and DEP (Sigma-Aldrich, St. Louis, MO) were dissolved in ethanol (Sigma-Aldrich). Phthalates were used at a final concentration of 1 μM, 2 μM, and 10 μM. The concentration range of 1-10 μM for tested EDC's was chosen based on previously reported phthalate concentrations linked to female infertility and on studies that evaluated DEHP plasma concentration in patients who undergo hemodialysis [93,94]. Vehicle controls were performed at the highest concentration.

Embryo collection from natural mating. 4- to-16- week-old female mice were super-ovulated by the standard procedure previously described [95]. Briefly, 5 IU of pregnant mare serum gonadotropin (PMSG; EMD Millipore) were administered via in*traperitoneal injection (i.p)* at 14:30. Forty-eight hours later, 5 IU of human chorionic gonadotropin (hCG; EMD Millipore) were injected. At the time of hCG injection, each female mouse was placed in an individual cage with one proven breeder (3-10 months old). The following morning, female mice were inspected for vaginal plugs. 20h after hCG administration, embryos were dissected out from the oviducts. The isolated oocyte-cumulus complexes were placed in pre-warmed 50 μL droplet of Hyaluronidase (80 IU/mL) (LifeGlobal) and were gently pipetted up and down repeatedly in a fine glass pipette until the oocytes were partially denuded. The oocytes were then transferred to a pre-warmed M2 media (Zenith Biotech) supplemented with 4 mg/mL BSA (Sigma-Aldrich) and washed in 4-5 droplets until all the corona cells were removed. Zygotes from each individual mouse were randomly allocated to different culture conditions for 20h of incubation. Since the tested EDCs show low water solubility and high oil solubility, the standard culture of embryos under oil could not be employed. Thus, we cultured the embryos in 500 μL KSOM (Zenith biotech) +/- EDCs at different concentrations for 20h in 4-well dishes (*Nunc*™,

Sigma-Aldrich) without oil. At the end of the 20h incubation, the two cell embryos were briefly washed and allocated to culture dishes, containing 10 µL droplets of KSOM (Zenith biotech) supplemented with 1 mg/mL BSA (Sigma-Aldrich) overlaid with embryo-suitable light mineral oil (Millipore) in 5% CO_2 and 37°C. Successful development was considered as morula or blastocyst – the final stage of embryonic development *before implantation.* To calculate the rate of embryo survival, we counted the number of embryos that developed to the morula or blastocyst stage and divided this number by the total number of the zygotes that were harvested.

In vitro fertilization. To investigate the influence of EDCs exposure on spermatozoa's ability to fertilize eggs, in vitro fertilization (*IVF)* experiments were conducted. *IVF* was performed as previously described [96] with a few modifications. Eggs were recovered from 4 to 16-week-old female mice by superovulation as described above. 13 hours after hCG injection, the female mice were euthanized, and the oviducts were dissected out. The cumulus masses were isolated from the ampulla region of the oviduct, and incubated in HTF medium (Embryomax, Specialty Media, Millipore MR-070-D), 5% CO_2, 37°C for 30 minutes prior to insemination. Sperm was obtained from a mature C57BL male mouse just before egg harvest. Spermatozoa were recovered by removing the caudae epididymis and placing each cauda separately in a petri dish containing pre-warmed HTF with or without EDCs. The tissue was cut five to six times, and sperm was allowed to swim out into the medium for 20-30 min. The cauda was then removed, and the resultant sperm suspension was left for an additional 30-60 minutes in the media at 37°C in 5% CO_2 to capacitate. Total time of capacitation was 60-90 minutes.

Four well plates were used for fertilization. Each well was filled with 700 µL of HTF. Sperm was added to each well to a final concentration of 210,000 spermatozoa/mL. Subsequently, the cumulus masses were added to the fertilization dish; care was taken to avoid carry-over of excessive amounts of solution to maintain sperm concentrations. Since the cumulus masses were obtained around the time of ovulation, they were highly compact, making it difficult to quantify the exact number of eggs in each mass. To ensure similar numbers of eggs in each tested condition, two-three cumulus masses were added to each fertilization well. Dishes were placed in the incubator and maintained at 37°C in 5% CO_2 for 4h. After that time, eggs were washed to remove excess sperm and then cultured in 10 µL droplets of KSOM supplemented with 1 mg/mL BSA and overlaid with embryo-tested light mineral oil in 5% CO_2 and 37°C. To assess the rates of successful fertilization, the number of morula or blastocyst embryos produced by IVF on day five post insemination was counted and then divided by the number of eggs that were initially used for insemination.

Electrophysiology. Sperm was collected as previously reported [97]. Giga-ohm seals between the patch pipette and mouse spermatozoa were formed at the cytoplasmic droplet. Seals were formed in HS solution comprising the following (in mM): 130 NaCl, 5 KCl, 1 $MgSO_4$, 2 $CaCl_2$, 5 glucose, 1 sodium pyruvate, 10 lactic acid, 20 HEPES, pH 7.4 adjusted with NaOH. Transition into the whole-cell mode was performed by applying short (1 ms) 499–611 mV voltage pulses, combined with light suction. Access resistance was 15- 25 MΩ. Cells were stimulated every 5 s. Data were sampled at 2–5 kHz and filtered at 1 kHz. Pipettes (15–20 MΩ) for whole-cell patch-clamp recordings of monovalent CatSper currents were filled with the following (in mM): 130 Cs-methanesulfonate, 70 HEPES/MES, 3 EGTA, 2 EDTA, 0.5 Tris-HCl, pH 7.4 adjusted with CsOH. Bath divalent-free solution for recording of monovalent CatSper currents contained the following (in mM): 140 Cs-methanesulfonate, 40 HEPES/MES, 1 EDTA, pH 7.4 adjusted with

CsOH. HS solution was used to record baseline current while measuring monovalent CatSper currents. 1 µL/mL EtOH (vehicle control), 10 µM or 100 µM DEHP were added to the bath solution right before electrophysiology experiments. $CaCl_2$ was added to this solution in accordance with WinMAXC version 2.05 (C. Patton, Stanford University) to obtain the required free Ca^{2+} concentration.

Capacitation of spermatozoa in the presence of 10 µM DEHP to test the level of tyrosine phosphorylation. Spermatozoa collection and the assessment of protein tyrosine phosphorylation was performed as previously outlined [45], with a few modifications. Spermatozoa were recovered by removing the cauda epididymis and placing it into a Petri dish containing HTF with either 1 µL/mL ethanol or 10 µM DEHP. The tissue was cut five to six times, and sperm was allowed to swim out for 15-20 minutes at 37°C in 5% CO_2. The cauda was then removed, and spermatozoa suspension was further incubated at 37°C in 5% CO_2. Sperm samples were collected after 30, 60, 90, and 120 minutes of capacitation and placed into a clean tube. After each sample collection, the sample was centrifuged at 21000 x *g* for 1 minute. The supernatant was discarded, and the cellular pellet was resuspended in 25 µL of 2x Laemmli sample buffer (BioRad) [98]. The sample was then boiled for 5 minutes at 95°C and centrifuged at 21000 x *g* for 1 minute. Supernatants were transferred to clean tubes, β-mercapto-ethanol was added (to a final concentration of 2.5%), and the sample was heated again to 95°C for 1 min. 20 µL of the total crude cell lysate from each sample was loaded onto a 4–20% gradient Tris-HCl Criterion SDS-PAGE (BioRad). After transfer to polyvinylidene fluoride membrane, blots were blocked in 0.1% PBS-Tween20 (Fisher Scientific) with 3% IgG-free BSA blocking solution for one hour and incubated with anti-phosphotyrosine antibody, clone 4G10 (Millipore, 05-321) at a dilution of 1:2000 in 1% IgG-free BSA blocking solution overnight at +4°C. The membrane was then washed three times in PBST and probed with a secondary horseradish peroxidase-conjugated antibody (Abcam) at a dilution of 1:15,000 in 1x PBST. After subsequent washing, the membrane was developed with an ECL SuperSignal West Pico kit (Pierce) according to the manufacturer's instructions. After detection, the membrane was stripped and re-probed with mouse tubulin-alpha ab-2 (Sigma-Aldrich), 1:5000 dilution. To quantify the global changes in tyrosine phosphorylation, rectangular boxes were drawn around each lane of the western blots' images. Each lane's optical density was normalized. First, the detected signals were normalized to the loading control, acetylated tubulin. Subsequently, each lane was normalized to the control lane at 120 minutes of capacitation.

Spontaneous acrosome reaction in the presence of 10 µM DEHP in capacitated spermatozoa. Assessment of the acrosomal status was done as previously reported [99] with a few adjustments. In summary, the right and left caudae epididymides were surgically removed. One cauda was placed in HTF medium supplemented with 1µl/mL ethanol while the second one was placed in HTF medium containing 10 µM DEHP. Each cauda was cut five to six times, and sperm were allowed to swim out for 15-20 minutes at 37°C in 5% CO_2. The cauda was then removed, and the resultant spermatozoa suspension was left to capacitate for 60 min. On average, the concentration of sperm in each condition was $2\text{-}5\times10^6$ cells/mL. After 60 minutes of capacitation, spermatozoa suspension was transferred to clean microtubes and centrifuged at 300 x *g* for 5 minutes at room temperature. The cells were then fixed in 4% PFA in 1X PBS for 15 minutes. At the end of fixation, an equal volume of 0.1 M ammonium acetate was added. The microfuges were centrifuged at 800 x *g* for 5 minutes. The supernatant was removed, and sperm

cells were resuspended in the remaining 100 µL. 30 µL of sperm suspension was spotted onto non-charged microscope slides and gently spread out with a glass pipette. The samples were allowed to air-dry for 15 min. Subsequently, the slides were washed in Milli-Q water followed by a methanol wash, and then Milli-Q water again, each wash step was done for 5 minutes. The slides were subsequently submerged in Coomassie brilliant blue (Sigma-Aldrich) solution for 2 minutes (0.11 g Coomassie brilliant blue, 20 mL water, 25 mL Methanol, and 5 mL glacial acetic acid). Next, the slides were rinsed in Milli-Q water to remove excess Coomassie and mounted with Mowiol mounting medium (Millipore). After the cells were mounted, the acrosomal status was immediately assessed to avoid diffusion of the stain. Acrosome intact cells had bright blue staining on the dorsal region of the acrosome. Acrosome reacted cells had patchy or absent staining. 500 sperm cells per condition (100-200 cells per slide, 3-5 slides per condition) were assessed.

Flow cytometry. Spermatozoa was capacitated in the presence of either 10 µM DEHP or vehicle control. To detect phosphotyrosine residues in capacitated sperm by flow cytometry we followed the methodology previously outlined [100], with few modifications. Sperm aliquots (3×10^6) were taken at 60 min of capacitation and fixed in 3.7% PFA in 1 X PBS for 10 min at room temperature. To remove the PFA, the cells were centrifuged at 500 x g for 10 min. The supernatant was removed, and the cellular pellet was resuspended in 1XPBS. The cells were washed twice. Next, the cells were permeabilized in 0.1% Triton X-100 for 10 min at RT. Non-specific binding sites were blocked by 0.1% BSA in PBST for 30 min at RT. To detect phosphotyrosine, we conjugated an anti-phosphotyrosine antibody clone 4G10 with a CF 647 dye (Mix-n-Stain™ Antibody Labeling Kit, Biotium), as per the manufacturer's instructions. To label the cells, sperm were incubated with 10 µg/ml of the conjugated antibody in PBS with 0.1% BSA for 1 hour at RT. Labeled spermatozoa were then washed in PBS and resuspended in 250 µL PBS for flow cytometric analysis. *10,000 cells* per sample were analyzed. Sperm fluorescence was quantified using the BD LSR Fortessa flow cytometer equipped with an argon laser tuned far red spectrum. flow cytometry analysis was performed with the aid of a positive and a negative control for each experiment. FlowJo™ Software was used for data analysis. The region of interest was selected based on sperm forward scatter (FSC, relative cell size) and side scatter (SSC, cell internal complexity) to eliminate cellular debris.

ROS production detection by chemiluminescence assay. Spermatozoa were recovered by removing both caudae epididymides and placing them into a 30 mm Petri dish containing HS media. Cells were allowed to swim out for 15-20 min. Subsequently, the sperm suspension was equally divided between three Eppendorf tubes and spun down at 300 x *g* for 7 min. After the removal of the supernatant, the cells were resuspended in an equal volume of HTF containing either ethanol or DEHP. The control tube contained 1 µL/mL ethanol and the treatment tube contained either 10 µM or a 100 µM DEHP. The suspensions were then capacitated at 37°C in 5% CO_2 for 60 min. Detection of reactive oxygen species generated by sperm cells was done using the chemiluminescent agent - luminol following a previously described procedure [55,101]. The chemiluminescent probe, luminol (Sigma-Aldrich, A8511-5G.) was freshly prepared before each experiment. After 60 min of capacitation, the samples were spun down at 300 x *g* for 7 min and resuspended in 125 µM luminol in DPBS. Negative control, test sample, and positive control were prepared. 100 µL of 30% hydrogen peroxide solution was added to the positive control. A 100 µL aliquot of the cell suspension was taken from each sample for sperm count. The samples

were then taken for Chemiluminescence measurements using the Lumicycle 32 (Actimetrics, Inc. Wilmette, IL). The luminometer measured Chemiluminescence at 37°C for 5 minutes. ROS production was expressed as counted photons per minute (CPM)/10^6 sperm. Data were recorded using Actimetrics Lumicycle Data Collection software and analyzed using the Actimetrics Lumicycle Analysis program.

Statistical analyses. For statistical analyses used in the manuscript the GraphPad Prism 5 software (GraphPad Software, Inc., La Jolla, CA) was used. Unpaired t-test was used to determine statistical significance for embryo survival, IVF and Chemiluminescence experiments, and assigning $p \leq 0.05$ as the limit. Paired t-test was used for the AR, PY and flow cytometry experiments. All results are shown with the standard error of the mean. The significance of changes is indicated as follows: * $p \leq 0.05$, ** $p \leq 0.01$, *** $p \leq 0.001$

Acknowledgments. This work was supported by March of Dimes, Pew Biomedical Scholars Award, Chau Hoi Shuen Foundation Women in Science Program, and Packer Wentz Endowment Will (to PVL), as well as Male Contraceptive Initiative grant to LGK and Summer Research Fellowship to JDR. We thank Dr. Andrew Modzelewski for his valuable advice and technical assistance with embryo work, and Monika Haoui for the help with manuscript editing.

Authors' contributions. LGK and PVL conceived the project, designed the experiments and wrote the manuscript. LGK performed all studies, data acquisition and analysis for the manuscript. JDR helped with acrosome reaction, tyrosine phosphorylation, Chemiluminescence and flow cytometry studies. NP assisted with flow cytometry experiments and JM and LJK helped with Lumicycle and data analysis of luminol studies. All authors discussed the results and commented on the manuscript.

Declaration of Interests. *The authors declare that the research was conducted in the absence of any commercial or financial relationships that could be construed as a potential conflict of interest*.

6.5 Figures

Figure 1

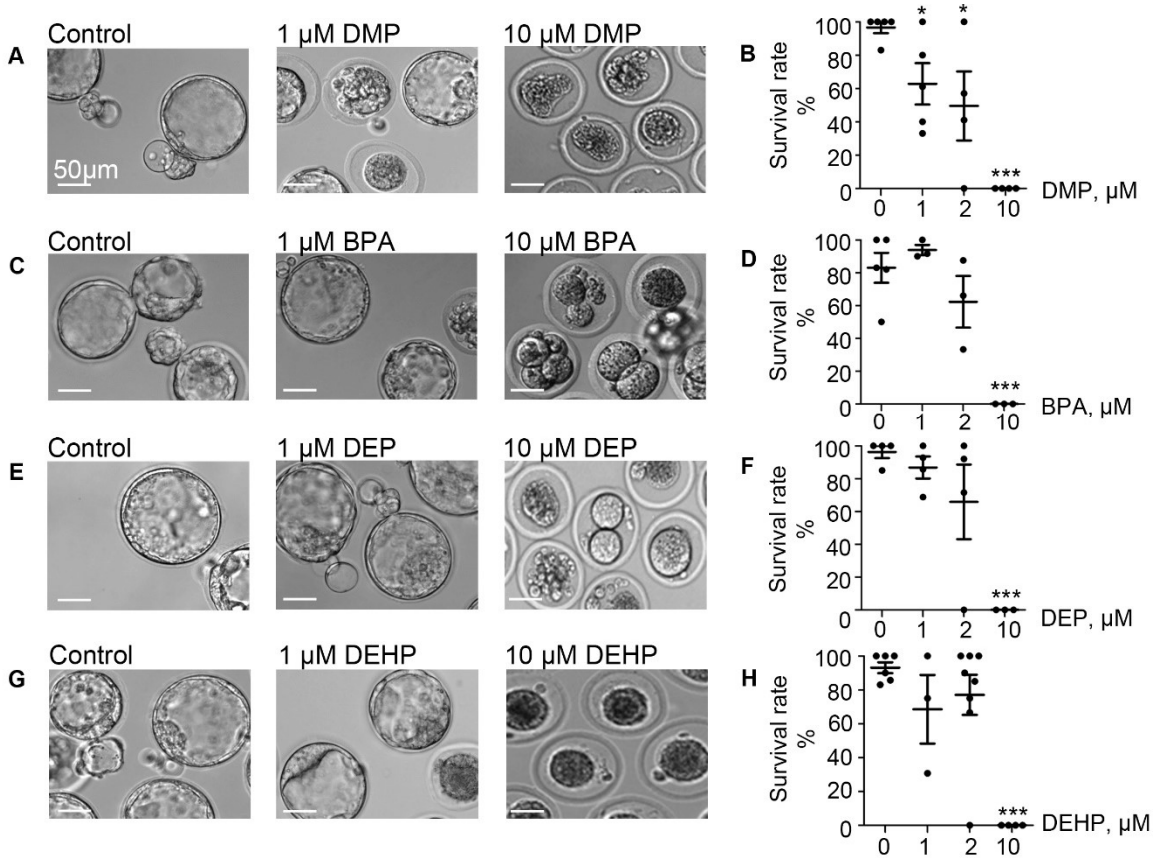

Figure 1. Murine embryo development is impacted by DMP, BPA, DEP and DEHP. In vitro embryo development on day 5 post fertilization. **A, C, E, G** are representative images of blastocysts previously exposed at the zygote stage to 0, 1 or 10 µM of the indicated EDC for 20 hours. The subsequent embryo culture was done in the absences of the indicated EDC. **A.** Shown are representative images of DMP-exposed embryos. **B.** The survival rate of DMP exposed zygotes was calculated based on the percentage of embryos that have reached the morula or blastocyst stage. **C.** Representative images of embryos previously exposed to BPA. **D.** The survival rate of BPA exposed zygotes was calculated as in (B). **E.** Representative images of embryos previously exposed to DEP. **F.** The survival rate of DEP exposed zygotes was calculated as in (B). **G.** Representative images of embryos previously exposed to DEHP. **H.** The survival rate of DEHP- exposed zygotes was calculated as in (B). Data are means +/- S.E.M. Asterisk indicates a statistical difference between control embryos and embryos exposed to EDCs. ** ($P<0.01$), *** ($P<0.001$). Scale bars for all images are 50 µm.

Figure 2

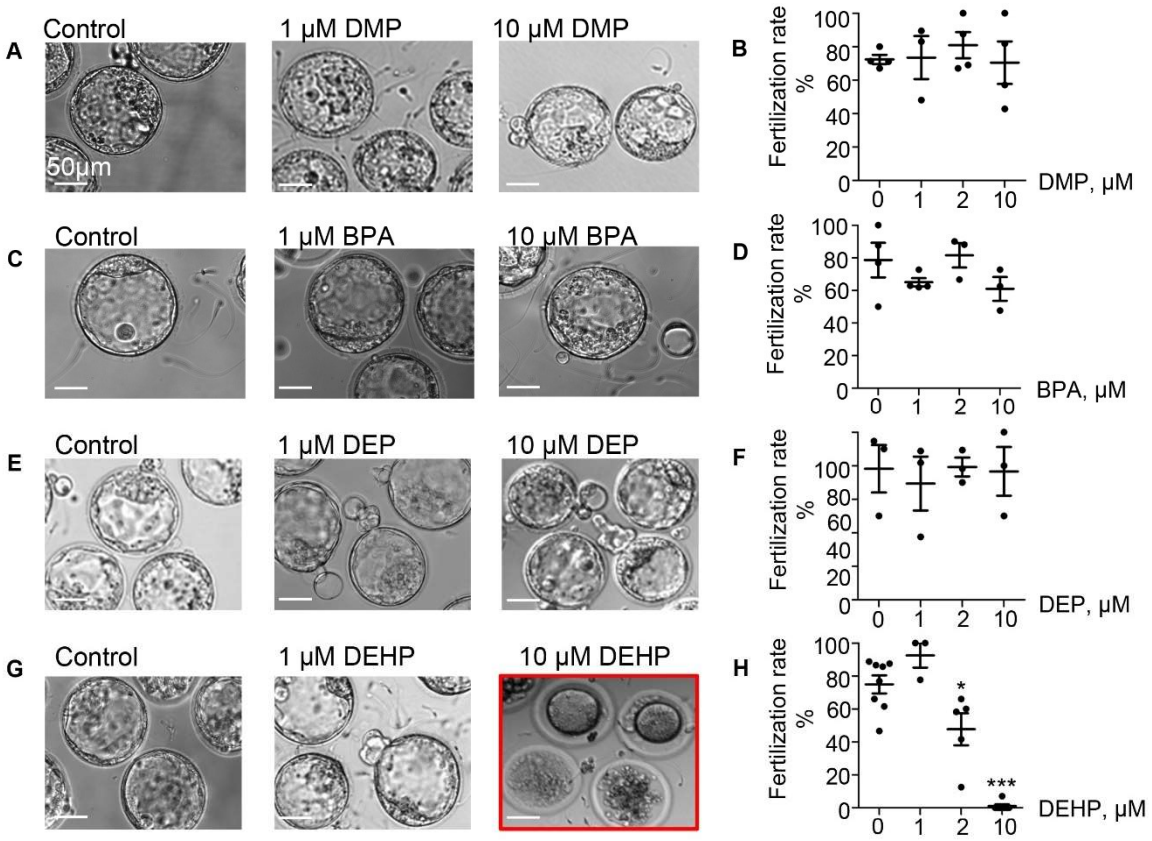

Figure 2. Fertilization rate of murine eggs exposed to EDCs treated spermatozoa. A, C, E, G are representative images of blastocysts obtained after murine eggs were introduced to sperm previously exposed to 0, 1 or 10 μM of the indicated EDC. Subsequent embryo culturing was done in the absences of EDCs, and the images were taken on day 5 post insemination. **A.** Shown are representative images of blastocysts obtained after murine eggs were introduced to sperm previously exposed to DMP. **B.** Percentage of eggs that were fertilized by DMP- treated sperm and were able to reach morula or blastocyst stage. **C.** Representative images of embryos obtained after IVF with BPA-treated spermatozoa. **D.** The percentage of eggs fertilized by BPA-treated sperm was calculated as in (B). **E.** Representative images of embryos obtained after IVF with DEP-treated sperm. **F.** The percentage of eggs fertilized by DEP-treated sperm was calculated as in (B). **G.** Representative images of embryos obtained after IVF with DEHP-treated sperm. **H.** The percentage of eggs fertilized by DEHP-treated sperm was calculated as in (B). Data are means +/- S.E.M. Asterisk indicates a statistical difference between control embryos and embryos exposed to EDCs. ** ($P<0.01$), *** ($P<0.001$). Scale bars for all images are 50 μm.

Figure 3

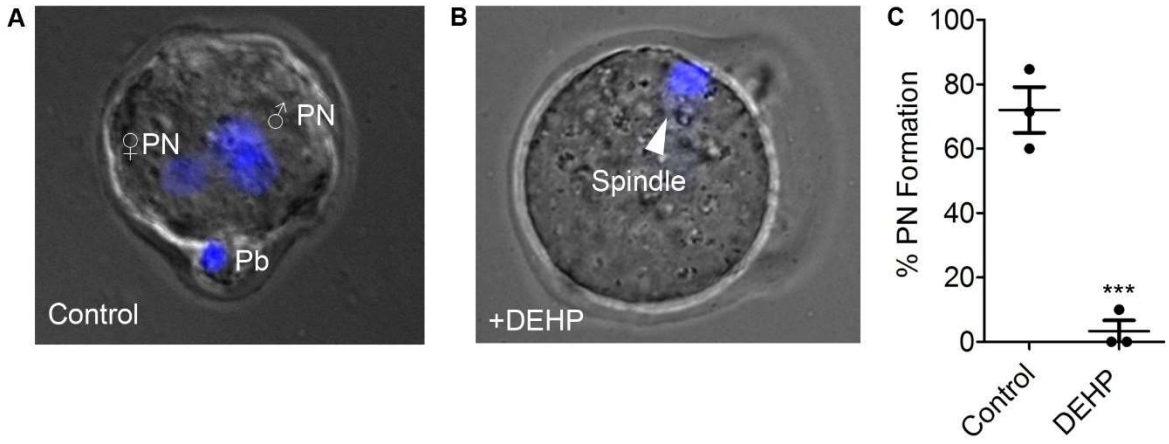

Figure 3. Pronuclei formation after in vitro fertilization by DEHP-treated sperm. Pronuclear formation was assessed 9 hours after IVF; genomic DNA staining was done with DAPI. **A.** Representative image of a successfully fertilized egg with two pronuclei (PN) and a polar body (Pb). The egg was inseminated with sperm treated with vehicle control solution. **B.** Shown are representative images of unfertilized eggs following an IVF with sperm that was treated with 10 μM DEHP. The arrowhead indicates the position of the second metaphase spindle. **C.** Percentage of fertilized eggs with PN detected. Each data point represents the mean of one of the three independent experiments +/- S.E.M. *** indicates statistical significance ($P<0.005$). The total number of eggs: 25 (control), 36 (+10μM DEHP).

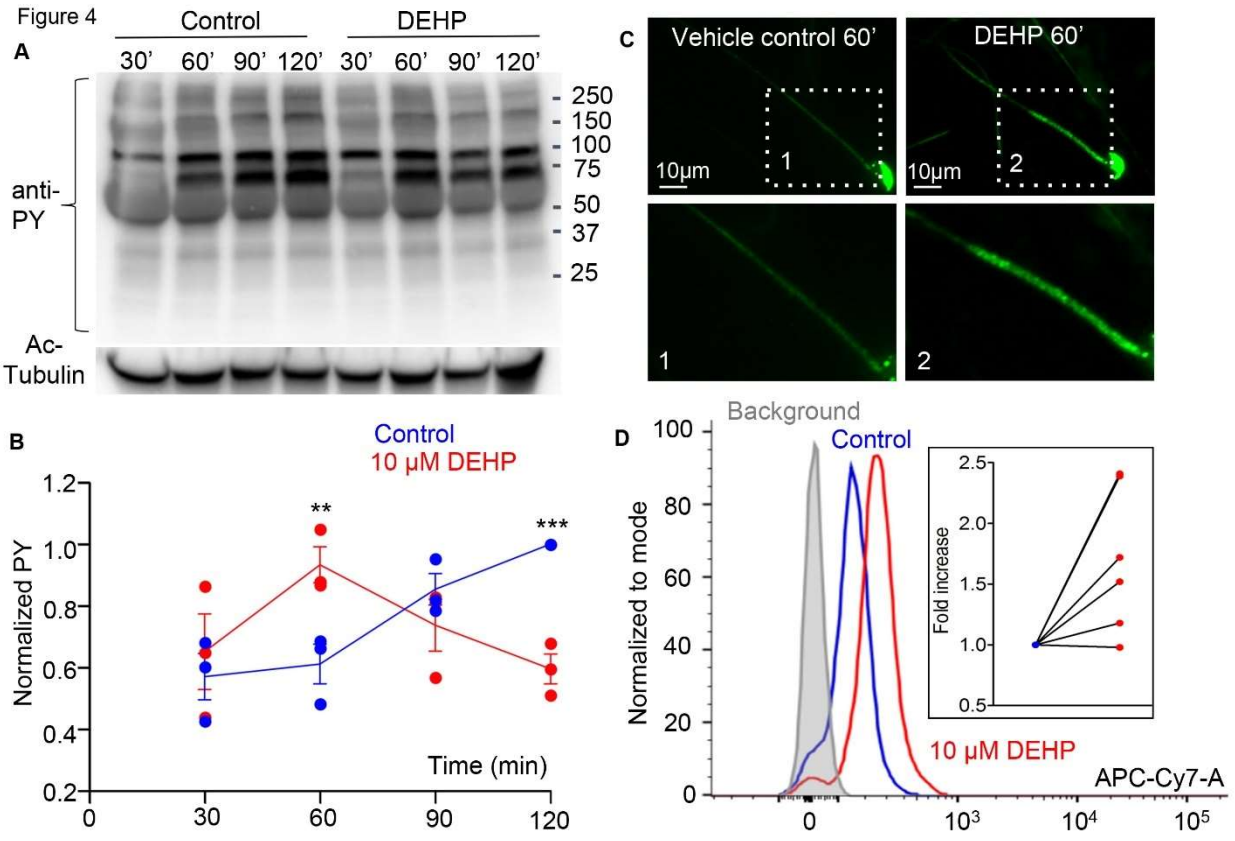

Figure 4. Capacitation-associated tyrosine phosphorylation of murine sperm is altered in the presence of DEHP. A. Representative western blot image shows the time course of protein tyrosine phosphorylation under capacitating conditions in the presence or absence of 10 µM DEHP. DEHP was added to the media immediately before the start of the capacitation process. Sperm lysates were obtained at the indicated times (30, 60, 90 and 120 minutes) and subjected to SDS-PAGE immunoblotting. Tyrosine phosphorylation was detected with a monoclonal phospho-tyrosine (PY) antibody. Acetylated-tubulin (Ac-Tubulin) was used as a loading control. **B.** Levels of relative tyrosine phosphorylation obtained as total densities extracted from (A) and normalized to the densities of the loading control. Each data point represents the mean of one of the three independent experiments. **C.** Immunofluorescent localization of tyrosine phosphorylated proteins as visualized by PY antibody. Increased phosphorylation detected after 60 minutes of capacitation in the mid-piece region of spermatozoa in DEHP- treatment group (right panels) as compared to control untreated spermatozoa (left panels). Lower panels represent insets from the corresponding region of interests indicated on the upper panels by dashed rectangular. **D.** A representative flow cytometry data showing an increase in global tyrosine phosphorylation in 10 µM DEHP- treated spermatozoa (red) at 60 minutes of capacitation compared to the vehicle control (blue). Tyrosine phosphoproteins were detected using a CF 647 dye conjugated to an anti-PY antibody. Inset: fold increase in mean fluorescent intensity normalized to mode as detected by the flow cytometer compared to control conditions. Data are means +/- S.E.M. ** indicates statistical significance ($P<0.01$) between control spermatozoa and spermatozoa exposed to 10 µM DEHP. *** indicates statistical significance ($P<0.001$)

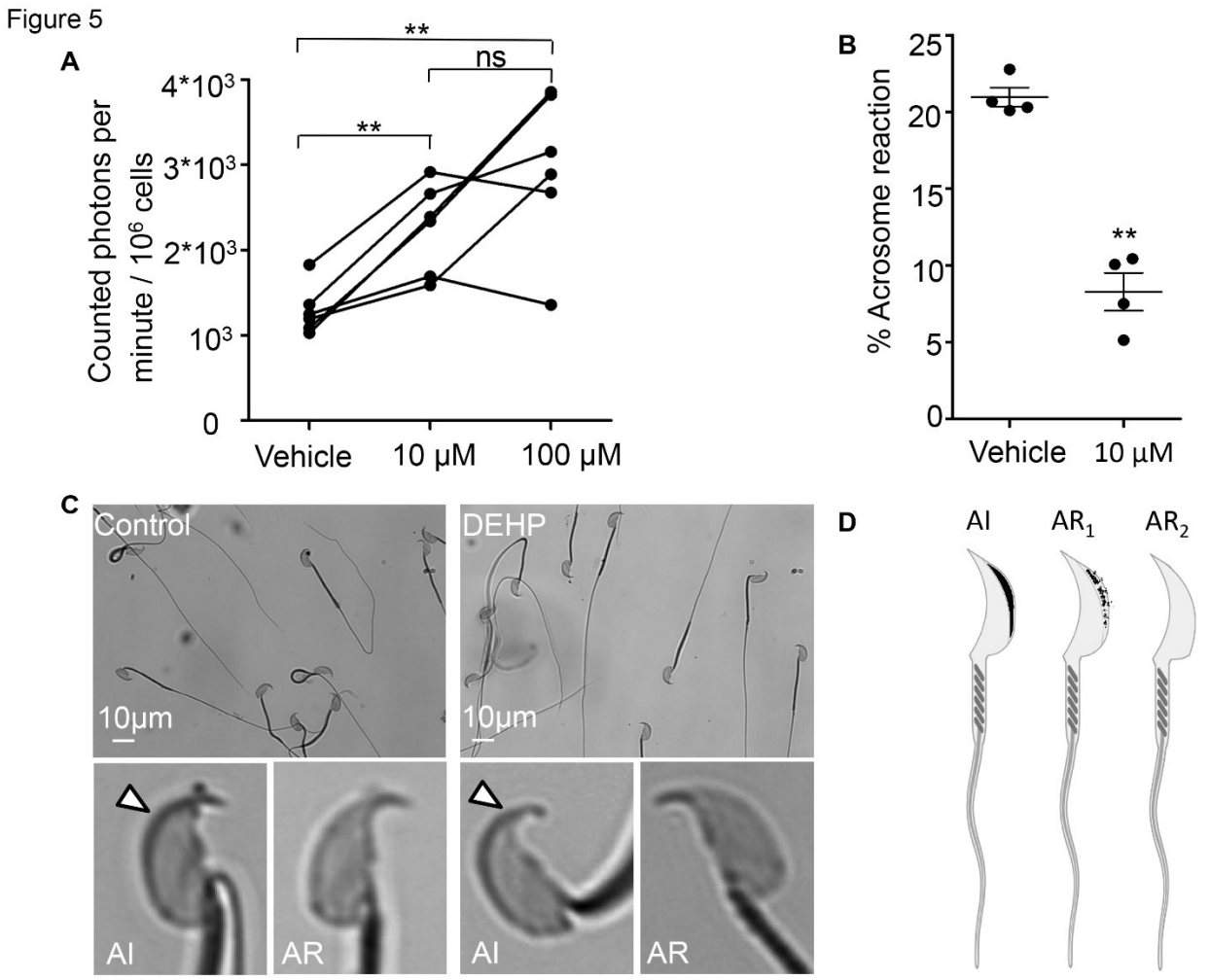

Figure 5. DEHP increases ROS production and decreases spontaneous acrosome reaction in capacitated sperm cells. A. Luminol-dependent chemiluminescence assay showed increased rates of ROS production in sperm treated with 10 and 100 µM DEHP in comparison to the vehicle control (0 µM DEHP). Connected dots represent spermatozoa extracted from the same mouse (total of six mice have been used for this experiment). Each sample was divided into three aliquots and subjected to different conditions. A minimum of $1.35*10^6$ sperm cells/mL was used per condition. **B.** Percentage of spontaneously acrosome-reacted spermatozoa subjected to 10 µM DEHP or vehicle control (0.1% ethanol) during capacitation. Each data point represents the mean of one of the four independent experiments. A minimum of 500 cells was evaluated per experiment. **C.** Acrosome-reacted (AR) and acrosome- intact (AI) spermatozoa in the control condition. **D.** AR and AI spermatozoa in 10 µM DEHP condition. Arrowheads point at intact acrosomes. AI cells have bright blue staining on the dorsal region of the acrosome, AR cells have patchy or absent staining. **E**. Diagram showing acrosome-reacted (two distinct patterns are indicated as AR_1 or partially reacted, and AR_2 as fully reacted) and acrosome- intact (AI) spermatozoa. Image made with Biorender.com. Data are means +/- S.E.M. ** indicates

statistical significance (P<0.01) between control spermatozoa and spermatozoa exposed to 10µM DEHP.

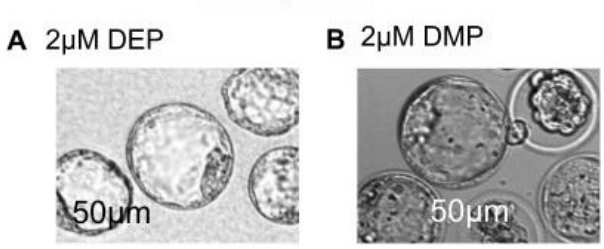

Supplementary Figure 1. Murine embryo survival post exposure to 2µM of tested EDCs. In vitro embryo development on day 5 post fertilization. **A**. Representative images of blastocysts previously exposed at the zygote stage to 2 µM DEP for 20 hours. **B.** Representative images of blastocysts previously exposed at the zygote stage to 2 µM DMP for 20 hours. Scale bars are 50 µm.

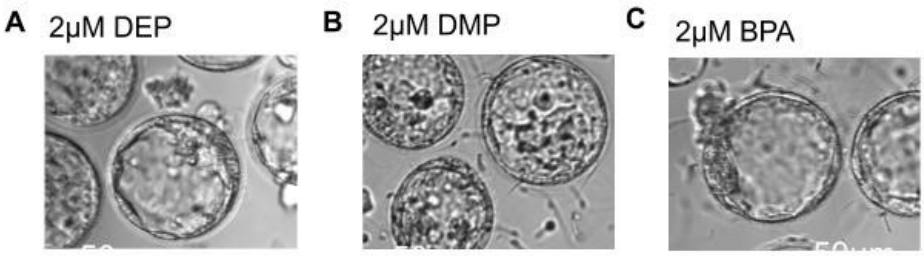

Supplementary Figure 2. Fertilization rate of murine eggs exposed to spermatozoa treated with 2 µM of tested EDCs. A. Representative images of blastocysts obtained after murine eggs were introduced to sperm previously exposed 2 µM DEP. **B**. Representative images of blastocysts obtained after murine eggs were introduced to sperm previously exposed 2 µM DMP. **C**. Representative images of blastocysts obtained after murine eggs were introduced to sperm previously exposed 2 µM BPA. Scale bars are 50 µm.

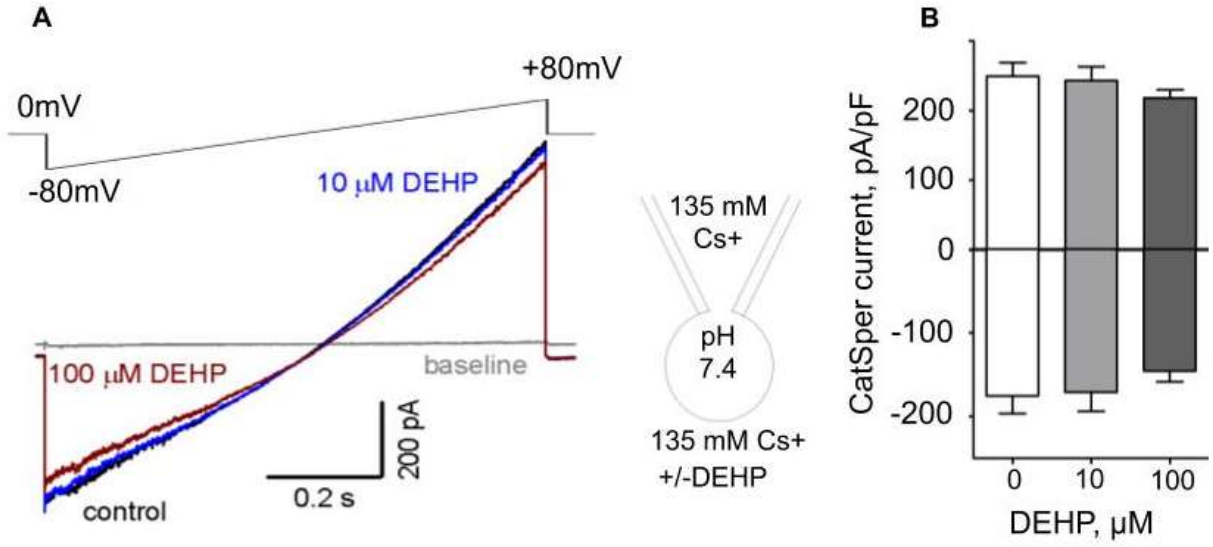

Supplementary Figure 3. Murine CatSper is not affected by DEHP. A. Representative monovalent whole-cell CatSper currents ($I_{CatSper}$) recorded from a murine spermatozoon in the absence (black) and presence of 10 μM (blue) and 100 μM DEHP (red). $I_{CatSper}$ were activated by a voltage ramp from -80 mV to +80 mV from a holding potential of 0 mV. Voltage protocol is shown above the currents. The panel on the right shows the main conducting ion of the pipette and bath solutions. **B.** Averaged $I_{CatSper}$ densities recorded from murine epididymal spermatozoa in the absence and presence of DEHP. Data are means +/- S.E.M. An average of 3 independent experiments is shown.

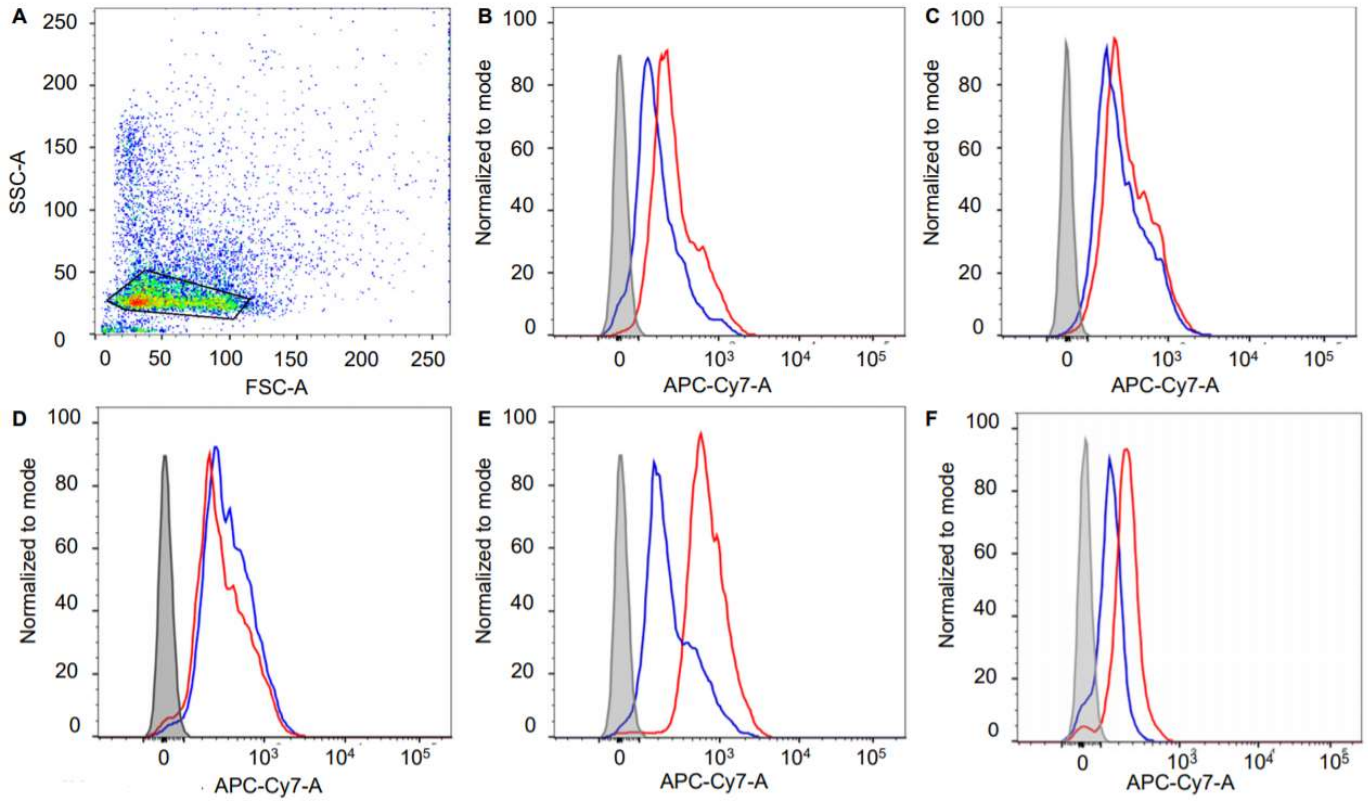

Supplementary Figure 4. Representative dot plot of side (SSC-A) versus forward (FSC-A) scatter showing flow-cytometry data obtained for sperm. A. The region of interest demarcated by solid lines was selected to eliminate cellular debris. **B-F.** Representative flow cytometry histograms from five independent experiments. Mean fluorescence intensities (MFI) normalized to mode show an increase in global tyrosine phosphorylation in 10 µM DEHP treated spermatozoa (red) at 60 minutes of capacitation compared to the vehicle control (blue). The background fluorescence detected in unstained spermatozoa is shown in grey. Tyrosine phosphoproteins were detected using a CF 647 dye conjugated to anti-PY (monoclonal antibody).

Supplemental Figure 5

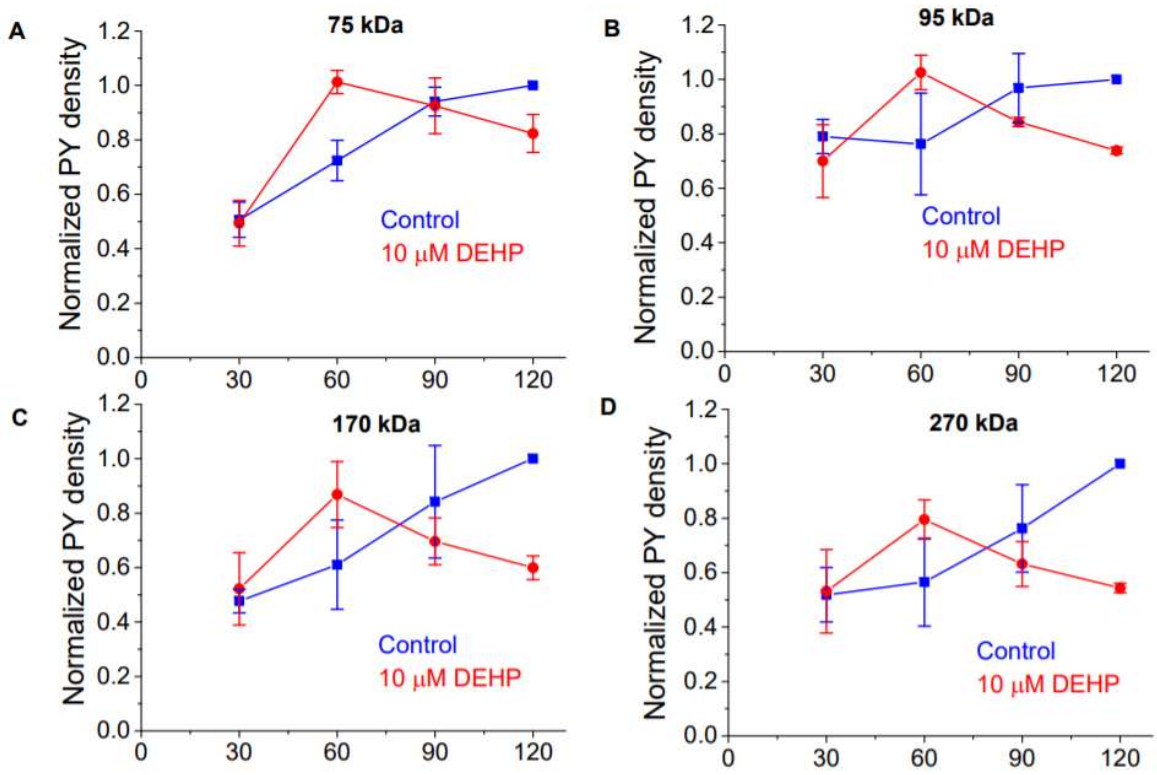

Supplementary Figure 5. Time course of capacitation-associated tyrosine phosphorylation of specific sperm proteins is altered by exposure to DEHP. Levels of relative tyrosine phosphorylation obtained from each of the four protein bands at the corresponding molecular weights: 75 kDa, 95 kDa, 170 kDa, and 270 kDa. **A.** The density of the 75 kDa protein band was normalized to the densities of the loading control, followed by normalization to the control at 120 min. Each data point represents the average of one of the three independent experiments. **B.** The 95 kDa protein band normalized as in (A). **C.** The 170 kDa protein band normalized as in (A). **D.** The 270 kDa protein band normalized as in (A). Normalization to the control band at 120 min was chosen as the strongest physiological phosphorylation signal.

Table 1A 20h exposure to DMP	Number of independent trials	Progression to blastocyst stage per experiment,%	Number of blastocysts/number of zygotes collected
Control	1	100%	37/38
	2	83%	
	3	100%	
	4	100%	
	5	100%	
1μM DMP	1	61%	26/46
	2	80%	
	3	33%	
	4	40%	
	5	100%	
2μM DMP	1	41%	14/34
	2	100%	
	3	57%	
	4	0%	
10μM DMP	1	0%	0/31
	2	0%	
	3	0%	
	4	0%	

Table 1B 20h exposure to BPA	Number of independent trials	Progression to blastocyst stage per experiment,%	Number of blastocysts/number of zygotes collected
Control	1	50%	35/42
	2	83%	
	3	82%	
	4	100%	
	5	100%	
1μM BPA	1	91.6%	25/27
	2	100%	
	3	90%	
2μM BPA	1	33.3%	13/20
	2	66.7%	
	3	87.5%	
10μM BPA	1	0%	0/37
	2	0%	
	3	0%	

Table 1C 20h exposure to DEP	Number of independent trials	Progression to blastocyst stage per experiment, %	Number of blastocysts/number of zygotes collected
Control	1	100%	27/29
	2	100%	
	3	85%	
	4	100%	
1μM DEP	1	68.75%	34/41
	2	100%	
	3	85.70%	
	4	92.80%	
2μM DEP	1	100%	21/34
	2	71.50%	
	3	0%	
	4	92%	
10μM DEP	1	0%	0/33
	2	0%	
	3	0%	

Table 1D 20h exposure to DEHP	Number of independent trials	Progression to blastocyst stage per experiment,%	Number of blastocysts/number of zygotes collected
Control	1	90%	44/48
	2	85.70%	
	3	100%	
	4	100%	
	5	100%	
	6	83%	
1μM DEHP	1	30%	13/23
	2	75%	
	3	100%	
2μM DEHP	1	100%	41/51
	2	66.7%	
	3	85%	
	4	75%	
	5	100%	
	6	0%	
	7	90%	
	8	100%	
10μM DEHP	experiments 1 to 4	0%, 0%, 0%, 0%	0/56

Supplementary Tables 1A-1D. **Murine embryo development after 20h exposure to DMP, BPA, DEP or DEHP**. Embryo development was assessed on day 5 post fertilization. The column "progression to blastocyst stage per experiment, %" represents the percentage of embryos that reached blastocyst or morula stage. This number was calculated by dividing the number of all embryos that reached blastocyst or morula stage to the number of all collected zygotes per each experiment. Zygotes were obtained from naturally mated super-ovulated females. Each condition was assessed by 3-8 independent experiments. **A.** Embryo development after 20 hours exposure to DMP at 0, 1, 2 and 10 μM and subsequent embryo culture in DMP-free media. **B.** Embryo development after 20 hours exposure to the indicated concentration of BPA and subsequent culture in BPA-free media. **C**. Embryo development after 20 hours exposure to the indicated concentration of DEP and subsequent culture in DEP-free media. **D.** Embryo development after 20 hours exposure to the indicated concentration of DEHP and subsequent culture in DEHP-free media.

20h exposure to Vehicle Control,1μL/mL	Number of independent trials	Progression to blastocyst stage per experiment,%	Number of blastocysts/number of zygotes collected
Vehicle Control,1μL/mL	1	100%	16/17
	2	83%	
	3	100%	

Supplementary Table 2. The development of murine zygotes isolated from naturally mated super-ovulated females and after their exposure to 0.1% ethanol for 20 hours in the culture media. Embryo development was assessed on day 5 post fertilization and represents the percentage of embryos that reached blastocyst or morula stage. This number was calculated by dividing the number of all embryos that reached blastocyst or morula stage by the number of all collected zygotes per experiment.

Table 3A IVF; DMP	Number of independent trials	Progression to blastocyst stage per experiment,%	Number of blastocysts/number of eggs collected
Control	1	71.4%	26/36
	2	71%	
	3	80%	
	4	67%	
1μM DMP	1	48%	30/42
	2	89.5%	
	3	83%	
2μM DMP	1	69%	28/36
	2	100%	
	3	87.5%	
	4	67%	
10μM DMP	1	57%	21/30
	2	43%	
	3	82%	
	4	100%	

Table 3 B IVF; BPA	Number of independent trials	Progression to blastocyst stage per experiment,%	Number of blastocysts/number of eggs collected
Control	1	100%	24/28
	2	88%	
	3	77%	
	4	50%	
1μM BPA	1	62%	56/88
	2	73%	
	3	63%	
	4	63%	
2μM BPA	1	90%	39/47
	2	88%	
	3	67%	
10μM BPA	1	73%	13/19
	2	63%	
	3	48%	

Table 3C IVF; DEP	Number of independent trials	Progression to the blastocysts stage per experiment, %	Number of blastocysts/number of eggs collected
Control	1	90%	28/31
	2	94.7%	
	3	50%	
1μM DEP	1	88.8%	20/28
	2	82%	
	3	38%	
2μM DEP	1	89%	35/42
	2	78%	
	3	70%	
10μM DEP	1	80%	18/20
	2	100%	
	3	50%	

Table 3D IVF; DEHP	Number of independent trials	Progression to the blastocyst stage per experiment,%	Number of blastocysts/number of eggs collected
Control	1	86%	72/92
	2	87%	
	3	89%	
	4	88%	
	5	77%	
	6	65%	
	7	47%	
	8	67%	
1μM DEHP	1	77%	16/18
	2	100%	
	3	100%	
2μM DEHP	1	58%	25/51
	2	60%	
	3	13%	
	4	66%	
	5	42%	
10μM DEHP	experiments 1 to 7	0%, 0%, 0%, 0%, 0%, 0%, 0%, 7%	1/63

Supplementary Tables 3A-3D. Development of in vitro fertilized mouse embryos obtained after murine eggs were introduced to the sperm previously exposed to DMP, BPA, DEP or DEHP for 60-90 minutes. Embryo development was assessed on day 5 post fertilization. The "Progression to the blastocyst stage per experiment, %" column represents the percentage of embryos that reached blastocyst or morula stage. This number was calculated by dividing the number of all embryos that reached blastocyst or morula stage to the number of all collected and inseminated eggs per each experiment. Each condition was assessed by 3-5 independent experiments. **A.** In vitro embryo development after eggs insemination with 0, 1, 2 or 10 μM DMP-treated sperm **B.** In vitro embryo development after eggs were inseminated with spermatozoa previously exposed to the indicated concentration of BPA. **C**. In vitro embryo development after eggs were inseminated with the spermatozoa treated with corresponding concentrations of DEP. **D.** In vitro embryo development after murine eggs were inseminated with spermatozoa treated with corresponding concentrations of DEHP.

20h exposure to Vehicle Control,1μL/mL	Number of independent trials	Progression to blastocyst stage per experiment,%	Number of blastocysts/number of zygotes collected
	1	100%	28/37
	2	80%	
	3	100%	
	4	50%	

Supplementary Table 4. Development of embryos derived from the murine eggs that were subjected to in vitro fertilization (IVF) with murine sperm previously exposed to 0.1% ethanol for 60-90 minutes. Embryo development was assessed on the day 5 post IVF and represents the percentage of embryos that reached blastocyst or morula stage. This number was calculated by dividing the number of all embryos that reached blastocyst or morula stage to the number of all collected eggs per each independent experiment.

Table 5 **PN formation**	Number of independent trials	Progression to blastocyst stage per experiment,%	Number of blastocysts/number of zygotes collected
Control	1	84.6%	21/25
	2	71.4%	
	3	60%	
DEHP 10µM	1	0%	2/36
	2	0%	
	3	10%	

Supplementary Table 5. Effect of 10 µM DEHP on fertilization and pronuclei formation. Pronucleus (PN) formation was assessed 9 hours after egg insemination with sperm cells previously exposed to 10 µM DEHP. Three independent experiments were carried out.

Table 6 **Flow cytometry** Mean Fluorescence Intensity (MFI) APC-Cy7-A normalized to mode	Number of independent trials	Control MFI	DEHP MFI	MFI Ratio DEHP/Control
	1	151	260	1.72
	2	374	442	1.18
	3	265	402	1.52
	4	523	514	0.98
	5	358	859	2.39

Supplementary Table 6. Assessment of the global tyrosine phosphorylation by flow cytometry. Tyrosine phosphoproteins were detected by flow cytometry using a CF 647 dye conjugated to anti-PY antibody. Five independent experiments were carried out. Sperm

concentrations were normalized between all conditions for each experiment. Values are mean fluorescence intensity (MFI) detected in the APC-Cy7-A channel normalized to mode. A ratio of the normalized detected MFI in the 10 μM DEHP-treated sperm cells vs the vehicle control was used to calculate the fold increase in global fluorescence.

Mouse #	cell/mL in vehicle	Vehicle CPM	CPM/ 10^6 sperm vehicle	cell/mL in 10μM	10μM CPM	CPM/ 10^6 sperm 10μM	cell/mL in 100μM	100μM CPM	CPM/ 10^6 sperm 100μM
1	$2.57*10^6$	4694	1826.459	$2.17*10^6$	6321.666	2913.210	$2.525*10^6$	6750.333	2673.399
2	$1.4*10^6$	1520	1085.714	$1.375*10^6$	3214	2337.454	$1.4*10^6$	5345.333	3818.095
3	$1.425*10^6$	1777.333	1247.251	$1.9*10^6$	3216	1692.631	$2.775*10^6$	3769	1358.198
4	$1.35*10^6$	1612	1194.074	$2.1*10^6$	3329.666	1585.555	$1.775*10^6$	5127.666	2888.826
5	$2.375*10^6$	3232	1360.842	$2.25*10^6$	5983.666	2659.407	$1.675*10^6$	5278	3151.044
6	$1.575*10^6$	1619.666	1028.359	$1.475*10^6$	3526.333	2390.734	$1.225*10^6$	4722.333	3854.965

Supplementary Table 7. Detection of reactive oxygen species (ROS) in murine spermatozoa treated with DEHP compared with vehicle control. The luminol-dependent chemiluminescence assay was used to detect ROS production. Six independent experiments were carried out. A minimum of $1.35*10^6$ sperm cells/mL were used per condition. ROS production was expressed as counted photons per minute (CPM)/10^6. Each row represents an individual experiment. For each experiment, sperm concentrations were normalized between all conditions.

6.6 References

1. Rudel, R. A., Camann, D. E., Spengler, J. D., Korn, L. R. & Brody, J. G. Phthalates, alkylphenols, pesticides, polybrominated diphenyl ethers, and other endocrine-disrupting compounds in indoor air and dust. *Environ. Sci. Technol.* **37**, 4543–53 (2003).

2. Hunt, P. A., Susiarjo, M., Rubio, C. & Hassold, T. J. The Bisphenol A Experience: A Primer for the Analysis of Environmental Effects on Mammalian Reproduction1. *Biol. Reprod.* **81**, 807–813 (2009).

3. Green, R. *et al.* Use of di(2-ethylhexyl) phthalate-containing medical products and urinary levels of mono(2-ethylhexyl) phthalate in neonatal intensive care unit infants. *Environ. Health Perspect.* **113**, 1222–1225 (2005).

4. Hauser, R. & Calafat, A. M. Phthalates and human health. *Occupational and Environmental Medicine* vol. 62 806–818 (2005).

5. Muncke, J. Endocrine disrupting chemicals and other substances of concern in food contact materials: An updated review of exposure, effect and risk assessment. *Journal of Steroid Biochemistry and Molecular Biology* vol. 127 118–127 (2011).

6. Pearson, S. D. & Trissel, L. A. Leaching of diethylhexyl phthalate from polyvinyl chloride containers by selected drugs and formulation components. *Am. J. Hosp. Pharm.* **50**, 1405–9 (1993).

7. Meeker, J. D., Calafat, A. M. & Hauser, R. Urinary metabolites of di(2-ethylhexyl) phthalate are associated with decreased steroid hormone levels in adult men. *J. Androl.* **30**, 287–97 (2009).

8. Toft, G. *et al.* Association between pregnancy loss and urinary phthalate levels around the time of conception. *Environ. Health Perspect.* **120**, 458–63 (2012).

9. Burdorf, A. *et al.* The effects of work-related maternal risk factors on time to pregnancy, preterm birth and birth weight: The seneration R study. *Occup. Environ. Med.* **68**, 197–204 (2011).

10. Lovekamp, T. N. & Davis, B. J. Mono-(2-ethylhexyl) phthalate suppresses aromatase transcript levels and estradiol production in cultured rat granulosa cells. *Toxicol. Appl. Pharmacol.* **172**, 217–224 (2001).

11. Svechnikova, I., Svechnikov, K. & Söder, O. The influence of di-(2-ethylhexyl) phthalate on steroidogenesis by the ovarian granulosa cells of immature female rats. *J. Endocrinol.* **194**, 603–9 (2007).

12. Bloom, M. S. *et al.* Associations between urinary phthalate concentrations and semen quality parameters in a general population. *Hum. Reprod.* **30**, 2645–2657 (2015).

13. Duty, S. M. *et al.* Phthalate Exposure and Human Semen Parameters. *Epidemiology* **14**, 269–277 (2003).

14. Hauser, R., Meeker, J. D., Duty, S., Silva, M. J. & Calafat, A. M. Altered semen quality in relation to urinary concentrations of phthalate monoester and oxidative metabolites. *Epidemiology* **17**, 682–91 (2006).

15. Brehm, E. & Flaws, J. A. Transgenerational effects of endocrine-disrupting chemicals on Male and female reproduction. *Endocrinology* vol. 160 1421–1435 (2019).

16. Patel, S., Zhou, C., Rattan, S. & Flaws, J. A. Effects of Endocrine-Disrupting Chemicals on the Ovary1. *Biol. Reprod.* **93**, 20 (2015).

17. Wang, W., Craig Z, B. M., K, H. & J, F. Mono-(2-Ethylhexyl) Phthalate Induces Oxidative Stress and Inhibits Growth of Mouse Ovarian Antral Follicles1. *Biol. Reprod.* **87**, 152 (2012).

18. Vandenberg, L. N., Hauser, R., Marcus, M., Olea, N. & Welshons, W. V. Human exposure to bisphenol A (BPA). *Reproductive Toxicology* vol. 24 139–177 (2007).

19. Calafat, A. M. *et al.* Urinary concentrations of bisphenol A and 4-Nonylphenol in a human reference population. *Environ. Health Perspect.* **113**, 391–395 (2005).

20. Hauser, R. *et al.* DNA damage in human sperm is related to urinary levels of phthalate monoester and oxidative metabolites. *Hum. Reprod.* **22**, 688–695 (2007).

21. Fernandez, M. F. *et al.* Bisphenol-A and chlorinated derivatives in adipose tissue of women. *Reprod. Toxicol.* **24**, 259–264 (2007).

22. Sun, Y. *et al.* Determination of bisphenol A in human breast milk by HPLC with column-switching andfluorescence detection. *Biomed. Chromatogr.* **18**, 501–507 (2004).

23. Zota, A. R., Calafat, A. M. & Woodruff, T. J. Temporal trends in phthalate exposures: findings from the National Health and Nutrition Examination Survey, 2001-2010. *Environ. Health Perspect.* **122**, 235–41 (2014).

24. Zhou, W. *et al.* Bisphenol A and Ovarian reserve among infertile women with polycystic Ovarian syndrome. *Int. J. Environ. Res. Public Health* **14**, (2017).

25. Fujii, S. *et al.* A TWO-GENERATION REPRODUCTIVE TOXICITY STUDY OF DIETHYL PHTHALATE (DEP) IN RATS. *J. Toxicol. Sci.* **30**, S97-116 (2005).

26. Mei, Y. *et al.* Effects of Dimethyl Phthalate (DMP) on Serum Sex Hormone Levels and Apoptosis in C57 Female Mice. *undefined* (2019).

27. Wang, Y., Zhu, H. & Kannan, K. A review of biomonitoring of phthalate exposures. *Toxics* vol. 7 (2019).

28. Zota, A. R., Phillips, C. A. & Mitro, S. D. Recent fast food consumption and bisphenol A and phthalates exposures among the U.S. population in NHANES, 2003–2010. *Environ. Health Perspect.* **124**, 1521–1528 (2016).

29. Api, A. M. Toxicological profile of diethyl phthalate: A vehicle for fragrance and cosmetic ingredients. *Food and Chemical Toxicology* vol. 39 97–108 (2001).

30. Kavlock, R. *et al.* NTP center for the evaluation of risks to human reproduction:

Phthalates expert panel report on the reproductive and developmental toxicity of di(2-ethylhexyl) phthalate. *Reprod. Toxicol.* **16**, 529–653 (2002).

31. Sumner, R. N., Tomlinson, M., Craigon, J., England, G. C. W. & Lea, R. G. Independent and combined effects of diethylhexyl phthalate and polychlorinated biphenyl 153 on sperm quality in the human and dog. *Sci. Rep.* **9**, 3409 (2019).

32. Pan, G. *et al.* Associations between hazard indices of di-n-butylphthalateand di-2-ethylhexylphthalate exposure and serum reproductive hormone levels among occupationally exposed and unexposed Chinese men. *Int. J. Androl.* **34**, e397–e406 (2011).

33. Austin, C. R. Observations on the penetration of the sperm in the mammalian egg. *Aust. J. Sci. Res. B.* **4**, 581–596 (1951).

34. Yanagimachi, R. Fertility of mammalian spermatozoa: Its development and relativity. *Zygote* **2**, 371–372 (1994).

35. Davis, B. K. Timing of fertilization in mammals: Sperm cholesterol/phospholipid ratio as a determinant of the capacitation interval. *Proc. Natl. Acad. Sci. U. S. A.* **78**, 7560–7564 (1981).

36. Chang, M. C. A detrimental effect of seminal plasma on the fertilizing capacity of sperm. *Nature* **179**, 258–9 (1957).

37. Ren, D. *et al.* A sperm ion channel required for sperm motility and male fertility. *Nature* **413**, 603–9 (2001).

38. Carlson, A. E. *et al.* CatSper1 required for evoked Ca2+ entry and control of flagellar function in sperm. *Proc. Natl. Acad. Sci. U. S. A.* **100**, 14864–8 (2003).

39. Qi, H. *et al.* All four CatSper ion channel proteins are required for male fertility and sperm cell hyperactivated motility. *Proc. Natl. Acad. Sci. U. S. A.* **104**, 1219–23 (2007).

40. Tamburrino, L. *et al.* The CatSper calcium channel in human sperm: Relation with motility and involvement in progesterone-induced acrosome reaction. *Hum. Reprod.* **29**, 418–428 (2014).

41. Schiffer, C. *et al.* Direct action of endocrine disrupting chemicals on human sperm. *EMBO Rep.* **15**, 758–765 (2014).

42. Kirichok, Y., Navarro, B. & Clapham, D. E. Whole-cell patch-clamp measurements of spermatozoa reveal an alkaline-activated Ca2+ channel. *Nature* **439**, 737–40 (2006).

43. Salicioni, A. M. *et al.* Signalling pathways involved in sperm capacitation. *Society of Reproduction and Fertility supplement* vol. 65 245–259 (2007).

44. Visconti, P. E. Understanding the molecular basis of sperm capacitation through kinase design. *Proc. Natl. Acad. Sci. U. S. A.* **106**, 667–8 (2009).

45. Visconti, P. E. *et al. Capacitation of mouse spermatozoa I. Correlation between the capacitation state and protein tyrosine phosphorylation*. (1995).

46. Naz, R. K. & Rajesh, P. B. Role of tyrosine phosphorylation in sperm capacitation / acrosome reaction. *Reprod. Biol. Endocrinol.* **2**, 75 (2004).

47. Sepideh, J. *et al.* Tyrosine phosphorylation pattern in sperm proteins isolated from normospermic and teratospermic men. *J. Reprod. Infertil.* **10**, 185–91 (2009).

48. Nassar, A. *et al.* Modulation of sperm tail protein tyrosine phosphorylation by pentoxifylline and its correlation with hyperactivated motility. *Fertil. Steril.* **71**, 919–923 (1999).

49. Alvau, A. *et al.* The tyrosine kinase FER is responsible for the capacitationassociated increase in tyrosine phosphorylation in murine sperm. *Dev.* **143**, 2325–2333 (2016).

50. Huang, Y. *et al.* The Increase of ROS Caused by the Interference of DEHP with JNK/p38/p53 Pathway as the Reason for Hepatotoxicity. *Int. J. Environ. Res. Public Health* **16**, (2019).

51. Kasahara, E. *et al.* Role of oxidative stress in germ cell apoptosis induced by di(2-ethylhexyl)phthalate. *Biochem. J.* **365**, 849–56 (2002).

52. Schaedlich, K. *et al.* DEHP deregulates adipokine levels and impairs fatty acid storage in human SGBS-adipocytes. *Sci. Rep.* **8**, 3447 (2018).

53. Ochsendorf, F. R. *et al.* Chemiluminescence in semen of infertile men. *Andrologia* **26**, 289–293 (1994).

54. Williams, A. C. & Ford, W. C. L. Relationship between reactive oxygen species production and lipid peroxidation in human sperm suspensions and their association with sperm function. *Fertil. Steril.* **83**, 929–36 (2005).

55. Agarwal, A., Cocuzza, M., Abdelrazik, H. & Sharma, R. K. *Oxidative stress measurement in patients with male or female factor infertility*. *Chemiluminescent Methods in Oxidative Stress Assessment* vol. 37 (2008).

56. Avella, M. A. & Dean, J. Fertilization with acrosome-reacted mouse sperm: implications for the site of exocytosis. *Proc. Natl. Acad. Sci. U. S. A.* **108**, 19843–4 (2011).

57. Zalata, A. A., Ahmed, A. H., Allamaneni, S. S. R., Comhaire, F. H. & Agarwal, A. Relationship between acrosin activity of human spermatozoa and oxidative stress. *Asian J. Androl.* **6**, 313–318 (2004).

58. Aitken, R. J. & Clarkson, J. S. Cellular basis of defective sperm function and its association with the genesis of reactive oxygen species by human spermatozoa. *J. Reprod. Fertil.* **81**, 459–69 (1987).

59. Ichikawa, T., Oeda, T., Ohmori, H. & Schill, W. B. Reactive oxygen species influence the acrosome reaction but not acrosin activity in human spermatozoa. *Int. J. Androl.* **22**, 37–42 (1999).

60. Griveau, J. F., Renard, P. & Le Lannou, D. Superoxide anion production by human spermatozoa as a part of the ionophore-induced acrosome reaction process. *Int. J. Androl.* **18**, 67–74 (1995).

61. Brehm, E., Rattan, S., Gao, L. & Flaws, J. A. Prenatal Exposure to Di(2-Ethylhexyl) Phthalate Causes Long-Term Transgenerational Effects on Female Reproduction in Mice. *Endocrinology* **159**, 795–809 (2018).

62. Hannon, P. R., Niermann, S. & Flaws, J. A. Acute Exposure to Di(2-Ethylhexyl) Phthalate in Adulthood Causes Adverse Reproductive Outcomes Later in Life and Accelerates Reproductive Aging in Female Mice. *Toxicol. Sci.* **150**, 97–108 (2016).

63. Wu, Y. *et al.* Primary neuronal-astrocytic co-culture platform for neurotoxicity assessment of di-(2-ethylhexyl) phthalate. *J. Environ. Sci. (China)* **26**, 1145–1153 (2014).

64. Kay, V. R., Bloom, M. S. & Foster, W. G. Reproductive and developmental effects of phthalate diesters in males. *Crit. Rev. Toxicol.* **44**, 467–498 (2014).

65. Latini, G., Del Vecchio, A., Massaro, M., Verrotti, A. & De Felice, C. Phthalate exposure and male infertility. *Toxicology* vol. 226 90–98 (2006).

66. vom Saal, F. S., Parmigiani, S., Palanza, P. L., Everett, L. G. & Ragaini, R. The plastic world: Sources, amounts, ecological impacts and effects on development, reproduction, brain and behavior in aquatic and terrestrial animals and humans. *Environmental Research* vol. 108 127–130 (2008).

67. Pant, N. *et al.* Environmental and experimental exposure of phthalate esters: the toxicological consequence on human sperm. *Hum. Exp. Toxicol.* **30**, 507–14 (2011).

68. Tanaka, A., Adachi, T., Takahashi, T. & Yamaha, T. Biochemical studies on phthalic esters I. Elimination, distribution and metabolism of di-(2-ethylhexyl)phthalate in rats. *Toxicology* **4**, 253–264 (1975).

69. Regnier, S. M. & Sargis, R. M. Adipocytes under assault: environmental disruption of adipose physiology. *Biochim. Biophys. Acta* **1842**, 520–33 (2014).

70. Tripathi, A., Pandey, V., Sahu, A. N., Singh, A. & Dubey, P. K. Di-(2-ethylhexyl) phthalate (DEHP) inhibits steroidogenesis and induces mitochondria-ROS mediated apoptosis in rat ovarian granulosa cells. *Toxicol. Res. (Camb).* **8**, 381–394 (2019).

71. Kim, J. H., Park, H. Y., Bae, S., Lim, Y.-H. & Hong, Y.-C. Diethylhexyl phthalates is associated with insulin resistance via oxidative stress in the elderly: a panel study. *PLoS One* **8**, e71392 (2013).

72. Ambruosi, B. *et al.* Correction: In Vitro Acute Exposure to DEHP Affects Oocyte Meiotic Maturation, Energy and Oxidative Stress Parameters in a Large Animal Model. *PLoS One* **6**, (2011).

73. Aitken, R. J., Paterson, M., Fisher, H., Buckingham, D. W. & Van Duin, M. Redox regulation of tyrosine phosphorylation in human spermatozoa and its role in the control of human sperm function. *J. Cell Sci.* **108**, 2017–2025 (1995).

74. Leclerc, P., De Lamirande, E. & Gagnon, C. Regulation of protein-tyrosine phosphorylation and human sperm capacitation by reactive oxygen derivatives. *Free Radic. Biol. Med.* **22**, 643–656 (1997).

75. Rahman, M. S. *et al.* Bisphenol-A affects male fertility via fertility-related proteins in spermatozoa. *Sci. Rep.* **5**, 9169 (2015).

76. Donà, G. *et al.* Evaluation of correct endogenous reactive oxygen species content for human sperm capacitation and involvement of the NADPH oxidase system. *Hum. Reprod.* **26**, 3264–73 (2011).

77. Villegas, J. *et al.* Reactive oxygen species induce reversible capacitation in human spermatozoa. *Andrologia* **35**, 227–32 (2003).

78. Alvarez, J. G. & Storey, B. T. Spontaneous Lipid Peroxidation in Rabbit Epididymal Spermatozoa: Its Effect on Sperm Motility. *Biol. Reprod.* **27**, 1102–1108 (1982).

79. Jones, R., Mann, T. & Sherins, R. Peroxidative breakdown of phospholipids in human spermatozoa, spermicidal properties of fatty acid peroxides, and protective action of seminal plasma. *Fertil. Steril.* **31**, 531–537 (1979).

80. Visconti, P. E. *et al.* Capacitation of mouse spermatozoa. II. Protein tyrosine phosphorylation and capacitation are regulated by a cAMP-dependent pathway. *Development* **121**, 1139–1150 (1995).

81. Piehler, E., Petrunkina, A. M., Ekhlasi-Hundrieser, M. & Töpfer-Petersen, E. Dynamic quantification of the tyrosine phosphorylation of the sperm surface proteins during capacitation. *Cytometry. A* **69**, 1062–70 (2006).

82. Rosado-Berrios, C. A., Vélez, C. & Zayas, B. Mitochondrial permeability and toxicity of diethylhexyl and monoethylhexyl phthalates on TK6 human lymphoblasts cells. *Toxicol. In Vitro* **25**, 2010–6 (2011).

83. Roth, Z. Symposium review: Reduction in oocyte developmental competence by stress is associated with alterations in mitochondrial function1. *J. Dairy Sci.* **101**, 3642–3654 (2018).

84. Aitken, R. J., Wingate, J. K., De Iuliis, G. N., Koppers, A. J. & Mclaughlin, E. A. Cis-Unsaturated Fatty Acids Stimulate Reactive Oxygen Species Generation and Lipid Peroxidation in Human Spermatozoa. **91**, 4154–4163 (2006).

85. Wathes et al. Polyunsaturated fatty acids in male and female reproduction. *Biol. Reprod.* **77**, 190–201 (2007).

86. Chen, S. J., Allam, J. P., Duan, Y. G. & Haidl, G. Influence of reactive oxygen species on human sperm functions and fertilizing capacity including therapeutical approaches. *Arch. Gynecol. Obstet.* **288**, 191–199 (2013).

87. Cocuzza, M., Sikka, S. C., Athayde, K. S. & Agarwal, A. Clinical relevance of oxidative stress and sperm chromation damage in male infertility: An evidence based analysis. *International Braz J Urol* vol. 33 603–621 (2007).

88. Sikka, S. Relative Impact of Oxidative Stress on Male Reproductive Function. *Curr. Med. Chem.* **8**, 851–862 (2001).

89. Inoue, N., Ikawa, M., Isotani, A. & Okabe, M. The immunoglobulin superfamily protein

Izumo is required for sperm to fuse with eggs. *Nature* **434**, 234–238 (2005).

90. La Spina, F. A. *et al.* Mouse sperm begin to undergo acrosomal exocytosis in the upper isthmus of the oviduct. *Dev. Biol.* **411**, 172–182 (2016).

91. Jin, M. *et al.* Most fertilizing mouse spermatozoa begin their acrosome reaction before contact with the zona pellucida during in vitro fertilization. *Proc. Natl. Acad. Sci. U. S. A.* **108**, 4892–4896 (2011).

92. Yanagimachi, R. Mammalian Sperm Acrosome Reaction: Where Does It Begin Before Fertilization? *Biol. Reprod.* **85**, 4–5 (2011).

93. Reddy, B. S., Rozati, R., Reddy, B. V. R. & Raman, N. V. V. S. S. Association of phthalate esters with endometriosis in Indian women. *BJOG* **113**, 515–20 (2006).

94. Nassberger, L., Arbin, A. & Ostelius, J. Exposure of patients to phthalates from polyvinyl chloride tubes and bags during dialysis. *Nephron* **45**, 286–290 (1987).

95. Hoogenkamp, H. & Lewing, P. Superovulation in mice in relation to their age. *Vet. Q.* **4**, 47–48 (1982).

96. Vergara, G. J., Irwin, M. H., Moffatt, R. J. & Pinkert, C. A. In vitro fertilization in mice: Strain differences in response to superovulation protocols and effect of cumulus cell removal. *Theriogenology* **47**, 1245–1252 (1997).

97. Wennemuth, G., Carlson, A. E., Harper, A. J. & Babcock, D. F. Bicarbonate actions on flagellar and Ca2+-channel responses: Initial events in sperm activation. *Development* vol. 130 1317–1326 (2003).

98. Laemmli, U. K. Cleavage of structural proteins during the assembly of the head of bacteriophage T4. *Nature* **227**, 680–685 (1970).

99. Larson, J. L. & Miller, D. J. Simple histochemical stain for acrosomes on sperm from several species. *Mol. Reprod. Dev.* **52**, 445–449 (1999).

100. Barbonetti, A. *et al.* Dynamics of the Global Tyrosine Phosphorylation During Capacitation and Acquisition of the Ability to Fuse with Oocytes in Human Spermatozoa1. *Biol. Reprod.* **79**, 649–656 (2008).

101. Saleh, R. A. & Agarwal, A. Oxidative stress and male infertility: From research bench to clinical practice. *J. Androl.* **23**, 737–752 (2002).

Chapter IV

7. Concluding remarks

The current work focused on two key roles of mitochondria- the regulation of calcium homeostasis and the generation of reactive oxygen species- and examined how endogenous and exogenous factors can regulate these two functions.

The first goal of this thesis was to examine the levels of PIP2 in the mitochondrial membranes and investigate whether this endogenous bioactive lipid can regulate the activity of the mitochondrial calcium uniporter (MCU). Using a targeted lipid mass spectrometry analysis, we detected thirteen different species of PIP2 in mitochondrial membranes and have shown that PIP2 concentration in the mitochondrial membranes is comparable to the levels of PIP2 in the plasma membrane. Also, by applying the mitochondrial patch-clamp technique, we have shown that the application of PIP2 analog potentiates calcium uptake via the MCU. In contrast, the removal of PIP2 a specific binding peptide (PBP10), reduces the calcium current amplitude. In addition, by showing that PIP2 does not activate calcium uptake in MCU KO mitochondria, we confirmed that the observed effect is specific to MCU. Based on these experiments, we conclude that PIP2 is an endogenous lipid in the mitochondrial membrane that regulates the MCU channel. Nonetheless, to gain a better understanding of PIP2's physiological role in the mitochondrial calcium uptake, it would be beneficial to do the following two experiments: an inside-out configuration of the patch-clamp technique and mitochondrial calcium imaging. The inside-out configuration of the patch-clamp method is characterized by a fast depletion of endogenous PIP2 after the inner leaflet of the patch is exposed [1,2]. The inner leaflet exposure also allows a rapid and direct application of exogenous PIP2 , after its depletion. This electrophysiological experiment will provide insight to the molecular mechanism of PIP2 regulation and determine if such regulation is physiologically relevant. In addition, performing mitochondrial calcium imaging in intact cells would help determine PIP2 contribution to mitochondrial calcium uptake[3]. Using intact cells will provide a better understanding of mitochondrial calcium handling in relation to the cellular function. Mitochondrial calcium imaging in intact cells can be done by utilizing a genetically encoded fluorescent reporter constructs targeted to the mitochondria[4–6].

The second goal of this thesis was to study the impact of acute exposure to di-2-ethylhexyl phthalate (DEHP) on sperm fertility. The outlined experiments revealed that a short exposure of 60-90 minutes to DEHP impairs sperm fertility. Exposure to DEHP triggered ROS overproduction, which led to altered capacitation and inhibited the acrosome reaction; two essential steps sperm must undergo to acquire fertility. These results add to the growing body of scientific evidence on the harmful impact of EDCs on health and fertility.

One major drawback of these studies is that they were done mostly in vitro. It would be advantageous for our understanding to do in-vivo experiments. With that being said, such experiments would be difficult to execute, namely because the assessment of acute exposure to unmetabolized DEHP requires either abrupt release from the adipose tissue [7] or release from medical devices, such as a urological catheter[8]. For the former, one has to ensure there are stores of unmetabolized DEHP in the adipose tissue. Generating stores of unmetabolized DEHP will

require exposing the animal to DEHP over prolonged periods. Such chronic exposure may lead to deterioration in the reproductive health of the animal or other unforeseen health issues [9–11]. Therefore, distinguishing between the chronic and the acute effects of such exposure will be difficult. Catheterization could be an alternative approach for this purpose.

Another drawback of our study is that all experiments were done using a murine model; thus, there is an inherent challenge of extrapolating these data to humans. Therefore, in the future, it would be ideal to repeat the same experiments using human spermatozoa.

Overall, the presented work revealed a new endogenous regulator of mitochondrial calcium uptake. It also characterized the effect of one of the most ubiquitous environmental toxins, DEHP, on reactive oxygen species production, using murine spermatozoa as a model.

7.1 References

1. Rodriguez, N. *et al.* Phosphatidylinositol-4,5-bisphosphate (PIP2) stabilizes the open pore conformation of the Kv11.1 (hERG) channel. *Biophys. J.* **99**, 1110–1118 (2010).
2. Remedi, M. S. & Nichols, C. G. KATP Channels in the Pancreas: Hyperinsulinism and Diabetes. Hyperinsulinism and Diabetes. in *Ion Channels in Health and Disease* 199–221 (Elsevier Inc., 2016). doi:10.1016/B978-0-12-802002-9.00008-X.
3. Duchen, M. R., Surin, A. & Jacobson, J. Imaging mitochondrial function in intact cells. *Methods Enzymol.* **361**, 353–389 (2003).
4. Gkerküçük, E. B., Tramier, M. & Bertolin, G. Imaging mitochondrial functions: From fluorescent dyes to genetically-encoded sensors. *Genes* vol. 11 (2020).
5. Hodneland Nilsson, L. I. *et al.* A new live-cell reporter strategy to simultaneously monitor mitochondrial biogenesis and morphology. *Sci. Rep.* **5**, 1–17 (2015).
6. Suzuki, J. *et al.* Imaging intraorganellar Ca2+ at subcellular resolution using CEPIA. *Nat. Commun.* **5**, 1–13 (2014).
7. Regnier, S. M. & Sargis, R. M. Adipocytes under assault: environmental disruption of adipose physiology. *Biochim. Biophys. Acta* **1842**, 520–33 (2014).
8. Green, R. *et al.* Use of di(2-ethylhexyl) phthalate-containing medical products and urinary levels of mono(2-ethylhexyl) phthalate in neonatal intensive care unit infants. *Environ. Health Perspect.* **113**, 1222–1225 (2005).
9. Kay, V. R., Chambers, C. & Foster, W. G. Reproductive and developmental effects of phthalate diesters in females. *Critical Reviews in Toxicology* vol. 43 200–219 (2013).
10. Mathieu-Denoncourt, J., Wallace, S. J., de Solla, S. R. & Langlois, V. S. Plasticizer endocrine disruption: Highlighting developmental and reproductive effects in mammals and non-mammalian aquatic species. *General and Comparative Endocrinology* vol. 219 74–88 (2015).
11. Chronic Toxicity of Di(2-ethylhexyl)phthalate in Mice | Toxicological Sciences | Oxford Academic. https://academic.oup.com/toxsci/article/58/2/377/1733981.